ANALYSIS OF HOLE QUALITY FOR PRE-TEMPERED FLOAT GLASS WHILE USING ROTARY ULTRASONIC MACHINING

A Thesis submitted in fulfillment of the requirement for the award of the degree of

DOCTOR OF PHILOSOPHY

IN

MECHANICAL ENGINEERING

Submitted by

ANKIT SHARMA

Roll No. 901508008

Under the supervision of

Dr. Vivek Jain
Associate Professor

Dr. Dheeraj Gupta
Associate Professor

Department of Mechanical Engineering,

Thapar Institute of Engineering & Technology, Patiala-147004, INDIA

(Deemed to be University)

July 2020

CONTENTS

CERTIFICATE

I, **Ankit Sharma**, Roll no. 901508008, hereby declared that the thesis entitled **"Analysis of Hole Quality For Pre-Tempered Float Glass While Using Rotary Ultrasonic Machining"** submitted to the Department of Mechanical Engineering at Thapar Institute of Engineering & Technology, Patiala, Punjab (India) is an authenticated record of my own work for the award of the degree "Doctor of Philosophy" under the supervision of Dr. Vivek Jain and Dr. Dheeraj Gupta. This report has not been submitted to any other institute for the award of any other degree.

Ankit Sharma

Roll No. 901508008

Patiala

Date: 28/July/2020

This is certifying that the above statement by the candidate is correct to the best of our knowledge

Verified by:

29/07/2020

Dr. Vivek Jain
(Supervisor)
Associate Professor
Department of Mechanical Engineering
Thapar Institute of Engineering & Technology
Patiala-147004, (Punjab), India

Dr. Dheeraj Gupta
(Supervisor)
Associate Professor
Department of Mechanical Engineering
Thapar Institute of Engineering & Technology
Patiala-147004, (Punjab), India

ACKNOWLEDGEMENT

First and the foremost, I wish to thank my supervisors **Dr. Vivek Jain** and **Dr. Dheeraj Gupta** for his valuable support and guidance. I am sincerely gratitude to him for judging my potential and providing me an interesting topic according to my capability. I am thankful for his positive suggestions, and meticulous guidance that helped me to improve my talent to write scientific research papers and carries out the new research. His patience and motivation enhanced me up to achieve in my goal. I feel really honored to have worked under his mentorship throughout my entire Ph.D. work.

I thank the doctoral committee members **Dr. T.P. Singh** (Chairman, Board of Studies), **Dr. Kulvir Singh**, **Dr. Vinod Kumar Singla** and **Dr. H. L. Bhowmick** for the feedback and reviews that were given on my research proposal and progress monitoring presentations. Their guidance was beneficial for me to improve my research work. I am also thankful to **Dr. Tarun Nanda**, our Ph.D. coordinator for his approachability and keeping me informed with all the relevant communication throughout E-mails.

I am thankful to Mr. Mukesh Kumar & Mr. Himmat Singh of LPS Bossard Pvt. Ltd, Rohtak, India and Mr. Aditya Kumar & Mr. L. K. Aneja of GSC Glass Pvt. Ltd, Noida, India for assisting me in arranging industrial visits and utilizing the materials for my research work. I am also encouraged by my colleagues and research team members Mr. Vishwas Grover, Mr. Kulwinder Singh Chani and Mr. Apoorv Jain.

From the core of my heart, I dedicated my thesis to my beloved parents **Mr. Brij Kishore Sharma** (Father) and **Late Sunaina Sharma** (Mother) and complete family members for their constant encouragement, love and blessing.

I thank to "**Almighty God and Guru**" for giving me the strength and patience for successfully completing my goal.

Ankit Sharma

ABSTRACT

In today's industrialization era, the innovation in the field of hard and brittle material such as float glass is still under investigation, because of its continuous demand as an operational application. It's fascinating features such as high thermal stability, strength, toughness, and high optical transmittance makes it a high-performance material. The major application of such materials is listed as optical lenses, automotive glass, thermal collector, solar concentrator, sensors, and solar panel etc. These materials are known as difficult to machine material, because of their brittleness. Analysis of a float glass during machining or drilling process is considered as a brainstorming research area. The drilled hole quality is characterized by the amount of chipping generated near hole edge corners on both sides of the hole as well as the surface roughness of the hole. Hence, the research endeavor of the present work is to pay attention and introduces their strategies to minimize the unwanted chipping near the entrance and exit periphery of the hole by deploying trending rotary ultrasonic machining technique. In the entire study, the hole entrance chipping is measured as average radial chip distance (RCD), hole exit chipping is quantified as the maximum chip radial distance (CRD) and the maximum chip thickness (t_c) in horizontal and vertical direction, respectively.

In the first case study, multi-shaped tools are used to create blind holes by rotary ultrasonic machining and conventional drilling. The intention is to select the best tool among all to get the negligible RCD along with least tool wear. It is noticed that according to the tool shapes, each tool has paying should be own path of drilling and effective contact area which influences the chip formation and the quality of the hole. The multi tool study for blind holes shows that rotary ultrasonic drilling process attained smallest measurement of radial chip distance as compare to CD for all types of tools. The concave circular tool is found as the best tool particularly to get the least radial chip distance (entrance chipping) during drilling i.e. 0.1145 mm.

In the second study, L 18 optimization technique is deployed to visualize the influence of various process parameters i.e. spindle rotation speed, feed rate and vibration amplitude during drilling of float glass specimen by rotary ultrasonic machining technique. After optimizing the process parameters, the least radial chip distance (RCD) is 0.425 mm at hole entrance, chip radial distance (CRD) is 0.70 mm at hole exit, chip thickness (t_c) is 0.55 mm at hole exit and hole internal surface roughness is 1.09 μm.

In the third case study, the comparison between the edge chipping (RCD) size; before and after

tempering process has been investigated at optimized parametric condition during conventional drilling and rotary ultrasonic drilling. It is investigated that after tempering process, the chipping (RCD) size near machined corners of the float glass specimen has been propagate. It is revealed that during the float glass tempering process, the combined effect of elevated temperature and high pressure creates some breakage (such as chipping) due to change in physical characteristics of the float glass material. Hence, the chipping amount should be as little as possible on pre-tempered float glass. It is noticed that RCD size is smaller in case of rotary ultrasonic drilling process as compared to conventional drilling process i.e. 36.92 %.

The mechanism behind the formation of chipping during float glass drilling by rotary ultrasonic machining and conventional drilling is also reported. It is revealed that during conventional drilling, abrasives loaded over the tool periphery are in continuous contact with the surface of the specimen to be drilled. It is one of the major reasons of chipping on the workpiece. During rotary ultrasonic drilling, the abrasive impregnated over the tool end face is travelled in definite sinusoidal paths along the axis of the workpiece with some specific tool revolution.

In the present study, a FE analysis is developed to investigate the effect of stress generation on hole exit during rotary ultrasonic glass drilling and conventional drilling of float glass.

The results showed that the present strategies would be appropriate and capable to overcome the challenges like severe chipping, poor surface finish, excessive tool wear and inappropriate machining parameter selection during float glass drilling. Therefore, rotary ultrasonic machining technique is suggested to get the better hole quality and tend to reduce heavy monetary loss expenditure in the form of machining cost and rejection cost.

LIST OF FIGURES

LIST OF TABLES

LIST OF ABBREVIATIONS

PVB	Poly-vinyl butyral
CD	Conventional diamond drilling
WJM	Water Jet Machining
AWJM	Abrasive water jet machining
LBM	Laser beam machining
EBM	Electron Beam machining
VAM	Vibration Assisted machining
USM	Ultrasonic machining
RUM	Rotary ultrasonic machining
RCD	Radial chip distance
CRD	Chip radial distance
t_c	Chip thickness
ANOVA	Analysis of variance
O.D	Outer Diameter (mm)
I.D	Inner Diameter (mm)
CBN	Cubic boron nitride
MRR	Material removal rate
FEM	Finite element method
CMC	Ceramic matrix composites
CCD	Central composite design
LAM	Laser assisted milling
CFRP	Carbon fiber reinforced plastic
RUD	Rotary ultrasonic drilling
SEM	Scanning electron microscope
CMM	Coordinate measuring machine
MCU	Machine controller unit
PC	Personal computer
FEA	Finite Element Analysis
CIP	Chip initiation point
CCP	Chipping conclusion point
W/P	Workpiece
S/N ratio	Signal noise ratio

LIST OF NOMENCLATURES

SiC	Silicon carbide
Al_2O_3	Alumina
Al_2O_3-SiO_2	Mullite fibers
SiO_2	Silicon oxide
MgO	Magnesium oxide
Na_2O	Sodium oxide
CaO	Calcium oxide
ZrO_2	Zirconia
$Li_2.Al_2O_3.SiO_2$	Lithium alumino silicate
BK 7 glass	Barium borosilicate glass
K9 glass	Chinese borosilicate crown crystal
KDP glass	Potassium di-hydrogen phosphate
Na_2CO_3	Soda ash
Na_2SO_4	Salt cake
$Ca.Mg(CO_3)_2$	Dolomite
Ra	Surface roughness
R^2	Coefficients of determination
S	Spindle speed (rpm)
f	Feed rate (mm/min)
F	Vibration frequency (KHz)
A	Vibration amplitude (μm)
Au	Gold
C	Carbon
Cr	Chromium
V_c	Volume of chipping (mm^3)
V_t	Volume of truncated portion (mm^3)
V_{cyl}	Volume of cylinder portion (mm^3)
r_c	Entrance radius of chip rod or Internal tool radius(mm)
R_c	Exit radius of chip rod (mm)
F_c	Critical cutting force (N)
σ_{von}	Von Mises stress (MPa)
σ_{ut}	Ultimate tensile strength of the workpiece (MPa)

CHAPTER 1: INTRODUCTION

1.1 Overview of Hard and Brittle Materials

The innovation in the field of hard and brittle materials such as ceramic, glass and ceramic composites, etc. are still under investigation, because of its distinctive features. These brittle materials have found wide applications because of their exceptional wear resistance, chemical, and thermal characteristics. The major application of such materials is listed as optical lenses, automotive glass, medical implants, sensors, pacemakers, and solar panels, etc. These materials are known as difficult to machine material, because of its high hardness and brittleness. Therefore, materials like ceramic and glass are still facing machining and fabrication related issues, where, researchers are focusing on such critical and vogue area, which is directly associated with the practical application of the hard and brittle materials. Instantly, researchers are working on the critical area, exemplify as profile accuracy, high precision machining, high tolerance, surface quality, chipping and cracking, etc. Recently, the machining quality of glass is characterized by the amount of chipping and cracking generated during the machining or drilling process. Hence, it is entail to resolve difficult to machine materials up to zenith level to boost its operational application. The types of brittle materials whose parent material is ceramic are illustrated in the following flow chart (Fig. 1.1).

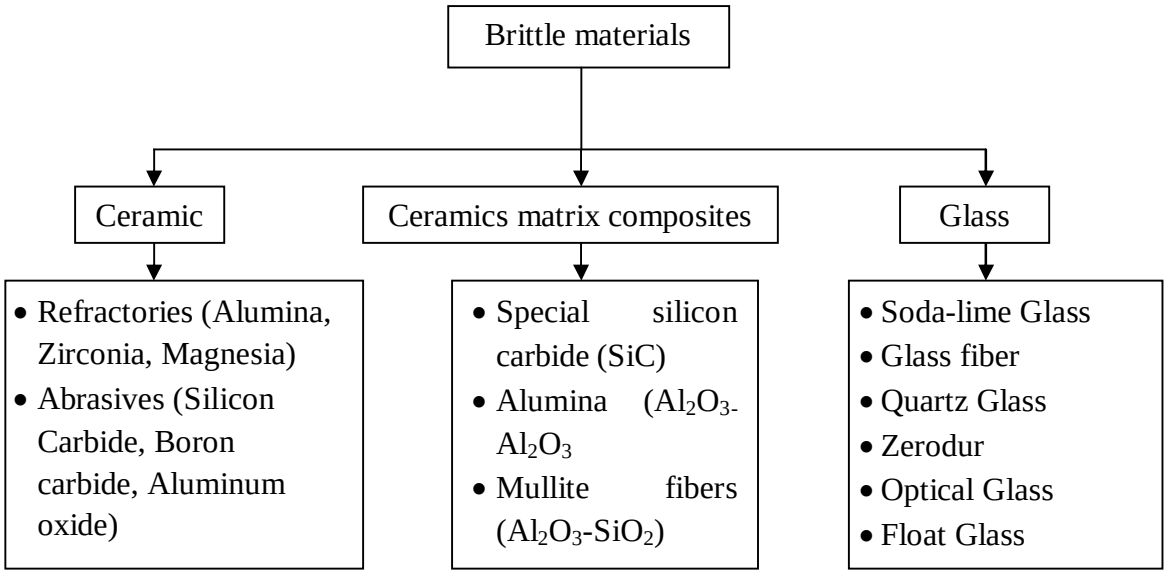

Fig. 1.1: Flow chart illustrates the types of brittle materials (ceramic based)

1.1.1 Ceramics

Industries based on automobiles, electronics, aerospace, and semiconductor are focusing on ceramics and its related application. Ceramic has some advanced mechanical properties i.e. high wear resistance, better hardness, high temperature constancy, and high strength. Although, these properties make the ceramic material a difficult-to-machine and therefore an innovative cost-effective method is needed (Liu et al. (2014)).

Alumina ceramic (Al_2O_3) is known as a challenging material to machine and utilize (Ahmed et al. (2012)). The chemical composition of alumina ceramic contains more than 90% of Al_2O_3 with some fraction of silicon oxide (SiO_2), magnesium oxide (MgO), sodium oxide (Na_2O) and calcium oxide (CaO) compound. It has some exceptional mechanical, thermal, and electrical properties. Alumina has characteristics as elastic modulus (375 GPa), poison ratio (0.25), density (3. 85 g/cm^3), tensile strength (275 MPa), compressive strength (2600 MPa) and vicker hardness (1440 Kg/mm^2). Generally, alumina ceramic is used in seal rings, electronic substrates, wear pads, grinding media, thread, and wire guides (Singh and Singhal (2017)).

Zirconia (ZrO_2) ceramic has admirable strength at room temperature, chemical, corrosion, and wear resistance property, which makes it a better option as a technical ceramic. It has possessed high density, superior fracture toughness, and high hardness with good frictional behavior (Nath et al. (2012)). The property of the zirconia (ZrO2) is explained as density (5.5 g/cm^3), Poisson ratio (0.31), Knoop hardness (1100 Kg/mm2) and elastic modulus (200 MPa). Zirconia has a wide application as insulating rings, dental frameworks, valves, and metrological components (Manicone et al. (2007)).

Silicon carbide material possessed high mechanical strength up to 1,400^{0}c. It has higher chemical and corrosion resistance characteristics than other ceramics. Applications of silicon carbide material are bushing, nozzle and sealing rings, etc (Yamada and Mohri (1991)). The major properties which defined its utility are density (3.1 g/cm^3), Poisson ratio (0.14), elastic modulus (410 MPa) and Knoop hardness value is 2800 Kg/mm^2 (Nath et al. (2012)).

1.1.2 Ceramic composites

Ceramic composites are an attractive choice for many industries based applications owing to their advanced properties such as high strength at elevated temperature as well as high wear resistance characteristics. However, extensive utilization of advanced ceramics is limited because

of the high machining cost. Therefore, it is an essential requirement of a cost-effective machining technique that could machine advanced ceramic materials. Mullite fibers (Al_2O_3-SiO_2) material is having some influencing features such as lower tensile strength and low thermal diffusivity (Rebro et al. (2004)). It has also acquiring fine chemical stability that fascinates to use it in some electronic and optical device applications. Mullite has density of $2.948*10^{-9}$ g/cm^3, micro-hardness (10 GPa), and flexural strength (500 MPa) (C. Paulmann (1996)).

The basic enhancement for ceramic matrix composites CMC as compare to conventional ceramics are anisotropic properties, incline in fracture toughness, fine thermal load resistivity, rupture elongation (nearly 1 %), and more life span as compared to metals. Ceramic matrix composites are generally used at high temperature application such as gas turbines; turbine blades, as combustion chambers and stator vanes (Bansal and Lamon (2014)).

1.1.3 Glass

The glass is a combination of several metallic silicates, where alkali metal is one of the major content in it. It is transparent, translucent, and amorphous in nature. Generally, glass is considered as solidified supercooled solutions consist of several metallic silicates, which possessed an infinite amount of viscosity. Moreover, it is known as a non-crystalline amorphous solid material that has numerous applications in technological and decorative e.g. electronics, optics, window panes, and many more. Glass can reflect, refract and transmit light. Hence, these properties motivate to use it as prisms, optical fibers, and lens for high speed data transmission by light by applying cutting, machining as well as polishing techniques to manufacture such parts (Rangwala (2010)).

Soda lime glass is also known as soft glass and soda glass. It is mainly a fusion of calcium silicate and sodium silicate. Its main properties are easily fusible at comparatively low temperatures, possible to blow or weld, and economical (Darvishi et al. (2012); Jawalkar et al. (2014)). Their applications are window glass, plate glass, glass tubes, and laboratory apparatus (Rawlings et al. (2006)). Another kind of glass is quartz crystal, it possessed the characteristics exemplify as hard, less porous as well as more flexible. It contained silicon dioxide (SiO_2) and it is also found in a wide variety of types and colors. Its properties are density (2.2 g/cm^3), young's modulus (76.7 GPa), Vicker hardness (9.5 GPa), and fracture toughness of 0.71 MPa/m^2 (Wang et al. (2018)).

Sapphire is considered as the purest form of aluminum oxide. It has characteristics such as no grain boundaries or porosity and arrangement of mechanical, electrochemical, optical, thermal durability. Its major properties are young's modulus (478 GPa), Vicker hardness (27.6 GPa), and fracture toughness (2 MPa/m^2) (Wang et al. (2016a)). These properties pointed sapphire as favorite materials with high performance system. Its major application is in several semi-conductor applications.

Zerodur is known as lithium alumino silicate ($Li_2.Al_2O_3.SiO_2$) glass ceramic material which was produced by Schott AG in 1968. It possessed some demanding properties such as low coefficient of thermal expansion, homogeneity in nature, and exceptional mechanical properties. It is widely used for the substrate of the EUV optics, astronautic mirror telescopes, and laser gyroscope reflectors (Yao et al. (2010)). Some other applications are precision optics, optical elements for comet probes, ring laser gyroscopes, mirror substrates of telescopes, and standards for precise measurements.

After some modification in the chemical composition of the glass, optical glasses are formed. These optical glasses are BK7 glass, K9 optical glass, KDP crystal, and pyrex, etc. There applications such as microscope in fighter aircraft, scientific instruments, and spectacles.

BK7 glass holds some superior features such as stable optical qualities, bubble-free characteristics as well as small quantity of inclusions. These properties stand BK7 glass separate from other glasses to use it in optical industries. The major properties related to BK7 glass are density (2.2 g/cm^3), young's modulus (63 GPa), Vicker's hardness (5 GPa), and fracture toughness of 0.6 MPa/m^2 (Jain and Pandey (2017)). Yet, because of large fabrication costs and deficiency to drill precise holes under dimensional tolerance, its application is still limited and the reason behind the least usability is hard and brittle nature of the material (Lv et al. (2016)).

K9 glass is a functional material for optics, electronics and fluidics applications. Some of the characteristics are described as young's modulus (85.9 GPa), Vickers hardness (7.2 GPa), and fracture toughness of 0.8 MPa/m^2. It has better qualities for instance high hardness, strength, thermal and corrosion resistance as well as wears resistance (Zhang et al. (2012)).

Crystal glass is known as potassium di-hydrogen phosphate (KDP) crystal. Due to its superior characteristics, various parts are made up of KDP crystal. Its key characteristic is stated as density (2.33 g/cm^3), young's modulus (63 GPa), Vickers hardness (2.5 GPa), and fracture

toughness of 0.1 MPa/m^2. These are optical harmonic generation lens and electro-optic switches etc. KDP crystal possessed comparatively inferior fracture toughness and hardness. Therefore, it is considered difficult to machine material (Lv et al. (2016)).

1.1.4 Float Glass

Float glass is known as a non-crystalline amorphous solid. It is fabricated by melting sand (SiO_2) and other elements such as soda ash (Na_2CO_3), salt cake (Na_2SO_4), dolomite ($Ca.Mg.(CO_3)_2$) and limestone ($CaCO_3$). Also, the broken cullet glass pieces are added to decline the melting temperature of silica compound and to stimulate the glass's optical clarity. The mixed cluster of above mentioned materials is heated between 1450 ^{o}c to 1650 ^{o}c of temperature, respectively. This method of fabrication of float glass is known as the Pilkington process. It is generally named as plain glass or plain float glass (Fig. 1.3 (a)). Glass will transmit, reflect and refract light; these qualities can be boosted by cutting, machining and polishing to make components such as optical lenses, optical fibers and prisms for high speed data transmission by light. High toughness, scratch resistance, superior safety, aesthetic appearance, high optical clarity, no refraction defect, high light transmission, and higher efficiency leads as a major solar application are an eye-catching property of float glass. Float glass could be further subdivided into two parts i.e. Basic float glass and processed float glass. Complete detail of float glass is mentioned in the below flow diagram (Fig. 1.2).

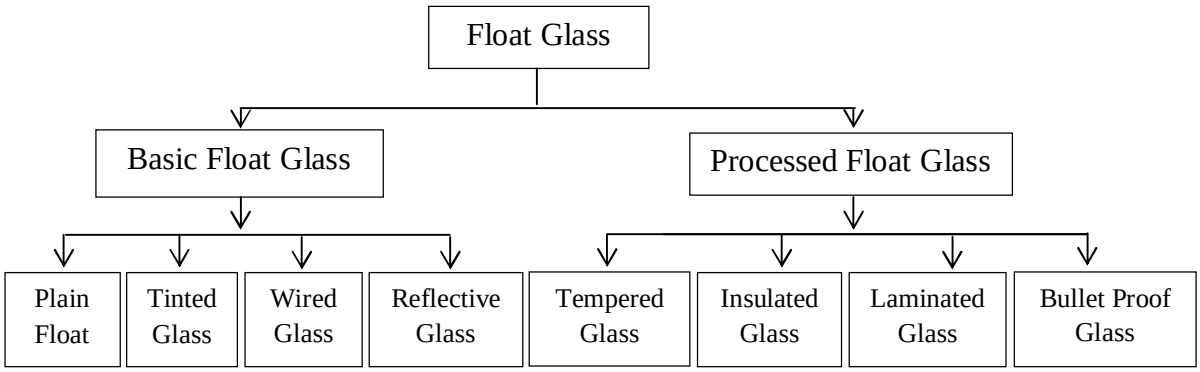

Fig. 1.2: Flow diagram illustrates the detail of float glass

Tinted glass is known as normal flat glass. Tinted glass is formed by the addition of very fine quantity (less than 1 %) of metal oxides as shown in Fig. 1.3 (b). In this type, various colors are mixed during the manufacturing process to attain the solar radiation absorption and tint

properties. These minor amounts of contents don't change the basic physical properties of the float glass excluding solar, optical transmission, and reflection [20]. Added, wired glass is a type of glass in which wire mesh has been included at the time of its production as shown in Fig. 1.3 (c). Another type of float glass is known as reflective glass (Fig. 1.3 (d)). It has been treated with a metallic coating, which aids to reflect heat. It is widely used in environmental friendly structure, whose main purpose is to reduce heat gain and loss. Also, making a building much cheaper to heat and cool.

Basic glass is further processed to make it more high performance finished product which could withstand at high wind pressure and to add more aesthetic features like better safety, ultraviolet filtration, solar screening, better sound absorption capacity, fire resistivity, pleasant interiors and exteriors to look good (Singh (2013)). Toughened (or tempered) glass is a type of processed glass as represented in Fig. 1.3 (e). It is an exceptionally strong glass, because of thermal heat treated process occurs. During heat treatment process, various sizes of glass panes are electrically heated in the furnace up to 650°c. After heating, the glass pane is carried to a chamber i.e. quenching chamber where it is cooled speedily by an explosion of air. It is approximately 4 to 5 times stronger than the annealed glass. Tempered glass is widely used as architectural glass and windscreen glass, because of the property like safety and strength. Major properties of tempered glass are great strength, high thermal resistance, injury-proof (difficult to break), and withstand during sudden impact (impossible to cut or drill). Therefore, all such prior works such as cutting, drilling, and machining, etc. are done before the tempering process. Hence, drilling is always performed before further processed.

Another type of processed glass is laminated glass, is consisting of two or more panels of glass with one or more layers of polyvinyl butyral (PVB) sandwiched between them and then finally used as shown in Fig. 1.3 (f). This sandwich has some exceptional benefits such as if the glass is broken or cracked, fragments remain strongly stick to the polyvinyl butyral (PVB) interlayer. Hence, it will reduce the peril of injury. Also, it will help to resist additional damage due to weather and impact. For getting more impact bearing applications, laminated glass is widely used. Table 1.1 describes the float glass properties.

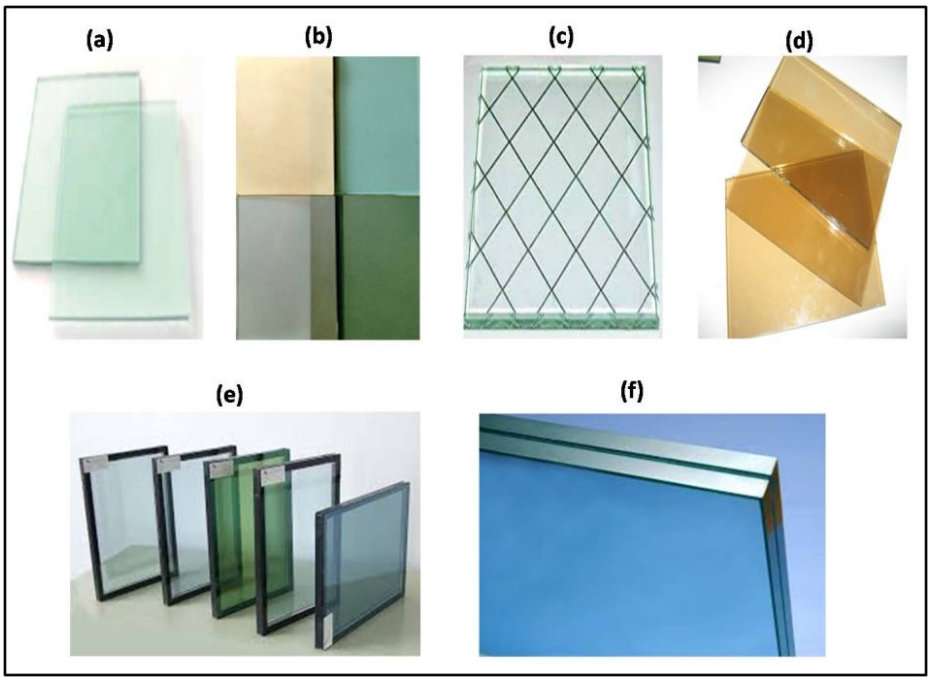

Fig. 1.3: Types of Float glass: (a) Plain Float glass (b) Tinted glass (c) Wired glass (d) Reflective glass (e) Tempered glass (f) Laminated glass

Table 1.1: Float glass properties (Wang et al. (2018); www.makeitfrom.com; Wang et al. (2017); Wang et al. (2016); Khan and Haque (2007)).

S. no.	Characteristics	Value
1.	Density (ρ)	2300 - 2500 Kg/m^3
2.	Thermal conductivity (k)	1.05 W/m°C
3.	Poisson ratio	0.20-0.23
4.	Modulus of elasticity (E)	38 GPa approx.
5.	Elastic modulus (Tensile)	70 GPa
6.	Compressive strength (St)	212 MPa approx.
7.	Tensile strength (UTS)	50 MPa approx
8.	Impact Strength	800 MPa
9.	Vickers hardness	4.59 MPa
10.	Specific Heat (C)	0.8 J/g/K
11.	Transformation range	520 - 550°C
12.	Glass transition temperature (T_g)	564 °C

Where, the basic laminated glass is as a glass-PVB-glass sandwich which is safe for small intrusions. To bear the larger impact, finally, it is used as a multiple layered sandwich of 'GLASS + PVB + GLASS + PVB + GLASS'. This sandwich will additionally escalate the toughness and it is known as bullet proof glass.

Float glasses are generally used as residential and commercial building glass, solar panels, automobile glass, optical lenses, prisms, etc. It has tremendous decorative, practical, and technological applications i.e. window panes, medical implants, sensors, pumps, and pacemakers, etc. Fig. 1.4 illustrates the final products of float glass: a) Glass plate used in Bajaj gas stove; b) Glass plate used in solar panel.

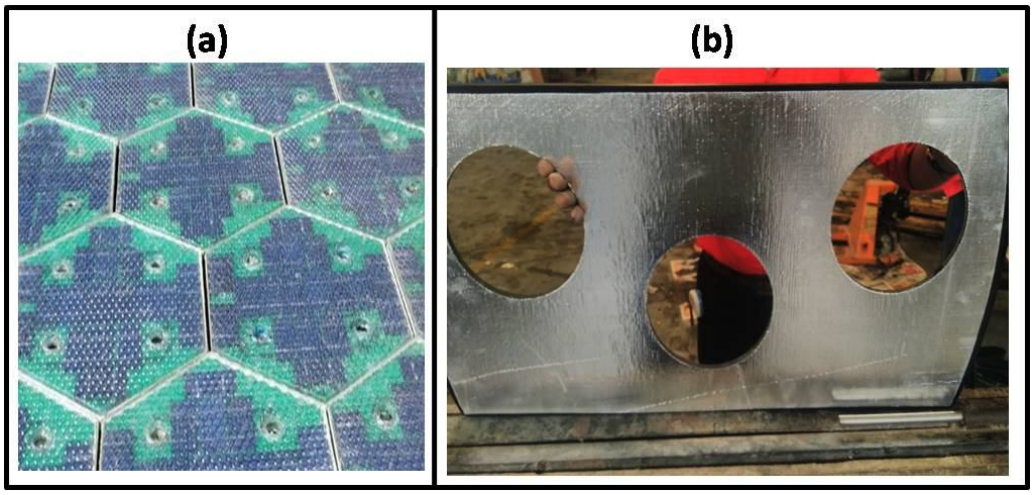

Fig. 1.4: Final products of float glass: a) Glass plate used in bajaj gas stove; b) Glass plate used in solar panel *(Courtesy: GSC GLASS Pvt. Ltd, Noida)*

Even though, researchers are still facing some machining and fabrication related issues, which are directly associated with its practical application. It was discussed in some research studies that traditional machining techniques such as conventional milling machine, water jet machine, etc. are not providing efficient outcomes, because of their high hardness and brittleness (Moriwaki et al. (1992)). Some of the trending glass drilling or machining techniques that are employed in the industries and research institutes explained in the next section.

1.2 Overview of Glass Machining Processes

In today's era, owing to hard and brittle materials exemplify as ceramics, glass, quartz, silicon carbide, and ceramic composites are challenging to machine by the traditional machining

techniques. Instantly, researchers are working on parameters such as machining accuracy, high precision machining productivity, and better surface quality. Therefore, machining of such materials mainly focused on emerging new techniques for instance: conventional diamond machining (CD), water jet machining (WJM), abrasive water jet machining (AWJM), laser beam machining (LBM), electron beam machining (EBM) (Imran et al. (2015), vibration-assisted machining (VAM), ultrasonic machining and rotary ultrasonic machining (RUM), etc. The following machining processes have been used for most of the hard and brittle materials. But, here in this report, the processes are explained in context with the machining of glass only.

1.2.1 Conventional Diamond Drilling

Conventional diamond tool based glass machining is generally used in creating holes and profile shape of glass material. It is also adopted in various applications related to glass machining. But still, because of its operational limitation, which is occurring nearby hole region or corner surface of the glass, it declines its usability where precise work is required frequently during mass production (Fanara et al. (2017)). Fig. 1.5 shows the conventional diamond drilling machine.

Fig. 1.5: Conventional diamond drilling machine (Navanth and Sharma (2013))

Conventional drilling is a traditional machining technique used in creating components in industrials. But still, engineers are facing various unwanted defects i.e. as fatigue fracture, low hole accuracy, micro-cracks, and chipping (Xing et al. (2017)).

1.2.2 Water Jet Machining

Challenging to machine materials such as glass and ceramics are commonly fabricated by water jet machining (WJM). WJM is a versatile and non-traditional process that is performed in several industrial operations, particularly in the industrial machining and impulse fragmenting. But still high consumable (slurry) cost, time consuming for large diameter of workpiece and high energy consumption are the critical issues during water jet machining. Therefore, engineers are moving ahead of the alternate machining options (Khan and Haque (2007)).

1.2.3 Abrasive Water Jet Machining

Abrasive water jet machining (AWJM) technique (Fig. 1.6) is known as a non-traditional process that is used for cutting difficult-to-machine materials such as float glass. It is an updated version of WJM technique. This process is particularly appropriate for brittle materials. The various abrasives which are used during the process are named as silicon carbide (SiC), glass bead, silica-sand, and garnet (Khan and Haque (2007)).

Fig. 1.6: Abrasive Water Jet Machining (AWJM) process (Khan and Haque (2007)).

During machining, there is least heat generation and the residual stresses have been noticed nearby machined surface (Eneyew and Ramulu (2016)). But still, AWJM process has high consumable (slurry) cost, time consuming for large diameter of the workpiece, and high energy consumption which motivates researchers to go for alternate machining techniques.

1.2.4 Laser Beam machining

The laser is a coherent and amplified beam of electromagnetic radiation (Darvishi et al. (2012). The mechanism behind the LBM is a combination of melting, vaporization, and chemical

degradation (Salama et al. (2016a); (Salama et al. (2016b); Singh et al. (2011)). Fig. 1.7 illustrates the laser beam machining process. It is widely used in the aircraft, electronics, and medical industries for machining of complex parts of the material such as ceramics, glass, and titanium (Dubey and Yadava (2008)). It helps to create micro-channels as well as to form complex shapes.

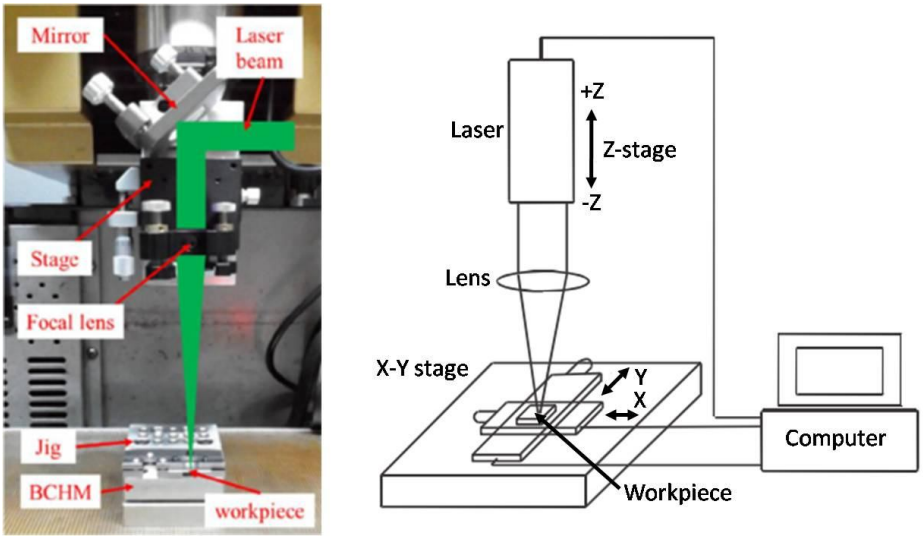

Fig. 1.7: Laser beam machining (Chang et al. (2017); Nikumb et al. (2005))

The major constraints that happened during machining are challenging to control the two or more laser beams at diverse angles during 3-D machining, difficult to form high thickness parts, and complex to machine transparent or shiny materials (Tsai and Chen (2003)).

1.2.5 Electro-Chemical Discharge Machining (ECDM)

Electro-chemical discharge machining (ECDM) is known as a non-conventional machining technique which is used for drilling and machining electrically non-conducting workpiece such as glass, quartz, and ceramic. The machining mechanism is based on the melting, vaporization and thermal erosion, owing to the heat discharge during the process. But, it is difficult to create intricate and complex shapes of glass workpiece (Goud and Sharma (2017); Goud et al. (2016)).

1.2.6 Vibration Assisted Machining

Vibration assisted machining is a process that provides a micro-level high frequency vibration to the motion of a tool tip to make the tool and workpiece interaction a discontinuous process. It

would affect the tool to vibrate along with the cutting or thrust direction at a high frequency of 15 kHz approx with an amplitude of 1 to 15 micron (Xu and Zhang (2015)). Vibration assisted machining (VAM) is specifically helpful in machining difficult-to-cut materials. A wide number of applications make the vibration-assisted machining more effective than the conventional machining process. Fig. 1.8 demonstrates the vibration-assisted machining (VAM) process (Kumar et al. (2014).

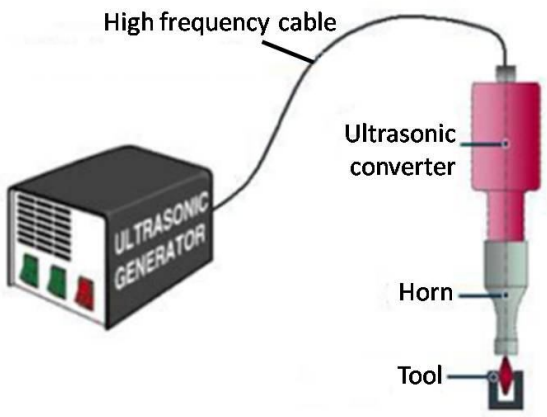

Fig. 1.8: Vibration assisted machining (VAM) (Kumar et al. (2014)

This technique is used to improve the machinability of float glass. Nowadays, researchers are more focused on the various vibration-based machining technique exemplify as vibration-assisted machining, stationary ultrasonic machining, and rotary ultrasonic machining (Xu et al. (2014). In the case of vibration-assisted machining process, the tool and workpiece carried out the discontinuous interaction between them. It could enhance the machining quality up to a certain level. Still, the chances of crack propagation, when parameters are not optimized are brain storming problem (Kumar et al. (2014).

1.2.7 Ultrasonic Machining

Ultrasonic machining is satisfying the market demand for machining glass-like materials. It is also known as stationary (or conventional) ultrasonic machining (Zhang et al. (1998)). There are three renowned material removal mechanisms are explained in several researcher studies such as the hammering action by the larger grits particles when the tool, abrasive and workpiece are in contact, the impact action by the smaller size moving grit particles in the working gap and the cavitations-erosion action in which the bubble collapses in the working gap by absorbing

ultrasonic vibration energy (Guzzo and Shinohara (2004; Ya et al. (2002)). Ultrasonic machining is used to machine the non-thermal and non-chemical material specimens. There is no significant change in the chemical and physical properties of the workpiece and proposed a stress free machined surface (Xu and Zhang (2015)). Fig. 1.9 shows the ultrasonic machining process. However, during float glass ultrasonic drilling some limitations are needed to be sought out.

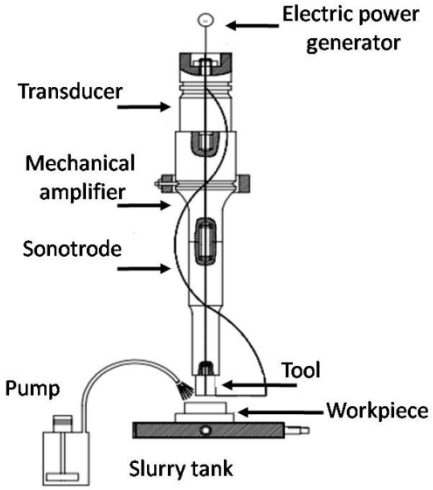

Fig. 1.9: Ultrasonic machining (Guzzo and Shinohara (2004))

These are the poor abrasive slurry flow in drilling deep holes, low form accuracy in drilling small holes, and considerable tool wear prohibit the wider application of float glass. Another two major concerns during USM are the chipping at the corners and edges of the hole entrance and the exit. To overcome these shortcomings during float glass machining, rotary ultrasonic machining was invented in 1964 (Wang et al. (2016b)).

1.2.8 Rotary Ultrasonic Machining

Rotary ultrasonic machining (RUM) is considered as a cost-effective machining process which is presented for creating holes in glass and advanced ceramics (Jain and Pandey (2017)). It is known as a hybrid machining technique which merges the material removal mechanism of ultrasonic machining and diamond grinding; consequently, it fascinates the better material removal rate than ultrasonic machining or by diamond grinding (Phadnis et al. (2012); Phadnis et al. (2013); Roy Roy et al. (2012)). In this process, a metal bonded drill tool with diamond abrasives electroplated over it has been moved in a rotational motion along with ultrasonic vibration are simultaneously fed in the direction of the workpiece specimen at a constant feed

rate. During machining, the high-frequency electrical energy is converted into the mechanical vibrations through a piezoelectric or magnetostrictive transducer which is then transmitted through horn assembly. Where, horn assembly is known as an energy focusing device. It would affect the tool to vibrate along with the cutting or thrust direction at a high frequency of 15 kHz (approx) and amplitude of 1 to 15 micron (Li et al. (2005)). Finally, material has been removed from the machined to be surface. Rotary ultrasonic machining (RUM) could achieve deep holes drilling, better hole accuracy, greater surface finish, minimum cutting force, and lesser tool pressure (Jiao et al. (2005); Zeng et al. (2005); Kuruc et al. (2015)). Usually, coolant is circulated from the core of the drill tool to wash away the unwanted scrap particles and keep both drill and workpiece cool. Fig. 1.10 (a) shows the rotary ultrasonic machining process and Fig. 1.10 (b) illustrates the 3-D view of the rotary ultrasonic machining (RUM) tool.

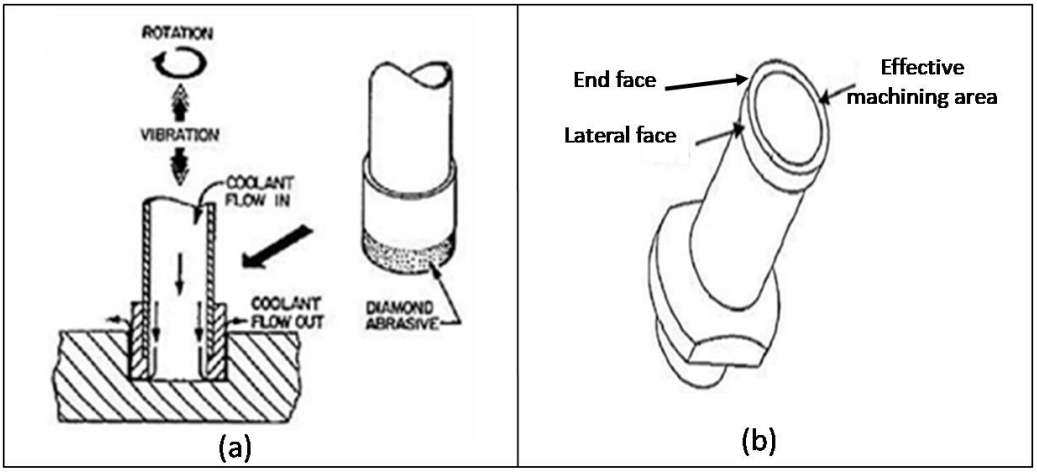

Fig. 1.10: (a) Rotary Ultrasonic Machining (RUM) process (Li et al. (2005)), (b) 3-D view of RUM tool (Jain and Pandey (2016))

1.3 Application of Rotary Ultrasonic Machining

A list of applications based upon their respective material properties during RUM is mentioned in Table 1.2.

Table 1.2: Applications of Rotary ultrasonic machining ((Wang et al. (2016b); Kuruc et al. (2015); (Li et al. (2005); Singh and Singhal (2015))

Materials	Properties	Application
Dental ceramics, Bone, CMC	High strength, low tensile strength, superior wear resistance	Molar crowns, veneers, knee joints, aesthetics restorations
Optical K9 glass	High Hardness, Strength, low fracture toughness, corrosion resistance	Optics, thermodynamics, electronics, fluidics
Glass BK7, Quartz, Float glass	High hardness and brittleness	Optical glass, automobile glass, reflective solar glass etc.
Sapphire, Silicon carbide	Great hardness, good thermal stability, chemical inertness, good light transmission	IC chips, thin film substrates, various electronics, and mechanical components

1.4 Key Terminology

Some of the major terminologies used in the present research study are explained in this section.

1.4.1 Hole Quality

Hole quality is an expression which explained that the purpose of the hole is achieved or not. The purpose or function of the product is described by its application. For instance, in the case of solar panel glass, the product should be defect free and reliable. The product which has no or negligible defects occurred during fabrication or machining processes, is stated as good quality. During machining (drilling, slot cutting, milling, grinding) processes, various types of defects could occur (Singh et al. (2008); Bhatnagar et al. (2004); Singh and Bhatnagar (2006); Davim (2010); Davim et al. (2004); Balogun and Mativenga (2017)). These defects or challenges are exemplified as chipping (edge and surface chipping), cracking, and surface roughness. However, chipping is the key obstacle during drilling high-quality holes (Zhang et al. (1998); Jiao et al. (2005); (Li et al. (2005); Singh and Singhal (2015); Abrao et al. (2007)). During drilling of brittle material like float glass, surface damage caused by the propagation of chipping over the

workpiece periphery is a vital notion to work by researchers. These damages have significantly affected the float glass usability (Arif et al. (2012)).

1.4.2 Chipping

A defect in which a small section of a workpiece is broken on the top or side corners is called chipping. The chipping generally occurs during the machining or drilling process. Some causes of chipping could be high temperature machining or improper coolant. The general remedies to avoid chipping could be controlled by selecting the best machining parameters. Normally, it can be sub-divided into two types: (a) Hole entrance chipping and (b) Hole exit chipping.

1.4.2.1 Hole Entrance chipping

The chipping occurred at the entrance corner of the hole is stated as entrance chipping. As shown in Fig. 1.11, hole entrance view shows the chipping occurrence near hole corners. It is noticed that the break out part is evaluated in form of radial chip distance (RCD).

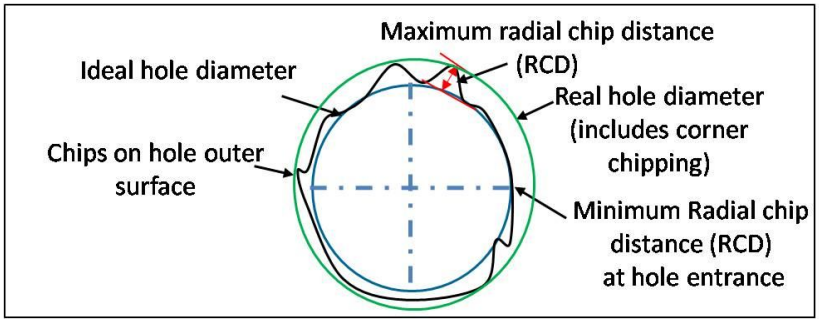

Fig. 1.11: Schematic hole entrance view

The radial chip distance (RCD) is defined as the difference between the maximum (actual) hole diameter (up to which chipping is reached) to the required (ideal) hole diameter.

1.4.2.2 Hole Exit chipping

In most of the cases, chipping at the hole exit corners (Fig. 1.12 (a)) are in huge amount. In actual practice, it is a challenging task for the engineers to measure the chipping in the exact amount. Therefore, the left out a portion of the hole i.e. machined rod (Fig.1.12 (b)) is used to validate the exit chipping on the hole. The reasons for using the machined rod as a means of exit hole chipping are 1. The edge chipping at the hole exit is expected to precisely follow the available chipping on the machined rod; 2. More suitable to quantify the chip radial distance and chip thickness by the machined rod. The depth of chipping in a hole is difficult to quantify whereas, it is easy to measure the height/thickness of chipping in a machined rod. Owing to these

reasons, the machined rod is used to quantify the amount of chipping in the form of chip thickness and chip distance radial at the exit side. Here, some terminologies are used which help to quantify the chipping amount. Fig. 1.13 depicts the microscopic image of the machined rod and its related measurement.

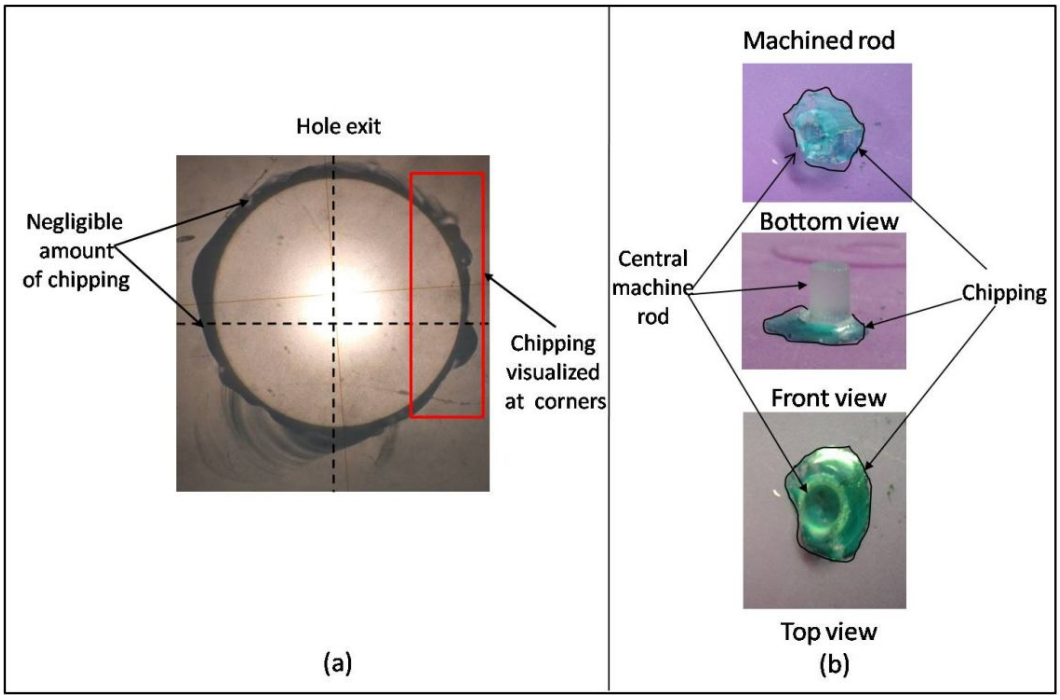

Fig. 1.12: Hole back side view (a) Hole Exit chipping (b) Different views of Machined rod

Chip radial distance (CRD) is defined as the difference between the (maximum) exit radius of chip rod (R_c) and the entrance radius of chip rod (r_c). Chip thickness (t_c) is stated as the depth of chipping at hole exit portion. The detailed explanation is discussed in Chapter 3.

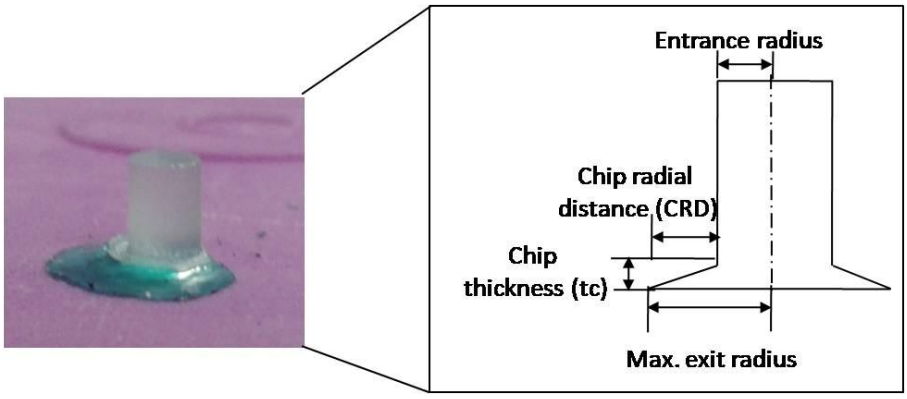

Fig. 1.13: Illustration of the microscopic image of the machined rod and its related measurement

1.5 Benefits of Float Glass's Hole Quality Enhancement

Nowadays, Ceramic and glass industries are facing plethora of hole quality problems. The float glass's hole quality enhancement could improve the impact bearing capacity and leads to the reduction in chances of fatigue failure which would provide a better hole tolerance limit. Once the drilled hole quality is improved, it would reduce the effect of wear and tear loss and directly decline the monetary losses bear by the industries during glass fabrication. Subsequently, the float glass's applications would have been increased along with its service life span.

1.6 Organization of the Thesis Chapters

The thesis is organized into the following chapters including the references.

Chapter 1: Introduces the different types of glass and ceramic types, its properties, demand, and applications. Various glass machining processes (especially: rotary ultrasonic machining) are explained including mechanism, advantage, limitation, and application.

Chapter 2: The available literature is grouped in two categories. One category is material specific i.e. machining (drilling, grinding) of glass composites by various methods and the second category is machine specific i.e. rotary ultrasonic machining. Also, some glass industry visits have been carried out to check the feasibility of the present research work. The chapter ends with the main objectives of the present research work and organization of the thesis chapters.

Chapter 3: Reports the development of rotary ultrasonic machining setup. The workpiece detail (measurements, properties) and tools detail (specifications, properties, and dimensions) have been elaborated. Further, experimentation procedure and parametric conditions are explained in three categories such as multi-shaped tool based experimentation (for the blind hole), process optimization experimentation (for through hole), the effect of tempering on pre-tempered float glass experimentation. The chapter describes the detail of characterization techniques such as coordinate measuring machine, SEM, optical profilometer, surface roughness tester, and digital microscope which are used for measuring and computing the hole quality and tool wear.

Chapter 4: States the results related to the effect of multi-shaped tools on entrance chipping. The effect on the multi-shaped tool wear is also explained. The detailed study about the effect of various parameters such as spindle speed, feed rate, vibration amplitude, and tool diameter on the hole entrance and exit chipping are reported. This chapter also incorporated the effect of similar input parameters on average surface roughness at hole internal region. The comparison of chipping before and after tempering process during conventional drilling (CD) and rotary ultrasonic drilling (RUD) has also been carried out.

Chapter 5: Deals with the FE analysis of stress generation at hole exit during rotary ultrasonic drilling of float glass specimen. Paying attention to minimizing the unwanted chipping measurements such as chip radial distance and chip thickness which are generated during drilling of float glass.

Chapter 6: Reflects with the conclusions and important findings of the present research work and also the scope of the future work.

CHAPTER 2: Literature Review

To carry out the study on float glass drilling and its related machining conditions and results, the available literature is grouped in two categories. One category is material specific i.e. machining (drilling, grinding) of glass composites by various methods and the second category is machine specific i.e. rotary ultrasonic machining. Also, the categories further contain their experimental aspects and theoretical studies.

In the first category, traditional and non-traditional machining processes such as ultrasonic machining, vibration-assisted machining, laser beam machining, conventional machining, and water jet machining excluding rotary ultrasonic machining are discussed while considering glass material. In the next category, the extensive literature specifically relevant to the rotary ultrasonic machining of miscellaneous hard and brittle materials exemplify as float glass, ceramics, quartz, soda lime, borosilicate glass, and zerodur, is discussed.

These above sections contain the various machining based issues which are unhealed or still under the researcher's eye. These are hole exit quality, chipping in glass, micro-cracks, surface topography, damage portion analysis, and ductile mode of machining up to its zenith level, metal removal rate, cutting force, tool wear, and surface roughness. Also, some ceramic and glass industries visits have been carried out to check the feasibility of the proposed work. The detailed observations of the industrial visits are explained precisely. Subsequently, the research gaps and objectives of the work have been postulated.

2.1. Glass Machining

Investigations related to glass machining by several traditional and non-traditional machining processes are discussed below.

Park et al. (2002) worked on micro-drilling of glass plates, to investigate the cracks that occur at the hole exit portion. A back-up glass plate was aided to prevent the exit crack up to certain limit. A tungsten carbide based drill tool with diameters of 0.1, 0.2, and 0.4 mm was used for glass drilling. Fig. 2.1 shows the shapes of the drilled hole which include: (a) Hole entrance (b) Hole exit.

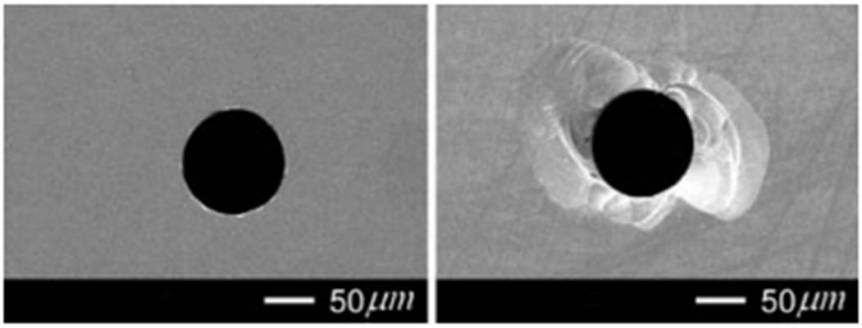

Fig. 2.1: Shapes of drilled hole (a) Hole entrance (b) Hole exit

Simulation results showed that tensile stress has possessed a significant role in crack propagation. It was found that the tensile stress near the drilled corner has been reduced while using back-up plates as compared to drilling without back up plates.

Gan et al. (2003) considered the fused silica material for carry out the ultra-precision diamond turning aided by ultrasonic vibration-based machining technique. The parameters and tool conditions mentioned as the feed rate (5μm/rev), spindle speed (90 rpm), vibration amplitude (3 μm), vibration frequency (40 kHz) with tool's clearance angle and rake angle as 11° and 0°, respectively. Consequently, the surface roughness (R_a) near the transition area was approximately 100 nm at a consistent feed rate of 5 mm/rev during the ductile mode of machining.

Azmir and Ahsan (2008) performed experimentation on workpiece made up of glass fiber reinforced epoxy composites to optimize the process working parameters that affect the machining. Also, the analysis of variance (ANOVA) and Taguchi methods was deployed. Here, the mathematical model was established in predicting the machining response of abrasive water jet machining. The analysis was approached with 95 % confidence level. Lastly, the value of coefficients of determination (R^2) was determined as 0.791 for the mathematical model. In nutshell, after this comparative study based upon experimental and mathematical model, it was noticed that the stand-off distance, hydraulic pressure, transverse rate, and abrasive types, had a significant effect on surface roughness.

Karim et al. (2011) performed an experimental study to minimize the edge chipping for soda lime glass specimen during milling operations using a cubic boron nitride (CBN) tool by optimizing the machining parameters i.e. depth of cut, feed rate, spindle speed, and coolant

pressure. It was found that at the lower depth of cut as well as feed rate values, the edge chipping width was reduced. As a result, it would reduce the cutting forces acting on the workpiece specimen. It was also noticed that as the spindle speed increased, the transition from brittle to ductile machining mode take place. Consequently, the higher cutting temperature linked with the higher spindle speed increased the workpiece ductility. Afterward, it reduced the cutting forces that created lesser chipping width. Lastly, it was mentioned that the spindle speed should be in the optimum range.

Baek et al. (2013) did an investigation on the glass coated with wax and as well as glass without wax coating while deploying on ultrasonic machining. In this work, blind holes were fabricated. Here, the specifications of the tool were as: diameter is 1.6 mm, thickness is 1 mm and feed rate was noted as 10 m/s. Fig. 2.2 represents a view of glass machined hole generated by traditional USM.

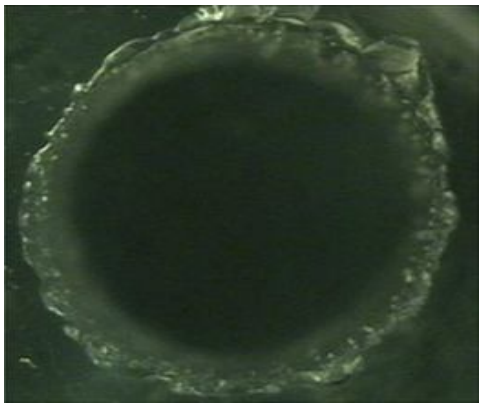

Fig. 2.2: Glass machined hole view generated by traditional USM (Baek et al. (2013))

Moreover, flat end shape tools were used and the wax coatings were applied with the thickness range of 0.0, 0.3, 0.6, and 1.0 mm, respectively. It was found that the wax coating shields the surface of the glass so that cracks are created in the wax in spite of the surface. In a nutshell, the surface quality of the glass holes is improved in ultrasonic machining.

Feucht et al. (2014) mentioned that the ultrasonic grinding/ machining of glass, ceramics, and similar materials were achieved by diamond impregnated tools through undefined cutting edges. Moreover, the mechanism behind machining was that material was removed by abrasion and the formation of micro fractures due to ultrasonic impacting at the surface of the workpiece. It was notified that the feed force was declined by 30 % while using vibration-assisted conventional

drilling. Ultrasonic machining technique could able to enhance surface roughness values and edge quality too. Subsequently, lesser temperatures at the tool, a perpetual machining quality, and reduced tool wear were achieved. Lastly, the ultrasonic machining technique fascinated the productivity nourishment and inclination in component quality compared to traditional techniques.

Pawar et al. (2015) did review study on machining of glass-like brittle materials to improve its machining characteristics. Also, Fig. 2.3 represents the pie chart related to the percentage of research focused on various types of results on glass material. It was reported that glass material is mostly machined or drilled by ultrasonic machining (USM), abrasive water jet machining (AWJM), laser machining (LM), and electro-chemical discharge machining (ECDM). On another side, rotary ultrasonic machining (RUM) is still under investigation for glass and ceramic machining. During machining of glass specimens, most of the output results were focused on material removal rate (MRR), surface roughness, and surface quality.

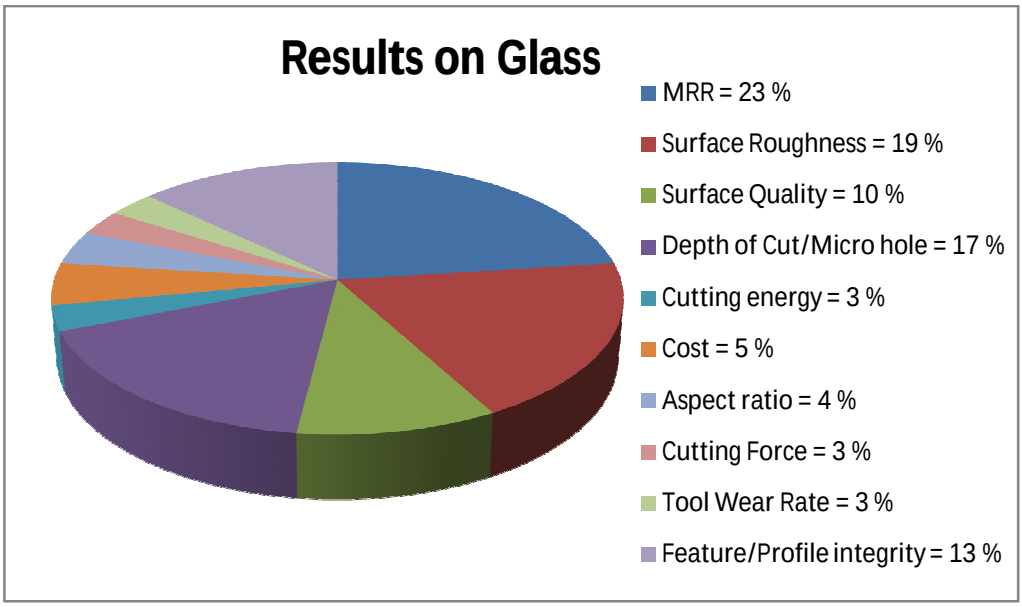

Fig. 2.3: Percentage of research focused on various types of results on glass related brittle materials (Pawar et al. (2015))

Ahmed (2016) did an investigation on the drilling portion of carbon fiber epoxy composite using an electrical discharge machining (EDM) process. The machining quality of the drilled hole was evaluated by considering the delamination extent, deviation in hole size, and hole taper. It was

found that after drilling process some deep cavities were observed on the specimen. These cavities were arising because of decomposition and evaporation of the epoxy specimen. It was mentioned that the cracks were formed owing to the pressure of the decomposition gasses. Also, thermal residual stresses were the reason behind the occurrence of fracture at the sharp edges of the hole.

Hasan et al. (2017) worked on the various shapes and features of tools such as single flute, compound drill tool, twist drill tool, multi-shaped tools, and coated drill tools have been used for micro-drilling purpose. It was mentioned that the micro-drilling of the product, boost the utility in medicine, automobiles, and electronics based the industries.

2.2 Rotary Ultrasonic Machining (RUM)

The literature regarding the rotary ultrasonic machining process of ceramic and glass-like materials i.e. float glass, ceramics, quartz, soda lime, borosilicate glass, zerodur etc. are discussed as below. It is sub-divided into two parts: experimental based and modeling related to stress generation based studies.

2.2.1 Experimental Studies

In the research study of **Prabhakar et al. (1993)**, experimental results have been represented and the machining rate obtained from RUM was nearly 6 to 10 times greater than that from a conventional grinding process under similar conditions. While comparing, RUM was found 10 times faster than USM. Especially, it was much easier to drill deep and small holes with RUM than with USM process. Additional benefits of improved hole accuracy and low tool pressure were also reported.

Wiercigroch et al. (1999) involved in the prediction of a mathematical model based on metal removal rate by rotary ultrasonic drilling on glass samples with high amplitudes forces produced by the impact. These forces were further acted on the workpiece samples and generated micro-cracks in the cutting zone. It was encapsulated that the ultrasonic machining based method created relatively mediocre material removal rate (MRR), poor accuracy, and significant tool wear while comparing with rotary ultrasonic machining.

Li et al. (2005) found that the experimental set up was consisting of an ultrasonic spindle system, a data acquisition system, and a coolant system. Added, it was observed that the metal removal rate (MRR) was 10% higher in RUM than diamond drilling for both CMC and alumina

workpieces. Moreover, in the case of RUM, the cutting force was reduced to 50 % as compared to diamond drilling. Results revealed that the high quality holes on CMC panels can be achieved by RUM with proper machining parameters exemplify as spindle speed, feed rate, and ultrasonic power. It was notified that the feed rate has the most significant effects on cutting force. In a nutshell, it was considered that all three machining process parameters i.e. spindle speed, feed rate, and ultrasonic power has crucial effects on hole quality.

Zeng et al. (2005) have investigated the cutting force and observed the topography of the end face and lateral face of a diamond tool in RUM for SiC workpiece. During the wear analysis of tool end face, the tool wear in RUM has two diverse stages. In the first stage, attritious wear dominates. In the second stage, bond fracture dominates. The tool fails to function any longer when the bond fracture becomes too severe. Here, it was detected that, in the first 6 drilling tests, as the number of drilling tests increased the maximum cutting force was also started inclining. Though, after the completion of six drilling tests, the maximum cutting force reduced. The reason was mentioned that it was happening because of the blunting of diamond grains. In a nutshell, it was concluded that the maximum cutting force in RUM of SiC was interrelated to the tool wear stage.

Yang et al. (2009) did an investigation base on the mechanism of edge chipping occurred during laser-assisted milling (LAM) on silicon nitride ceramics. It was found that as the temperature reached above the softening point and below the brittle/ductile transition temperature during machining, then the values of the cutting forces have been decreased that caused decreased in chipping. When the temperature is reached above the brittle/ductile transition temperature, it would increase the toughness of the specimen edges. The combination of the softening and toughening mechanisms has reduced the chipping form the edges.

Cong et al. (2012) analyzed the power consumption in rotary ultrasonic machining (RUM) while machining of carbon fiber reinforced plastic (CFRP) material. Moreover, different CFRP workpieces significantly affected the power consumption of ultrasonic power supply, coolant pump, and spindle motor.

Lv et al. (2013) were evaluated the surface formation mechanisms analysis on BK7 glass, which was incorporated by rotary ultrasonic machining (RUM). Additionally, it was notified that the stress imbalance on the workpiece specimen surface brought by the dramatic fluctuation of the

abrasive inertia load triggered ample tortuous cracks develop on the rotary ultrasonic machining grooves generated in the ductile material removal stage in 0.2 m sized length. Also, a theoretical model based upon the surface formation mechanisms were established on RUM by considering the ultrasonic effects, exemplify as the lower dynamic fracture toughness of workpiece, the larger abrasive inertia force and cyclical variation in the effective work angle of the abrasive. Here, while execution of experiments; it was notified that the ultrasonic vibration could significantly decline the cutting force of the diamond tool owing to the ductile behavior of thee BK7 glass. Nevertheless, the surface quality of the RUM workpiece samples was marginally degraded. In a nutshell, the ultrasonic superposition delivered a superior processing performance.

Zhang et al. (2014) worked on drilling of K9 glass specimens using RUM process by applying compressed air like a coolant. The input experimental factors are feed rate (mm/sec), spindle speed (r/min) and ultrasonic power (% age). The output factors were opted as surface roughness, edge chipping and power consumption. It was found that surface roughness over the drilled region has been reduced by adding more spindle speed. Opposite trend of surface roughness increased was noticed by increasing ultrasonic power and feed rate. Also, mentioned that the chipping size has been diminished by increases of spindle speed.

Ding et al. (2014) conducted experimental tests on machining of C/SiC composites while using rotary ultrasonic machining (RUM) and conventional drilling (CD) tests with a diamond core drill. Fig. 2.4 describes the experimental setup of RUM and CD.

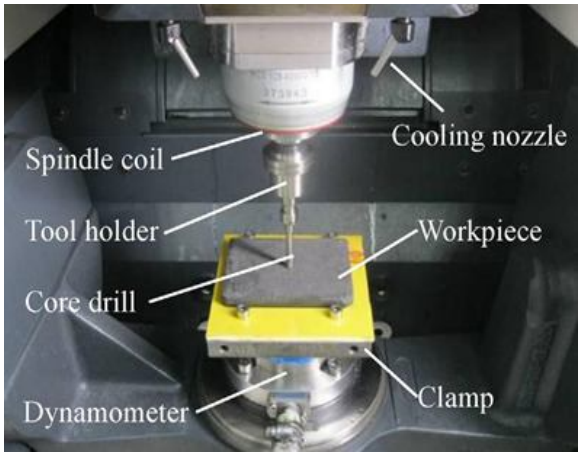

Fig. 2.4: RUM and CD experimental setup (Ding et al. (2014))

Here, the outcomes showed, while compared to conventional drilling (CD) that the drilling force

and torque for RUM were reduced by 23% and 47.6%, respectively. It was also notified that the drilling force and torque in RUM were smaller than CD when the spindle speed was 8000 rpm. The value of the drilling force for RUM was lower than CD and it was evaluated as 8.9% to 12.6% and the value of torque was 23% to 28.8%, respectively. It was found that the RUM created drilled holes of improved surface quality under similar operating conditions.

Liu et al. (2014) discussed that during drilling of brittle material by RUM, the proper consideration of tool wear was lead to the minimization of the micro-chipping and cracking near hole exit. It was revealed that during experimentation, exit crack was reduced to 25.375 μm as well as the tool wear was declined by 16.891 μm, respectively. Hence, the approach was verified and validate that it was effective for decreasing exit chipping while limiting tool wear.

Xu et al. (2014) suggested rotary ultrasonic machining/texturing to generate hybrid periodic micro/nano-textures on flat surfaces. Here, the diamond tool dimensions were noticed as length and diameter of 28 mm and 3 mm, respectively. Added, the cutting locus also evaluated mathematically, to get accurate and control the texturing process. During research study, several parameters for instance cutting edges, various tool faces, tool tip's geometry, cutting corner, the cutting locus and the surface textural features were analyzed. In the end, it was mentioned that there is a vital demand for rotary ultrasonic machining/ texturing method in the field of machining hard and brittle materials.

In this study, **Kuruc et al. (2015)** major concern was machining of poly-crystalline cubic boron nitride (PCBN) by Rotary Ultrasonic Machining (RUM). Here, the machining parameters were spindle speed of 8000 rpm, feed rate 300 mm/min, depth of cut 0.003 mm, vibration frequency 21.6 kHz and vibration amplitude was 6 μm, respectively. The results mentioned that the rotary ultrasonic machining could attain low level of surface roughness, i.e. Ra 0.24 μm through machining of PCBN for the welding tool.

In the study of **Ning et al. (2015),** a comparison between the conventional grinding and RUM for CFRP workpieces was considered for the output variables i.e. cutting force, torque, surface roughness, hole diameter, and material removal rate (MRR). Fig. 2.5 illustrates the tool used in both RUM and grinding and Fig. 2.6 shows the rotary ultrasonic machining (RUM) experimental setup.

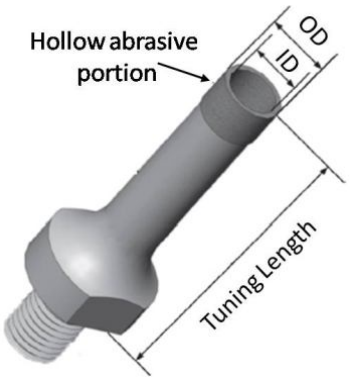

Fig. 2.5: Illustration of the tool used in RUM (Ning et al. (2015))

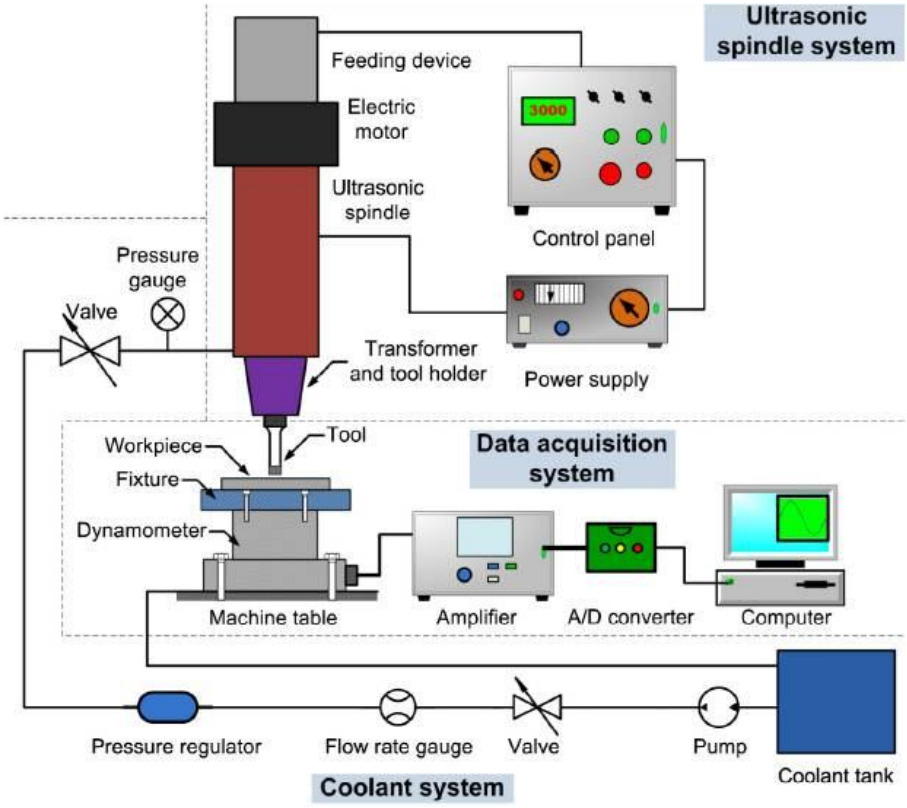

Fig. 2.6: Rotary ultrasonic machining (RUM) experimental setup (Ning et al. (2015))

Here, with the increase of tool rotation speed from 1000 to 5000 rpm, cutting force decreased in both RUM and grinding. It was found that as the tool rotation speed hiked from 1000 rpm to 5000 rpm, cutting force declined in both RUM and grinding. At last, it was concluded while comparing with the grinding process, the RUM process accomplished better in the drilling of

CFRP, including lower cutting force, lower torque, and better surface roughness. As well as, it was mentioned that the RUM machine required an ultrasonic generation system and special tools.

Lv et al. (2016) demonstrated a high-frequency vibration-based mechanism based on hole entrance chipping in RUD process of BK7 glass. It was mentioned that the deformation characteristics of the glass induced by the ultrasonic superposition would extensively influence the nucleation as well as propagation of entrance chipping during rotary ultrasonic drilling. Hole entrance quality was significantly determined by the nucleation of the lateral cracking systems between the initial tool's abrasive and workpiece material extrusion phase. After RUD process, scale-like cracking appeared nearby the hole. In the case of CD process, after the tool's abrasive unloading phase, the immense residual stress would generate which depicts as lateral cracks initialization. Whereas, the superimposing ultrasonic vibration controlled the intensification of the lateral cracking nearby hole entrance. Specifically, it was found that the superimposition of ultrasonic leads to the drastic improvement in the holes edge quality.

Singh and Singhal (2016) investigated that the maximum research study has been performed on examining the outcome characteristics such as surface roughness, cutting force, and material removal rate (MRR) during RUM process i.e. 25 %, 25 % and 15 %, respectively. Subsequently, it was noticed that the hole quality, subsurface damages, and edge chipping size have least examined outcomes as represented in this article i.e. 4 %, 4 %, and 3 %, respectively. Various machining performances are described as per its investigation by RUM process (Fig. 2.7).

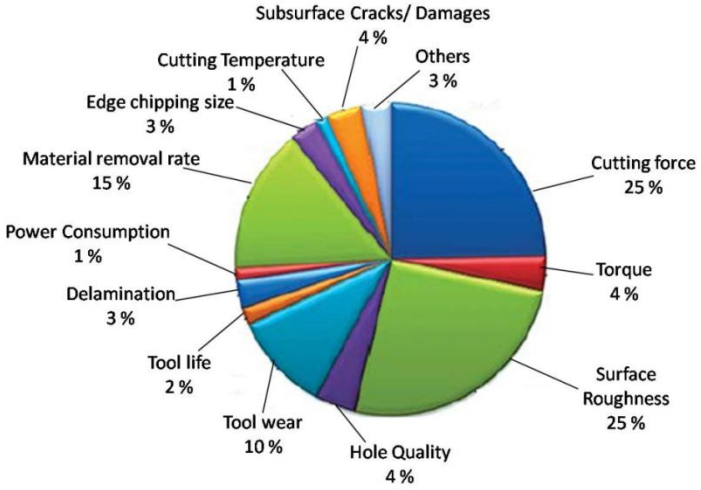

Fig. 2.7: Based on various machining performances investigated in RUM (Singh et al. (2016)**)**

It was noticed that the machining of hard and brittle materials exemplify as float glass, ceramics, quartz, soda lime, borosilicate glass, zerodur, and ceramic matrix composites (CMC) have been carry out using RUM process.

Wang et al. (2016a) developed an edge chipping size based analytical model. In this model, the effect of subsurface cracks and cutting force has been taken during RUD process. The experimental test had been conducted on the K9 optical glass samples to found the modeling coefficients. Analytical model and experimental results stated that edge chipping size were having greater influence of spindle speed and feed rate. On another hand, ultrasonic vibration amplitude was having least impact on chipping size. Overall, it was mentioned that the RUD process has a worthy method in drilling of brittle material.

Wang et al. (2016c) worked on the edge chipping reduction by making a hole on quartz glass by RUD process. The edge chipping initiation is estimated by the correlation between the machining-induced crack and the driving force. Vickers indenter technique is used to estimate the size of the crack. The elastic fracture mechanics theory is used for crack evaluation. Where, it has been noticed that the edge chipping fracture is strongly influenced by the toughness of the brittle material. It was concluded that the reduction in cutting force leads to crack size reduction. Subsequently, it was noticed that the cracks induced by RUD process are smaller in size than induced by conventional drilling.

Hu et al. (2017) carried out an experimental study of Rotary ultrasonic machining (RUM) and grinding process on optical BK7 and K9 glass samples. Effect of ultrasonic power on cutting forces, edge chipping, and torque were considered. It was found that at higher ultrasonic power rate, the cutting force, as well as torque, is reduced. A similar effect is also noticed in the case of edge chipping. The least size of edge chipping is noticed between 40 to 80 % of ultrasonic power.

Jain and Pandey (2017) established a mathematical model based upon the chip thickness and cutting forces during RUM process on borosilicate glass. It was revealed that the ductile mode of fracture and surface finish were superior in RUM process to the grinding process.

Ning et al. (2017) established a mathematical model to estimate the ultrasonic vibration amplitude at various combinations of input factors in the rotary ultrasonic machining of CFRP specimens. The vibration amplitude-based theoretical model is further validated by experimental

outcomes, which were confirmed by the microscope observation method. Finally, it was revealed that the ultrasonic vibration amplitude is one of the significant key input variables during rotary ultrasonic machining. It has a noteworthy impact on cutting force, cutting temperature, and chipping.

Wang et al. (2017b) worked on estimating a critical feed rate with respect to amplitude and spindle speed. Sapphire and quartz glass work samples have been carried out. A critical feed rate based analytical model was predicted which considering the indentation fracture mechanic and the impact of vibrating systems theory. It was found that when the feed rate exceeds up to a critical value, the cutting force increased rapidly, along with a considerable decline in ultrasonic amplitude. It was also noticed that as the tool thickness reduced in size, the critical feed rate significantly improved.

Wang et al. (2018a) used a compound step-taper tool installed on RUM process to reduce the chipping defects. Quartz glass was used in the experimental study. It was mentioned that the mechanism behind the chipping reduction near hole exit stated that the decrease in cutting force leads to decline in undrilled thickness. The reason for lesser cutting force could be the formation of wedge type contact structure between the taper face of the tool with respect to the workpiece specimen. The size of chipping at hole entrance has been reduced owing to the shielding impact of the residual cracks. It was found that the compound tool has reduced the chipping size at the hole entrance and exit between 35 % to 50 % and 60 % to 80 %, respectively. Hence, it was concluded that the compound tool has an effective impact on improving the hole exit quality by adjusting the angle of the tool taper face.

Wang et al. (2018b) did a review study on the damage and defects that occur during Rotary ultrasonic machining (RUM) process on hard and brittle materials. It was stated that the RUM process has a combined effect of diamond grinding and small amplitude of tool vibration, to enhance the machining quality of brittle specimens. In this study, the mechanism related to the chipping formation, subsurface damages, and tearing defects have been elaborated. It was noticed during the ultrasonic vibration of the tool, the trajectory motion of the diamond abrasive is sinusoidal which leads to enhancement of hole quality.

2.2.2 Theoretical Studies

Jiao et al. (2005) analyzed Al_2O_3 (Alumina) specimen during the formation of edge chipping by rotary ultrasonic machining (RUM). Also, the FEM analysis was taken place along with the integration of designed experiments. Furthermore, the author was established a cutting force based model under a uniform pressure acting on the work component surface during machining. Moreover, FEM analysis was delivering the stress and strain distributions in work component during occurring of rotary ultrasonic machining. Additionally, the relationship between cutting force and chipping thickness was revealed from the FEM simulations and then compared with the outcomes of the designed experiments. It was concluded that as the spindle speed increase and reduction in feed rate take place, it would lead to smaller chipping thickness. Subsequently, cutting force was the key influencing parameter on edge chipping and the greater edge chipping was achieved at higher cutting force. Yet, there was limited research study on edge chipping by rotary ultrasonic machining was revealed.

Li et al. (2006) performed ceramic drilling by RUM process. In the study, a 3-D finite element analysis was established to investigate the effects of support length, pre-tightening load, and cutting depth on the von Mises stress near the chipping initiation region. Added, von Mises stress failure criterion was applied to find the relationship between the support length and the edge chipping thickness. It was also noticed that the chipping thickness was decreased from 0.80 to 0.79 mm, as the support length increases from 4.5 to 10.5 mm, respectively. A fine agreement was predicted between FEA simulation and experimental chip thickness outcome.

Singh et al. (2008) did a comparative study using experimental and finite element study by drilling of glass fiber reinforced plastics using a twist drill of 6 mm diameter with 90^0, $104^{0,}$ and 118^0 point angles. The study was aimed at tool geometry, optimization of drilling variables, and thrust force modeling. The simulation was focused on direct stresses and shear stresses which was noticed near hole edges. The maximum stress failure criterion signifies the specimen failure in the principal direction only and Tsai Wu Failure criteria carried out as the interaction of the stress components in all the directions. Fig. 2.8 illustrates the Tsai Wu failure plot on workpiece specimen using twist drill of point angle 90^0.

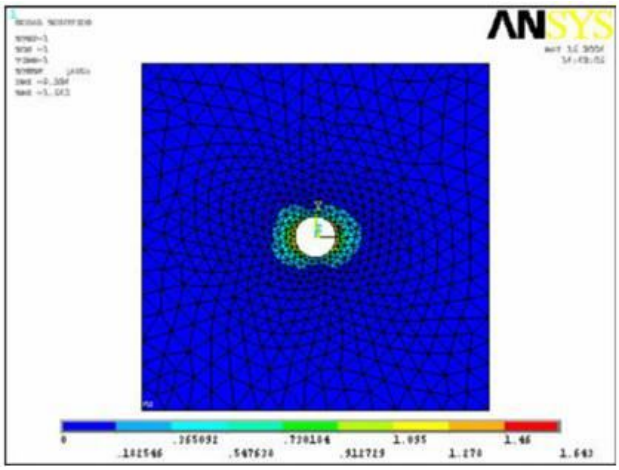

Fig. 2.8: Tsai Wu failure plot on workpiece specimen using twist drill of point angle 90^0 (Singh et al. (2008))

Results showed that the lower point angle of the tool tends to reduce the damage portion while drilling. Consequently, it was stated that the decrease in feed rate and point angle of the tool significantly decrease the drilling forces, that has been further influence the hole quality.

2.3 Tabular Summary of Glass machining outcomes

A summary of glass machining outcomes is reported in the following Table 2.1 which includes workpiece detail, input parameters/tool details, and findings of the different research articles.

Table 2.1 Tabular Summary of Glass machining and Rotary ultrasonic machining (RUM) outcomes

Author and Year of Publication	Workpiece detail	Input Parameters/ Tool detail	Findings/Results
Park et al. (2002)	Soda-lime glass **Properties:** Young modulus (E)- 69 (GPa), Poisson ratio- 0.22,	**Machining detail:** Spindle speed (rpm) - 20000 to 40000, Cutting speed (m/min) - 6.28 to 50.3, Feed rate (μm/rev) - 0.1 to 2.	Hole exit crack size decreased, as the feed rate and thrust force reduced too. At the same thrust force, the average crack size is smaller when the spindle speed is higher.

	Density (ρ)- 2490 Kg/m^3	**Tool detail:** Twisted drill tool of tungsten carbide, Drill diameter (d) - 0.1, 0.2 & 0.4 mm. Back up plate installed.	Least thrust force value and the exit crack size was 0.8 N and 0.015 mm, respectively. Tensile stress plays a key role in crack propagation. With back-up plates, lower tensile stress has been observed near the drill hole exit.
Singh et al. (2008)	Glass fiber Reinforced Plastics **Properties:** Tensile modulus (GPa) - 48, Poisson ratio - 0.25	**Machining detail:** Spindle speed (rpm) - 375, 938 & 1500, Feed rate (mm/rev) - 0.075, 0.188 & 0.300, Tool Point angles - 90^0, 104^0 &118^0. **Tool detail:** HSS twist drill used of 6 mm. 27 experiments was performed.	FEA model was established while considering Tsai Wu failure criteria in all directions. It was found that the direct stresses and the shear stresses were extreme at the hole edges. It was mentioned that the amount of damage at hole corners was reduced by implementing lower point angles.
Karim et al. (2011)	Soda-lime glass chemical Properties: Density (g/cm^3) - 2.53, Young's modulus (Gpa) - 74, Thermal conductivity (W/m*K) - 0.9 to 1.3.	**Machining detail:** Lubrication pressure (MPa) - 0.4 to 1, Spindle speed (rpm) - 5000 to 20000**,** Feed rate (mm/min) - 0.5 to 2**,** Depth of cut (mm) - 0.25 to 1. Taguchi optimization technique used.	As the feed rate and depth of cut decreased, the required amount of energy was declined. As a result, it reduced the cutting force and generated smaller chipping size. It was stated that the spindle speed should be in optimum range because it influenced the temperature and considerably influence cutting force, tool life, and chipping. It was found that the highest

			lubrication pressure i.e. 1MPa, the utmost cutting speed i.e. 20000 rpm, least feed rate i.e. 0.5mm/min and least depth of cut i.e. 0.25 mm are confirmed as best parameter condition to get the least chipping.
Baek et al. (2013)	Soda lime glass	**Machining detail:** Ultrasonic frequency (KHz) - 20, Ultrasonic amplitude (μm) - 20, Feed rate (μm/sec) - 10. **Tool detail:** Tool diameter (mm) - 1.6, Flat end face tool shape.	USM technique used. Wax coated on the workpiece. The thickness of the wax-coated wax as 0.0, 0.3, 0.6, and 1.0 mm. Crack has been reduced in the coated hole entrance chipping. Good surface quality using USM.
Feucht et al. (2014)	Silicon carbide	Diamond impregnated hollow tools used.	As compared to conventional drilling, 30% reduction in feed force was noticed using USM.
Jiao et al. (2005)	CMC and Alumina	**Machining detail:** Spindle speed (rps) - 50, Feed rate (mm/sec) - 0.09, Ultrasonic frequency (KHz) – 20 and Coolant pressure (MPa) - 0.207. **Tool detail:** Metal bonded diamond grain-based drill tool with O.D. (9.54 mm) and I.D. (7.82 mm), respectively, Grain mesh size- 140 to	RUM technique used. At high rate of spindle speed, the chip thickness has been reduced. It was mentioned that the cutting force during RUM of alumina specimen was 66 % lesser than conventional drilling. It was observed that the cracks in the alumina specimen propagate along a direction that is about 45^0 from the workpiece surface and accordingly generates chipping in

		170.	a brittle fracture mode. The chipping of CMC panel has been reduced by using sharp tools. It was found that the best hole has chip thickness of 0.35 mm and chip size was less than 1 mm.
Li et al. (2005)	Ceramic matrix composites (CMC) and Alumina	**Machining detail:** Spindle speed (rps) - 50, Feed rate (mm/sec) - 0.09, Coolant pressure (MPa) - 0.207. **Tool detail:** Diamond core drill tool, Drills with O.D. and I.D. of 9.54 mm and 7.82 mm, Abrasive mesh size - 140 to 170. Testing with and without RUM.	It was found that the cutting forces were decreased while drilling CMC-1, CMC-2, and alumina specimens i.e. 60 %, 40 %, and 60 %, respectively. Metal removal rate (MRR) was 10 % higher with RUM than CD. As the chip size and chip thickness decreased, accordingly it produced enhanced hole quality.
Zeng et al. (2005)	Silicon carbide	**Machining detail:** Depth of drilling - 1.5 mm, Spindle speed (rpm) -4000, Feed rate (mm/sec)-0.09, Vibration frequency (khz) - 20, Coolant pressure (KPa) – 276. **Tool detail:** Metal bonded diamond core drill tool, Outer	The experimental study between RUM and CD. Wear of diamond grains on the tool lateral face was insignificant after 16 tests were performed. It was suggested diamond grains on the tool's lateral face were required in smaller quantities. Grains wear at the edge of the lateral face (close to the end face) were dislodged.

		diameter (OD) - 9.6 mm, Inner diameter (ID) - 7.8 mm, Grit mesh size - 100 to 120.	Abrasive pulled out phenomenon occurs during RUM.
Ding et al. (2014)	C/SiC composites panel	**Machining detail:** Spindle speed (rpm) - 10000, Vibration frequency (kHz) - 20 to 30.4. **Tool detail:** Sintered diamond core drill with O.D. and I.D. of 6 and 5 mm, respectively, Grain mesh size – 126.	Experimental study between RUM and CD. Back-up plate used. RUM reduced the drilling force between 7.4 % to 23 %, During RUM, higher quality of holes was achieved with less tear.
Liu et al. (2014)	Alumina oxide ceramic	**Machining detail:** Spindle speed (rpm) - 3000, Ultrasonic frequency (kHz) - 40, Amplitude (μm) - 8. **Tool detail:** CVD diamond coated drill.	Exit crack (μm) 25.378 at optimized parametric condition. Also reduced tool wear.
Lv et al. (2016)	BK7 glass **Properties:** Density, (g/cm^3)- 2.52, Young's modulus (GPa)- 82, Poisson ratio - 0.203	**Machining condition:** Spindle speed (rpm) - 4500 to 9000, Feed rate (mm/min) - 5, Amplitude (μm) - 2 to 5, Coolant- Water based solution. **Tool detail:** Nickel bonded diamond	Hole entrance chipping was evaluated. It was mentioned that the increase in spindle speed noticeably expanded the abrasive trajectory and reduced the periodic fluctuation; as a result, it shrinks the inhibitory effect of the lateral

		drill tools with different diameters.	crack propagation. Consequently, the chipping width was reduced.
Wang et al. (2016a)	K9 optical Glass (Young modulus- 85.9 GPa), Sapphire ((Young modulus- 478 GPa)	**Machining condition:** Spindle speed (rpm) - 3000 to 6000, Feed rate (mm/sec) - 0.01 to 0.1, Amplitude (μm) - 7 to 27. **Tool detail:** Electroplated hollow diamond tool with thickness of 1 mm, diamond grit size - 100.	It was mentioned that the chipping near hole corners of a brittle material occurred because of crack propagation owing to cutting force. It was revealed that the chip size achieves from RUD has been smaller than CD process.
Wang et al. (2016c)	Quartz Glass **Properties:** density= 2.2 g/cm3, elastic modulus E = 76.7 GPa, Vickers hardness Hv = 9.5 GPa, Poisson's ratio v = 0.17	**Machining condition:** Ultrasonic spindle speed (rpm) – 8000, Power - 300 W, Vibration frequency (kHz) - 20, Amplitude (μm) - 1 to 10. **Tool detail:** Electroplated diamond core tool with OD of 5 mm and thickness of 0.5 mm and abrasive mesh size - 126.	Reduction in the size of cracks due to the special material removal mechanism was introduced. During RUM, as the tool vibrates with some frequency, the tool's end face has not in continuous contact with the specimen. This type of impact reduced the crack size while more micro-cracks have been generated whereas long cracks could reduce. The decline in cutting force leads to decrease in cracks size during RUD process.
Wang et al. (2018a)	Quartz Glass	**Machining condition:** Spindle speed (rpm) - 3000 to 5000, Feed rate	The compound tool attains the reduction in chip size near hole exit by 60 % to 80 %.

		(mm/min)- 2 to 4, Ultrasonic frequency (kHz)-40, Amplitude (μm) -8. **Tool detail:** A compound tool with step taper and common tool was used.	The compound tool leads to reduction in chip size at the hole entrance by 35 % to 50 % owing to the shielding effect of residual cracks which were created by the second outmost abrasives from the tool's taper face.

2.4 Industrial Visits and Observation

During the Industrial observation, it was noticed that the ceramic and glass industries are facing a plethora of machining problems such as glass volume defects during machining or drilling, edge chipping, cracking, moderate surface quality, surface roughness, etc. Therefore, some industrial visits were planned to check the feasibility of the proposed work.

The following are the detail related to the visit to ceramic and glass based industries. These are:

- Asahi India Pvt. Ltd, Rewari, India
- GSC Glass, Greater Noida, India
- Nanda Glass, Noida, India
- Saint Gobain Glass, Bhiwadi, India

2.4.1 Asahi India Pvt. Ltd (AIS), Rewari, India

AIS group is established in 1984, AIS is India's prominent integrated glass producer of all kinds of glass and a leading competitor in the automotive and architectural glass value. It shares 70 % Indian automotive glass market. It manufactures several classes of glass such as plain float glass, tempered glass, tinted glass, reflective glass, solar glass, laminated glass, and bullet proof glass. Specifically, AIS group deploy conventional diamond drilling, CNC diamond drilling, and milling and water jet machining (WJM) processes to achieve various shape and sizes of hole, slots, and contour. Fig. 2.9 represents CNC diamond drilling machine used to drill glass specimen.

Fig. 2.9: A picture of CNC diamond drilling machine

(Courtesy: Asahi India Pvt. Ltd)

The various kind of abrasive tools which are used during glass drilling is mentioned in Fig. 2.10. Also, Fig. 2.11 and Fig. 2.12 represents the float glass workpiece with accepted as well as rejected holes due to volume defects like cracking and chipping. If there were no hole inaccuracy due to chipping or cracking, then these glass plates could be further functional in the building's infrastructure.

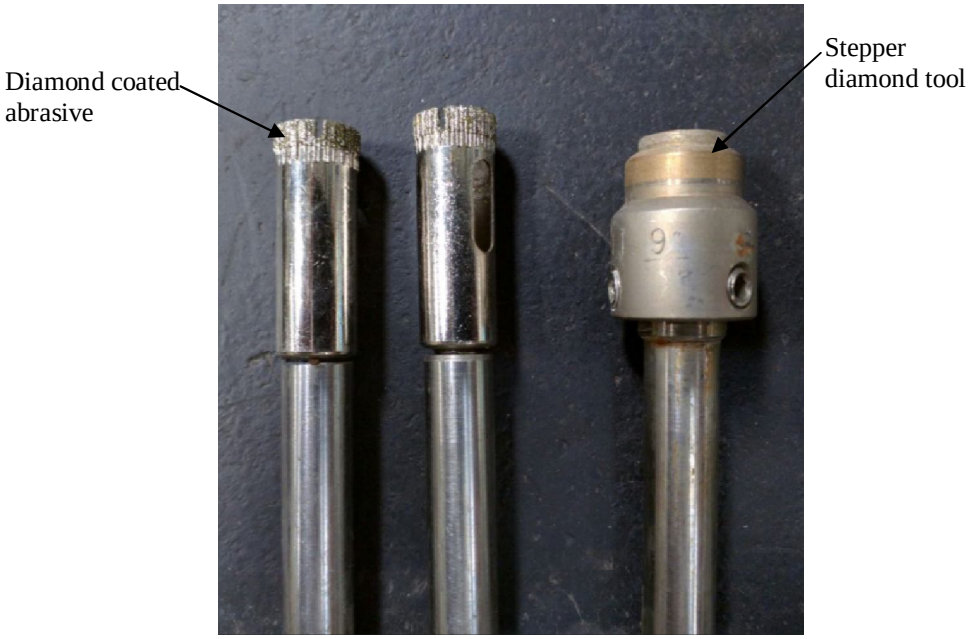

Fig. 2.10: Various kind of drill tool used during glass drilling

(Courtesy: Asahi India Pvt. Ltd)

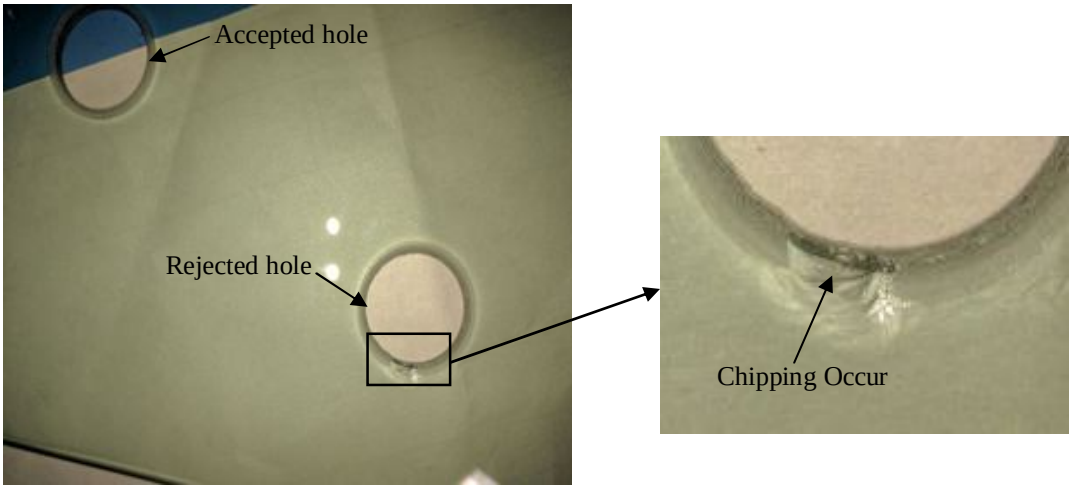

Fig. 2.11: A float glass workpiece drilled by diamond drilling

(Courtesy: Asahi India Pvt. Ltd

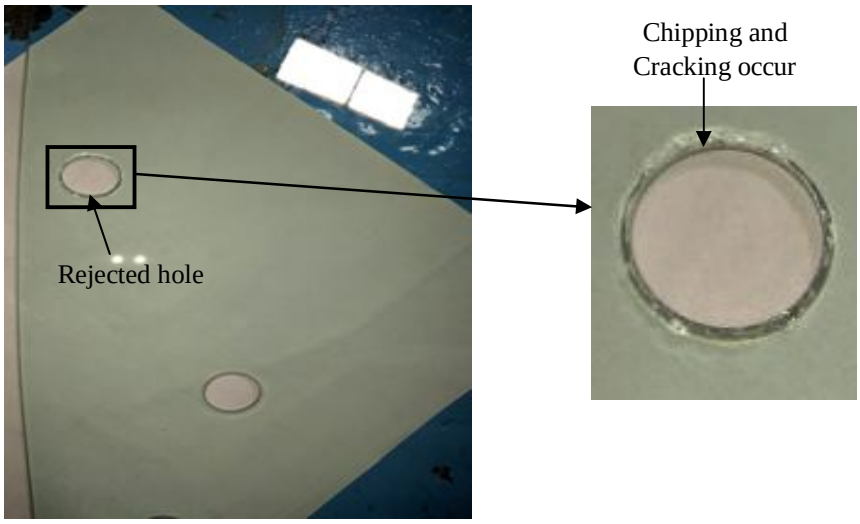

Fig. 2.12: Float glass workpiece by water jet machining (WJM)

(Courtesy: Asahi India Pvt. Ltd)

Based upon the working experience on conventional drilling machine and water jet machine, it is noticed that still, the percentage of precise hole accuracy is not optimum. Therefore, it is a brain storming problem for the industries as well as for the researchers that during drilling operation the chances of occurring of cracks and chips are significant.

2.4.2 GSC Glass, Noida, India

GSC has been into architectural glass processing since 1978. It possesses wide range of glass processing facilities using the most modern high tech machines and equipment. GSC manufactured wide range glasses exemplify as heat strengthened glass, tinted glass, laminated glass, insulated and tempered glass, etc. GSC supplies to numerous users for architectural, automotive, domestic appliances, solar collectors, photovoltaic, luminaries, and displays, etc. Fig. 2.13 mentions a CNC based water jet machine (WJM) and Fig. 2.14 shows a CNC double-ended drilling machine. During drilling, cut-outs, and slot cutting operations, GSC has automatic CNC double-ended drilling and milling machine, conventional diamond drilling and water jet machining (WJM) processes to achieve various shapes and sizes of the hole, cut outs and contour. Figures represent the water jet machine (WJM) and CNC double-ended drilling and milling machine along with their drilled holes.

Fig. 2.13: CNC water jet machine *(Courtesy: GSC GLASS Pvt. Ltd, Noida)*

Fig. 2.14: CNC double-ended drilling machine *(Courtesy: GSC GLASS Pvt. Ltd, Noida)*

Also, Fig. 2.15 shows a conventional diamond drilling machine courtesy GSC Glass, Noida, India.

Fig. 2.15: Conventional diamond drilling machine

(Courtesy: GSC GLASS Pvt. Ltd, Noida)

New and used abrasive coated type of drill tools were generally used in this company as shown in Fig. 2.16 and Fig. 2.17, respectively. It is noticed that the tool wear could also be a concern to investigate in further study. It is visualized that the abrasive particles are losing strength and wear out over the tool periphery. One of the major applications of float glass specimen is Bajaj gas stove (Fig. 2.18) on which drilling operation generally occurs.

Fig. 2.16: New diamond drill tool

(Courtesy: GSC GLASS Pvt. Ltd, Noida)

Fig. 2.17: Used diamond drill tool

(Courtesy: GSC GLASS Pvt. Ltd, Noida)

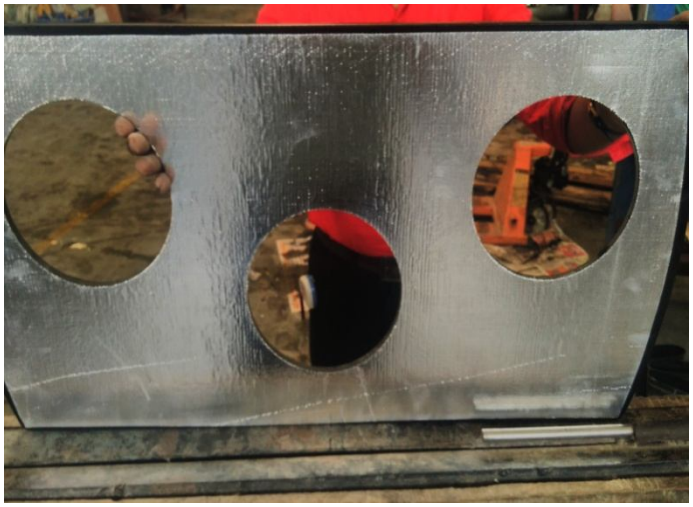

Fig. 2.18: Glass plate used in Bajaj gas stove

(Courtesy: GSC GLASS Pvt. Ltd, Noida)

As per the quality regimes of GSC plant, volume defects related problems as cracking and chipping (Fig. 2.19) are very common during drilling, cut off and slot cutting operation.

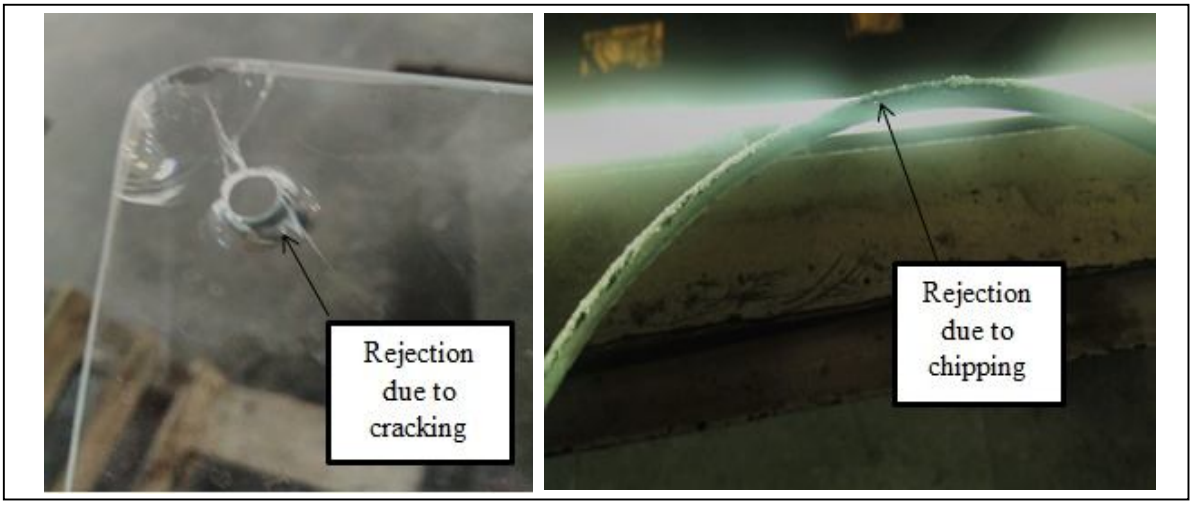

Fig. 2.19: Rejection due to cracking and chipping

(Courtesy: GSC GLASS Pvt. Ltd, Noida)

Hence, it should be the major concern to get rid of cracking and chipping that could decrease the rejection that occurred during manufacturing.

2.4.3 Nanda Glass, Noida, India

Nanda glass industries were founded in 1996. It supplied toughened glass to the appliances industry of India as well as fulfilling the needs of the architectural, automotive, and commercial sectors. Nanda plant is capable of processing mainly plain float glass, low E-glass, coated glass, and patterned glass. Nanda industries have several conventional glass drilling machine, which achieves various diameters and thicknesses of holes. Fig. 2.20 represents the glass drilling machine along with their drilled holes.

Fig. 2.20: Conventional drilling machine

(Courtesy: Nanda Glass Pvt ltd., Noida)

Fig. 2.21 shows the float glass workpieces which could be used as lighting and optics glasses if it is lack of irregularities. Yet again, similar drilling hole relevant volume defect problems (cracking and chipping) were revealed.

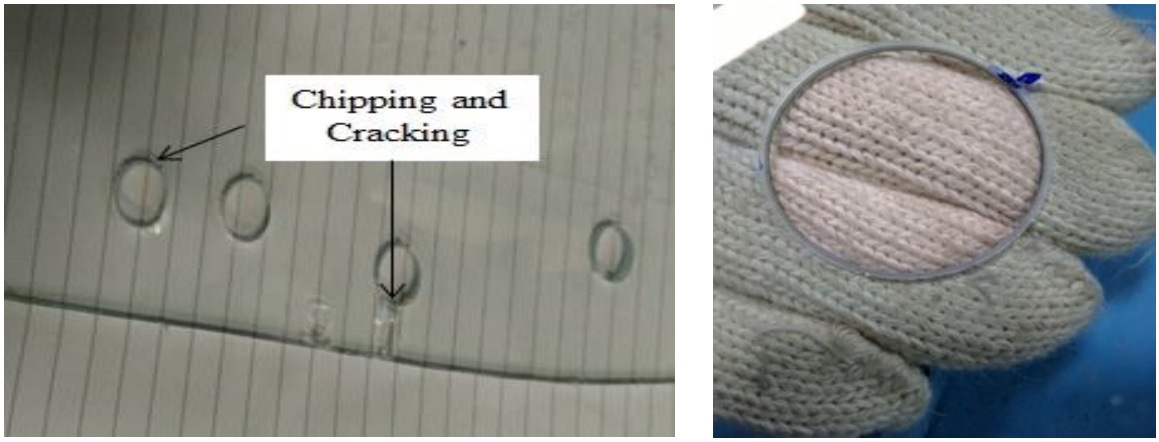

Fig. 2.21: A Float glass workpiece

(Courtesy: Nanda Glass Pvt ltd., Noida)

Also, the optimization of the machining parameter, while achieving refines surface quality is the decisive concern for the Nanda glass Group.

2.5 Rejection Rate and Monetary Loss during Float Glass Drilling for the Industries

The given Table 2.2 contains the rejection rate of plain float glass for the three well-known glass manufacturing industries during drilling operation by Conventional (Diamond drilling and Water Jet Machining) methods. Although, this rejection rate data sheet may vary some time which depends upon factors like diameter of hole, customer requirement regarding hole quality, types of float glass etc. It was found that each float glass workpiece of dimension (l*b*h) 500*500*8 mm^3contain cost price of Rs 500 approximately. It means cost price of 100 float glass plates would be Rs 50,000.

Monthly cost Estimation:

Total no. of days=30

Total shifts in 30 days= 80 shifts approx.

Cost price of 100 float glass plates= 100*500= Rs 50,000

Total cost price for each month= 80*50,000= Rs 4,000,000 = Rs 40 lakh approx.

Table 2.2: Rejection rate and monetary loss of float glass during drilling operation (*Courtesy: Heads of respective companies*)

Detail	Asahi India Pvt. Ltd., Rewari	Saint Gobain, Gujarat	GSC Glass, Noida
No. of glass plates drilled per shift (8 hours)	100	100	100
Total no. of holes	4 holes per plate	4 holes per plate	4 holes per plate
Total no. holes per shift	400	400	400
Rejection rate, If plate thickness varies from 3 to 8 mm.	**5 to 8 %** Or 20-32 holes per 400 holes	**8 to 12 %** Or 32-48 holes per 400 holes	**6 to 9 %** Or 24-36 holes per 400 holes
Monetary loss per shift (8 hours), If plate thickness varies from 3 to 8 mm.	Rs 2500 to 4000 approx.	Rs 4000 to 6000 approx.	Rs 3000 to 4500 approx.
Monetary loss in 30 days of the month, If plate thickness varies from 3 to 8 mm.	Rs. 2,00,000 to 3,20,000	Rs. 3,20,000 to 4,80,000	Rs. 2,40,000 to 3,60,000
Rejection rate, If plate thickness varies from 8 to 12 mm or more.	**3 to 5 %** Or 12-20 holes per 400 holes	**3 to 8 %** Or 12-32 holes per 400 holes	**3 to 7 %** Or 12-28 holes per 400 holes
Monetary loss per shift (8 hours), If plate thickness varies from 8 to 12 mm or more.	Rs 1500 to 2500 approx.	Rs 1500 to 4000 approx.	Rs 1500 to 3500 approx.
Monetary loss per shift (8 hours) in 30 days of month, If plate thickness varies from 8 to 12 mm.	Rs. 1,20,000 to 2,00,000.	Rs. 1,20,000 to 3,20,000	Rs. 1,20,000 to 2,80,000.

After analyzing Table 2.2, it was found that the glass companies bear heavy monetary loss. Because of poor hole quality during machining of glass. Therefore, this work intends to target the reduction in hole entrance and exit chipping and correspondingly enhancing the hole quality while using Rotary ultrasonic machining (RUM) technique.

2.6 Research Gaps

Based on the previous literature reported, the following research gaps can be postulated:

- It is noticed that the limited studies have been taken place in which various shape, size, and features of diamond drill tools were used in conventional diamond drilling (CD) and Rotary ultrasonic machining (RUM).
- Only few articles were focused on the comparison of drilling of float glass by CD and RUM process considering the effect of input parameters such as spindle speed, feed rate, vibration amplitude and tool diameter on hole quality.
- Least number of articles was focused on quantification of chipping; therefore, more elaborated examination is required for entrance and exit chipping with precise characterization technique.
- After conventional drilling (CD), the chipping size has been increased after tempering process. Therefore, a study should be made regarding chip size evaluation after rotary ultrasonic machining and to check its post processing consequences in form of chipping.
- Limited FE analysis has been found related to the stress generation at hole exit during rotary ultrasonic drilling of float glass.
- Subsequently analyzing the literature gap and industrial visits, it can be concluded that maximum work is done on the conventional diamond drilling and ultrasonic machining of glass. Additionally, various glass industries (GSC glass pvt ltd. etc.) are still facing glass machining (drilling) problems.

Although, few studies indicate the effect of non-conventional method or hybrid system used in drilling or machining of glass, very few papers reports the accuracy of hole, hole quality and damaged area on glass drilling. Keeping in mind the literature gap and industries real time problem, the present work is focused on **"Analysis of Hole Quality for Pre-Tempered Float Glass while using Rotary Ultrasonic Machining"**.

2.7 Research Objectives

The following objectives will be addressed to the proposed problem:

- To investigate and analysis the influence of various process parameters on performance characteristics of rotary ultrasonic machining (RUM) technique and process optimization.
- To evaluate the drilled hole quality and dimensional accuracy using Scanning electron microscope (SEM), atomic force microscope (AFM), optical profilometer and coordinate measuring machine (CMM).
- To compare the edge chipping reduction before and after tempering during conventional drilling and rotary ultrasonic drilling.
- To finite element (FE) analysis of stress generation at hole exit during rotary ultrasonic drilling of float glass.

2.8 Methodology

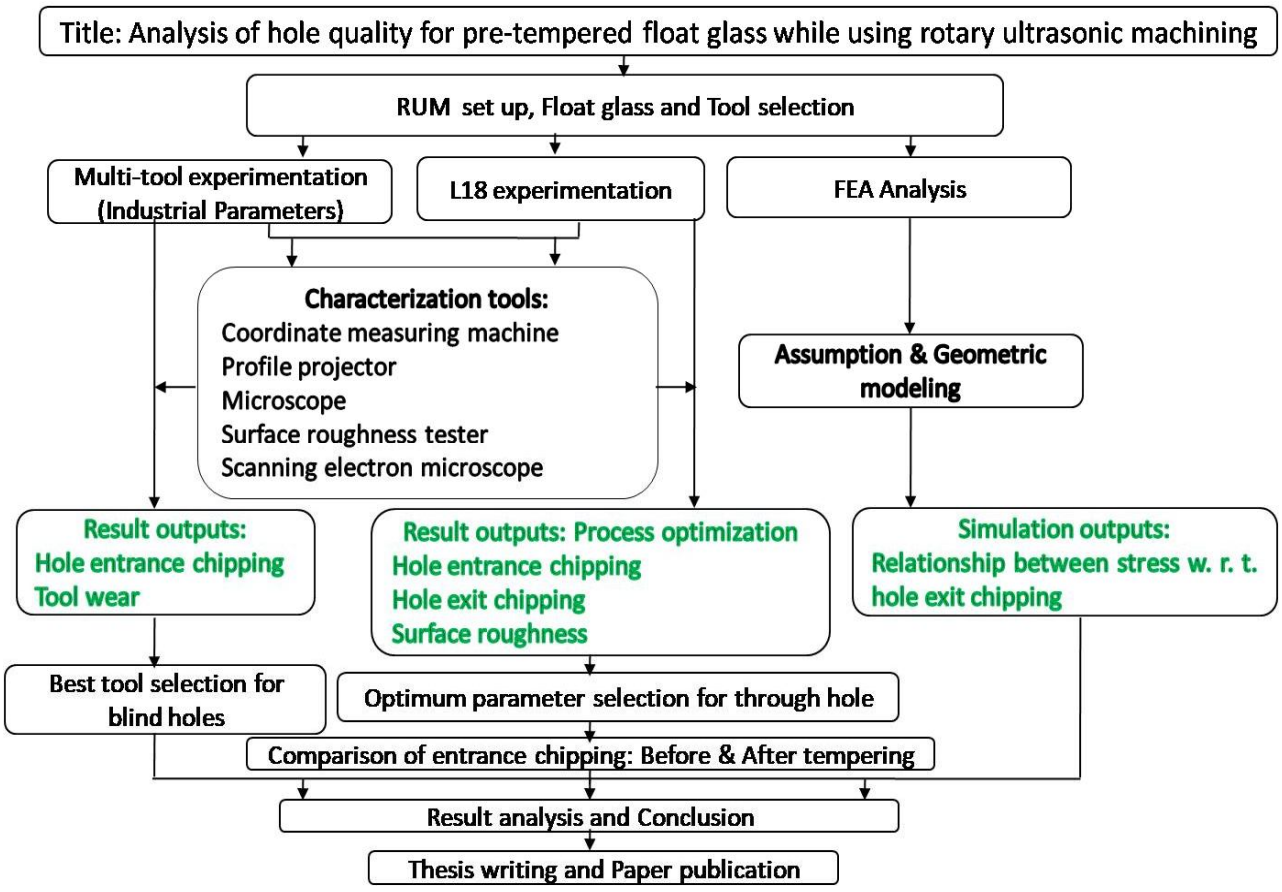

2.9 Summary

In the chapter, several machining processes such as ultrasonic machining, laser beam machining, conventional machining and water jet machining and rotary ultrasonic machining are discussed while processing hard and brittle materials such as float glass, ceramics, quartz, and soda lime glass, etc. It contains machining based issues that are still under investigation. These are hole exit quality, chipping in glass, surface topography, damage portion analysis, cutting force, tool wear, and surface roughness. Some glass industries visits have been carried out to check the feasibility of the proposed work. The detailed observations of the industrial visits are explained precisely. Research gaps and objectives of the work are described.

CHAPTER 3: EXPERIMENTATION

Rotary ultrasonic machining is expected to give the best results for machining of hard and brittle material. For the same reason, a rotary ultrasonic machining experimental setup is developed in the present study to machine the float glass specimen. Experimental trials are performed for achieving the proper industrial and real-time machining conditions.

3.1 Development of Rotary Ultrasonic Machining (RUM) Setup

Ultrasonic is a detailed branch of acoustics deals with the vibratory waves with a frequency range of 20 kHz and vibration amplitude of 0 to 20 μm. In this study, rotary ultrasonic machining set up is developed. Fig. 3.1 describes the manufacturing of shank fitting as well as cover part of piezoelectric transducer and booster by lathe machine. Consequently, the complete tool set up could aid in machining hard and brittle workpiece specimen i.e. Float glass. In tool set up, the cover part is made up of light weight Metalon nylon material. The key characteristics of grayish nylon are good chemical and corrosion resistivity, elevated durability and high strength. As shown in Fig. 3.2, Shank fitting is made up of aluminum alloy with 94 % of aluminum element and other related alloys (copper, manganese and magnesium). The reason of choosing aluminum alloy is to get adequate mechanical strength with low cost. Corrosion resistance is another influencing factor of aluminum that is much needed for the Shank fitting. After selection of materials, fabrication of RUM tool assembly has been done by turning, drilling, soldering, and machining processes. Fig. 3.1 portrays the fabrication part of the tool set up.

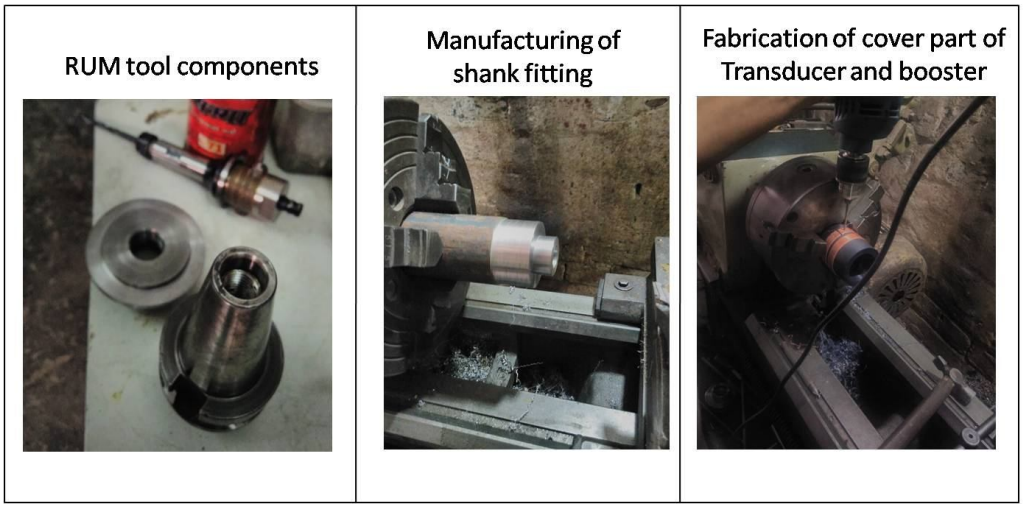

Fig. 3.1: Fabrication of RUM set up

The RUM tool assembly further consists of a piezoelectric transducer, cover part of the transducer and booster, shank fitting assembly, and the machining tool. For the smooth conversion of electrical energy into mechanical energy (vibration), the piezoelectric transducer is equipped in between the power generator and the tool-collet assembly. In the case of RUM tool setup, horn acts as a tool holder as well as an amplifier. Fig. 3.2 illustrates (a) The 2-D view of RUM tool, (b) 3-D view of RUM tool assembly.

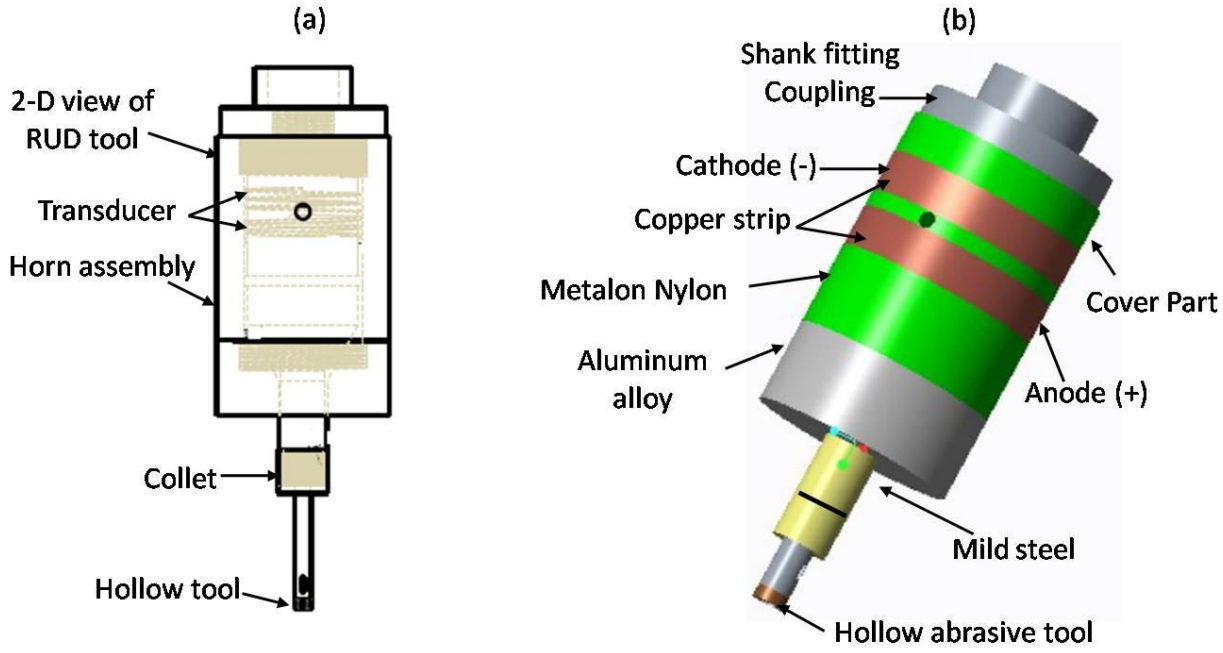

Fig. 3.2: Illustration of experimental set up (a) 2-D view of RUM tool and float glass specimen, (b) 3-D view of RUM tool assembly

The equipment used during fitting and manufacturing of set up is the ultrasonic power generator unit, CNC machine controller unit (MCU), coolant arrangement, glass holding fixture, and rotary ultrasonic machining (RUM) tool assembly. The ultrasonic power generator unit and piezo-electric transducer are outsourced. The machine controller unit (MCU) and coolant arrangement are auto fitted in CNC milling machine as shown in Fig. 3.3. A CNC milling machine is modified into RUM machine by fixing the attachments over it.

During RUM, the generator produces 20 kHz of high-frequency electrical energy. This electrical energy is converted into mechanical vibration using a piezoelectric transducer (Hu et al. (2017)). The mechanical vibrations are being transmitted towards horn assembly. These are focused and amplified further with the help of horn, to the required intensity for driving the tool which is

attached to the spindle. This set up is mounted on the CNC vertical milling machine for the tool rotation. Set up has spindle rotational capacity of 60 to 6000 rpm.

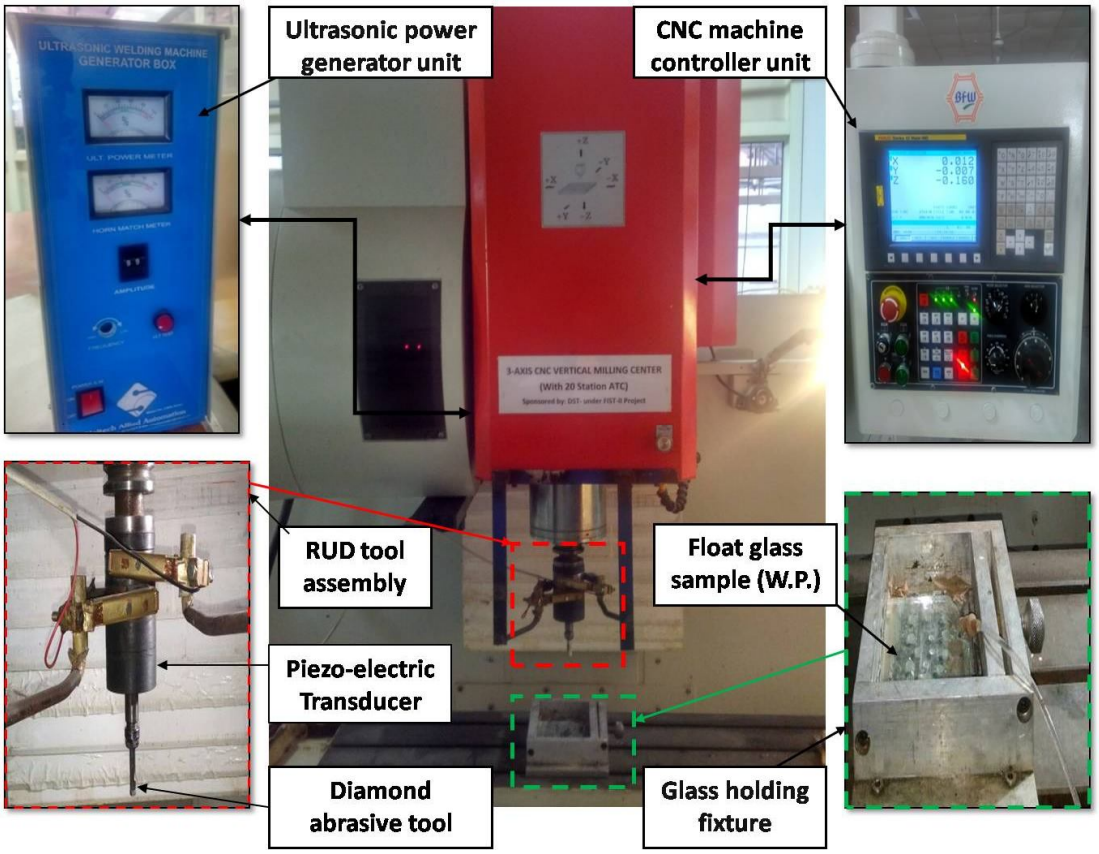

Fig. 3.3: A schematic flow diagram shows the RUM experimental setup and equipment used for generating blind and through holes

During conventional drilling (CD), the ultrasonic power supply is switched off. The spindle rotational speed and tool feed rate are controlled by CNC machine panel controller. Also, a coolant arrangement is installed on the machine for continuous feeding. Distilled water is used as a coolant. After installing the experimental setup, the other working conditions i.e. workpiece specimen, drill tool, and machining parameters are finalized.

3.2 Workpiece Detail

A float glass is deployed as a workpiece. The chemical ingredients of float glass are silica (60 %), soda ash (10 %), limestone (10 %), dolomite (10 %), salt cake (10 %), and cullet (glass waste pieces). A rectangular glass of 148*84 with 5 mm thickness is used in the experimentation. Table 3.1 mentions the mechanical properties of the float glass specimen.

Table 3.1: Mechanical properties of the workpiece material

(Wang et al. (2017); Wang et al. (2018); www.makeitfrom.com)

S. no.	Properties	Value
1.	Density	2500 Kg/m^3
2.	Compressive strength	212 MPa
3.	Elastic modulus (Tensile)	70 GPa
4.	Tensile strength (UTS)	50 MPa
6.	Vickers hardness	4.59 MPa
7.	Poisson's ratio	0.23

3.3 Tool Detail

Table 3.2 mentioned the 5 tools which are selected for the experimentation work along with their specification. During experimental trials, various shapes of solid and hollow abrasive coated tools are applied for generating blind hole as represented in Fig. 3.4. To analyze the hole entrance chipping and its corresponding tool wear, these 5 tools are used during trials. To create blind hole application, best tool among all is suggested at the end of the study.

Table 3.2: Detail specifications of tools *(Courtesy: GSC Glass Pvt. Ltd, Noida)*

S. No.	Tool Name	Type	Tool shank material	Abrasive/ grain type	Tool abrasive mesh size	Dimensions (mm)	Abrasive/grain coated method
1	Pin pointed Conical tool	Solid	EN 31	Diamond	90-140	Max. Dia.-7.94 Avg. Dia.-3.97	Electroplating
2	Flat cylindrical tool (Height > Dia.)	Solid	EN 31	Diamond	90-140	Dia.-4.92 Length-12	Electroplating
3	Flat cylindrical tool (Height < Dia.)	Solid	EN 31	Diamond	90-140	Dia.-7.92 Length-4	Electroplating
4	Hollow abrasive tool	Hollow	EN 31	Diamond	90-140	O.D-5.90 I.D-4.21	Electroplating
5	Concave circular tool	Solid	EN 31	Diamond	90-140	Dia.-9.94	Electroplating

Tool 1 (T1): Pin pointed Conical tool	Tool 2(T2): Flat pointed Cylindrical tool (Height > Dia.)	Tool 3(T3): Flat pointed Cylindrical tool (Height < Dia.)	Tool 4(T4): Hollow abrasive tool	Tool 5(T5): Concave circular tool

Fig. 3.4: List of tools used in experimentation

3.4 Experimentation Detail

The experimentation detail is divided into three categories. In the first category, blind holes are created using multi-shaped tools and blind hole samples are taken for analyzing the chipping at the **'hole entrance'** periphery. Correspondingly, the tool samples are also collected to analyze and estimate the tool wear. In the second category, parameter optimization experiments are performed to create through holes and then these hole samples are further carried out for evaluation of chipping at the **'hole entrance and exit'**. To evaluate the chipping at the hole exit, the machined rod is used to validate the exit chipping on the hole. The drilled hole internal region's surface roughness (R_a) is also evaluated to improve the overall quality of the hole. In the third category, conventional and rotary ultrasonic drilling experimentation is performed on pre-tempered float glass to compare the entrance edge chipping reduction **'before and after tempering'**. In the entire study, hole entrance chipping is measured as average radial chip distance (RCD), hole exit chipping is quantified as maximum chip radial distance (CRD) and maximum chip thickness (t_c) in the horizontal and vertical direction, respectively. The existed categories are explained in detail in the following section.

3.4.1 Multi-Shaped Tool Based Experimentation (For Blind Holes)

In this study, various shapes of solid and hollow abrasive coated tools are applied for generating blind hole as represented in Fig. 3.5. Each tool generates 6 holes, out of which 3 were produced with CD and the rest of 3 were with RUD to get more accurate and precise results. So in total 30

blind holes are achieved. As in Fig. 3.2, Tool 1 has an average diameter of 3.97 mm, and the maximum diameter is 7.94 mm. Tool 2 and Tool 3 both are named as flat cylindrical tools. The difference between them elaborated as: Tool 2 has a larger height (12 mm) than the diameter (4.92 mm), whereas Tool 3 has a larger diameter (7.92 mm) than the height (4 mm). Hence, both the tools have dissimilar lateral heights and diametrical endings. Subsequently, it could be chances of variation in the outcomes (in form of chipping and tool wear).

The parameters applied by glass industries are used in this experimental study. Based on industrial application and its working conditions following parameters are kept constant during blind drilling of float glass specimen by rotary ultrasonic machining. All the parameters will be the same during conventional drilling (CD) except the vibration frequency and amplitude. The vibration will be turned off during CD. Table 3.3 shows the machining conditions which are followed by experimentation trials.

Table 3.3: Illustration of machining conditions

S. no.	Parameter	Value
1.	Spindle speed (S)	4500 rpm
2.	Feed rate (f)	15 mm/min
3.	Vibration frequency (F)	20 KHz
4.	Vibration amplitude (A)	20 µm
5.	Coolant type (c)	Distill water
6.	Tool's abrasive type	Diamond

After outfitted all the working conditions and essential factors (such as tool and workpiece), the fabrication of blind holes is initiated. The whole process of hole creation is completed in a sequence of using multiple tools. The depth of drilling is considered as 3 mm. Later, the blind hole and used tool samples are further taken for analysis and estimation. For this case study, machining time (theoretically) is expected to be constant for each tool. The machining time (T_m) is estimated as 12 seconds using $T_m = L/f_r$ for all the cases. Where, L = length/depth of hole (3 mm), feed rate (f_r) is 0.25 mm/sec. All the tool wear studies have also been reported at constant machining time.

3.4.2 Parameter Optimization Experimentation (For Through Holes)

In another experimental case study, the Taguchi optimization technique is used that could optimize the input process parameters. It is the robust design technique that is widely used to improve the processing quality, reduce the number of experiments, minimize the processing variation and maintenance and promote the quality stability. The primary goal of Taguchi technique is to keep the variance in the output very low even in the presence of noise inputs. Therefore, Taguchi is stated as one of the most appropriate design for parameter optimization.

Here, an L18 orthogonal array has been carried out. Based on the industrial requirement and experimental setup capability, the process variables which are opted for the experimental study are: 1. Spindle speed (S); 2. Ultrasonic amplitude (A); 3. Feed rate (f). Table 3.4 shows the three levels of process variables considered during the study. A software package 'Minitab' is used to create a random test arrangement and aided in experimental processing. Based on objective i.e. to minimize the chipping, a 'smaller-the-better' condition is used here to estimate the responses and transformed into a signal-to-noise (S/N) ratio. Fig. 3.5 illustrates the specimen samples included (a) Front side (b) Back side and (c) Machined rod.

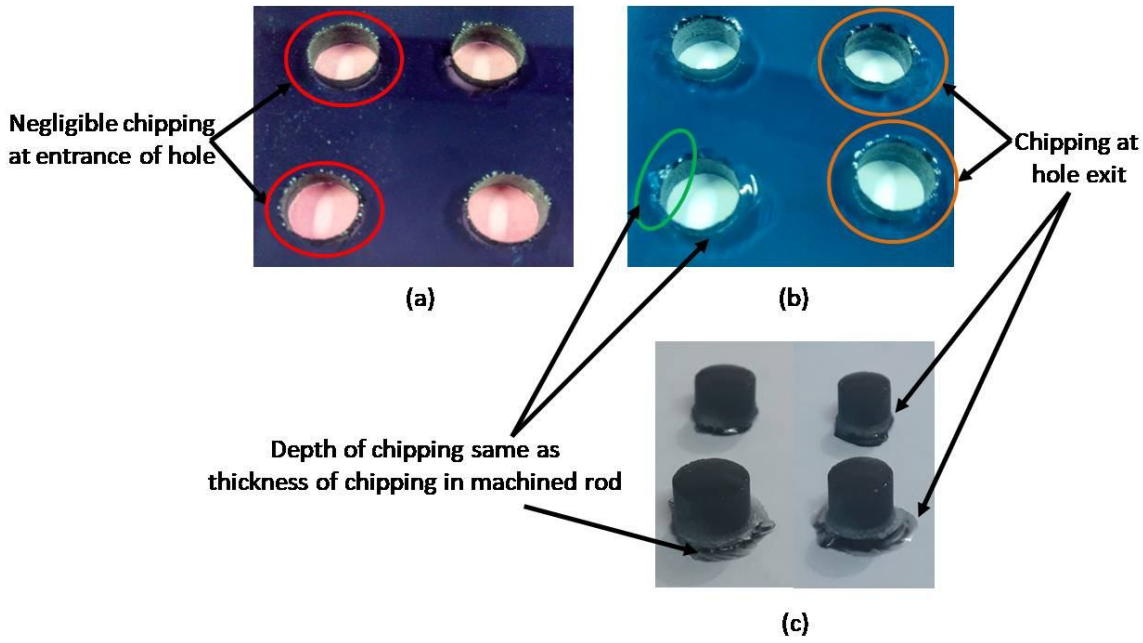

Fig. 3.5: Illustration of the specimen samples included (a) Front side (b) Back side and (c) Machined rod

To get the precise results and account for the unavoidable discrepancy, at each condition three holes are drilled, which compile 54 sets of trials. The samples were then characterized for chipping and average surface roughness at hole proximity at three locations i.e. at hole entrance, hole exit, and hole internal drilled region.

Table 3.4: Three levels of process factors/variables

S. no.	Control factors/variables	Low level	Medium Level	High level
1.	Spindle speed (rpm)	3000	4000	5000
2.	Amplitude (µm)	0	10	20
3.	Feed rate (mm/min)	6	12	18

These result responses are furthers described as: a) Radial chip distance (Average) at hole entrance; b) Chip radial distance (Maximum) at hole exit; c) Chip thickness (Maximum) at hole exit; d) Average surface roughness at the internal drilled region of float glass specimen. The same has already been explained in Section 1.4.2 using Fig. 1.11, 1.12 and Fig. 1.13.

3.4.3 Effect of Tempering on Float Glass Experimentation

In this experimental case study, the prime concern is to compare the edge chipping size (at hole entrance) before and after the tempering process. In industries, all the primary operations like cutting, drilling and machining are performed on a pre-tempered float glass as tempered float glass. After creating the desired hole or machined surface, finally tempering process has been carried out. The optimized parametric combination which is estimated after performing L18 experimental runs is further deployed in this experimental case study. The parametric combination is in form of spindle speed (S), feed rate (f), vibration frequency (F), and amplitude (A). Added, the hollow abrasive coated tool is used to drill the hole of 5 mm depth. Fig. 3.6 illustrates the complete glass tempering furnace which includes a personal computer (PC), control panel, furnace bench, and drilled hole samples.

In this case study, 10 experimental trials are performed. Out of them, 5 are created by CD process and the remaining 5 are drilled by RUM set up at optimized parameter. Later, these drilled hole samples have been taken for the entrance chipping characterization and analysis on both the conditions i.e. (a) before tempering and, (b) after the tempering process. Because, after the tempering process there is always increase in chipping, but the size of the chipping should

not exceed the certain limit up to which the workpiece is not considered as rejected. Hence, the effect of tempering on edge chipping is estimated.

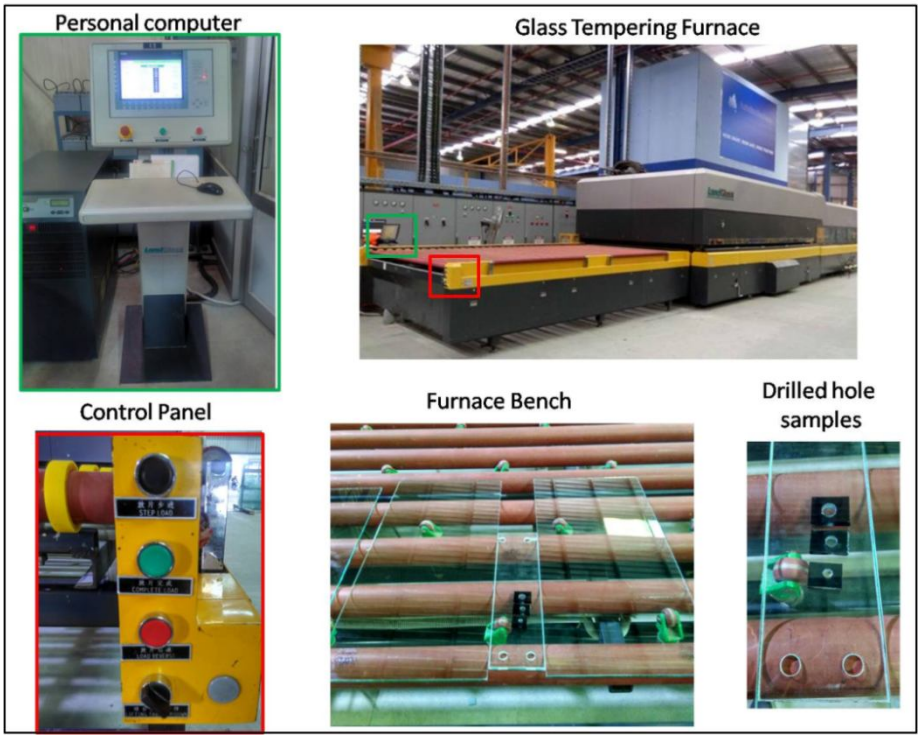

Fig. 3.6: Complete glass tempering furnace

(*Courtesy: ABS Toughened Glasses Pvt. Ltd. Pehowa, India)*

Along with it, the change in radial chip distance (RCD) by conventional drilling (CD) and rotary ultrasonic drilling (RUD) is also estimated precisely. For the same, a glass tempering furnace (*land glass*) is used with the assistance from the company names as 'ABS Toughened Glasses Pvt. Ltd. Pehowa, India'. Table 3.5 illustrates the working parameters during tempering process.

Table 3.5: Illustration of working parameters during tempering process

S. no.	Tempering working parameters	Value(s)
1.	Glass thickness	5 mm
2.	Workpiece load time	800 sec
3.	Temperature range	690-680^{0}c
4.	Heating time set	200 sec
5.	Oscillation speed range of furnace	35-100 mm/sec
6.	Quenching time	25 sec

During the float glass tempering process, working parameters specifically depend upon the thickness of the workpiece which is to be tempered. All the above tempering parameters are constant for 5 mm thickness of the workpiece samples.

3.5 Characterization

3.5.1 Hole Entrance and Exit Chipping

To evaluate the radial chip distance (RCD), chip radial distance (CRD) and chip thickness (t_c), scanning electron microscope (SEM), optical profilometer, digital microscope and coordinate measuring machine (CMM) are used. Fig. 3.7 describes the scanning electron microscope (SEM) device during samples examination. Fig. 3.8 portrays the digital microscope during sample examination.

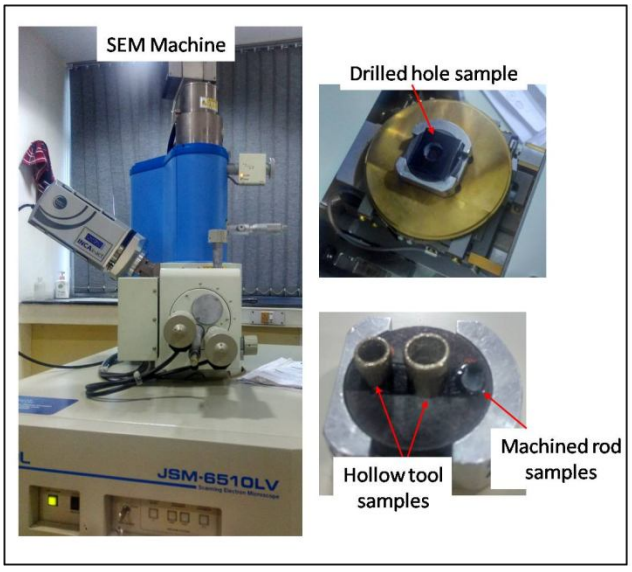

Fig. 3.7: Description of scanning electron microscope (SEM) device during samples examination

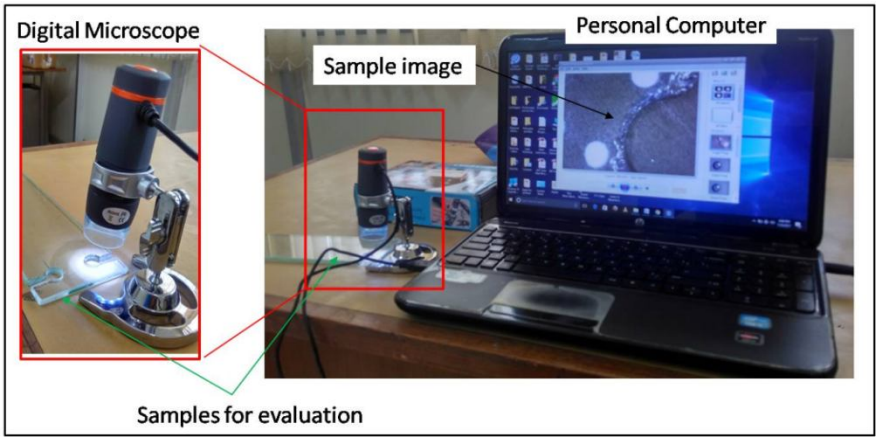

Fig. 3.8: Portray of the digital microscope during sample examination

A Profile projector apparatus (Nikon V-10) with the least count of 0.01 µm is used to characterize the chipping over the surface of blind holes. Also, the maximum, minimum, and average radial distance of edge chipping is quantified. Fig. 3.9 (a) showing the actual way of visualizing the chipping on the various blind hole. Fig. 3.9 (b) illustrates the instrument (Profile projector) used to estimate the average radial chip distance.

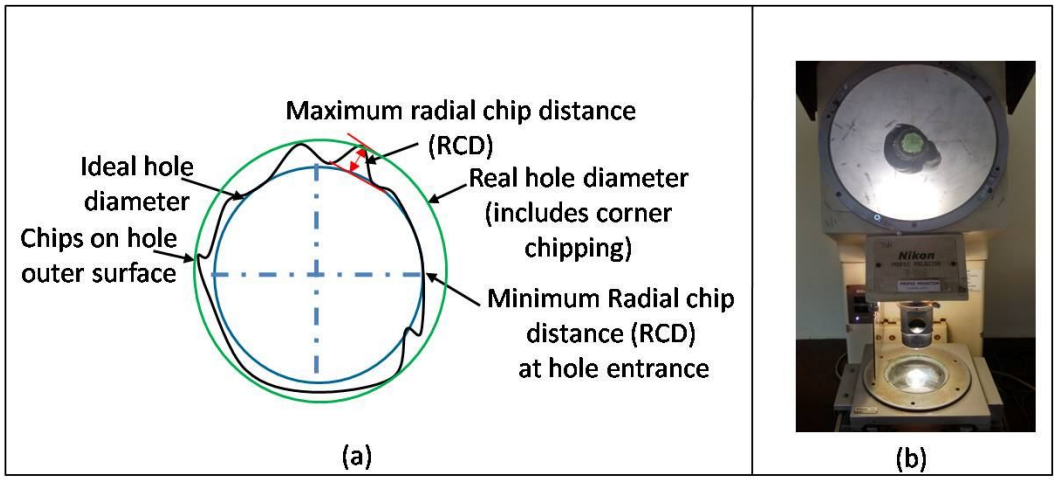

Fig. 3.9: (a) Pictorial view of chipping on a blind hole, (b) Profile projector

As shown in Fig. 3.10, to get the appropriate measurement outcome, radial chip distance (RCD) is measured at eight different points and then the average values of radial chip distance (at the entrance) are obtained as described in Equation 1.

$$RCD_{(Average)} = (RCD_1 + RCD_2 + RCD_3 + RCD_4 + RCD_5 + RCD_6 + RCD_7 + RCD_8)/8 \quad (1)$$

In the same manner, all the radial chip distances are evaluated at different points and then their average is calculated. Then, the obtained experimental average chipping values are further considered for the optimization of parameters. Fig. 3.10 represents the amount of chipping on the same hole using a digital microscope and Profile projector.

Coordinate measuring machine (Accurate 564 spectra) is used to examine the hole's exit chipping, where the removed machined rod is taken into consideration for analyzing exit chipping of the hole. First time in the scientific world a coordinate measuring machine (*CMM-MH20i*) is used to quantify the exit chipping through the machined rod. An improved study has been carried out which compute and traces the height and radius of the conical shape which encourages trying CMM for the chipping quantification (Prakasvudhisarn et al. (2004).

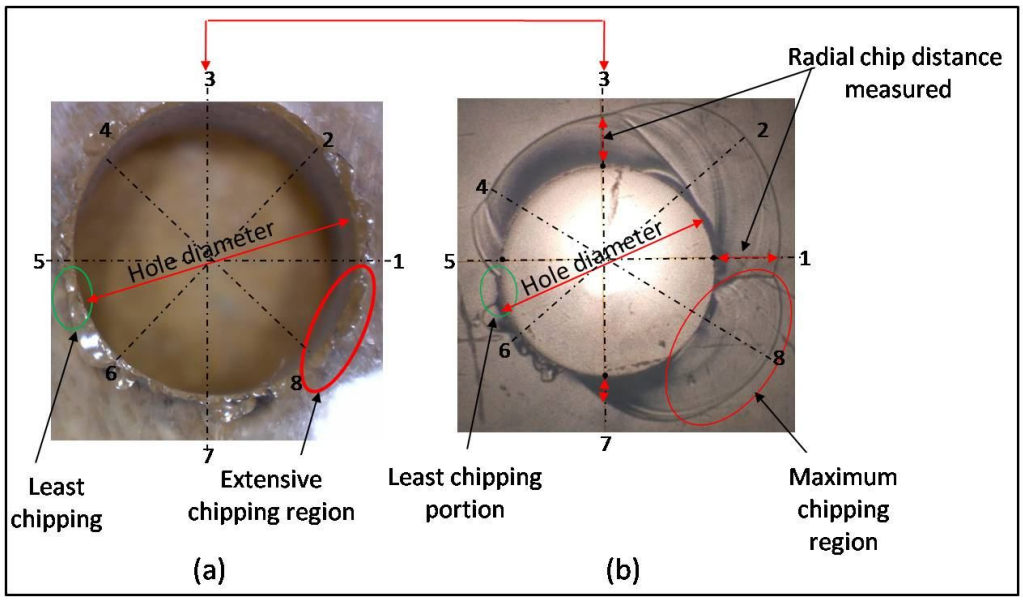

Fig. 3.10: Representation of amount of chipping on the same hole using: (a) Digital microscope; (b) Profile projector

CMM technique is based upon reverse engineering which compares the accuracy of various shapes and size of workpiece's profile. Its working is based upon stylus movement in which the touch-trigger probes collected discrete points on the workpiece surface; this system obtains enormous readings (errorless) of surface data that represent the shape of the sample. Several sizes of the probe can also be equipped with the CMM as per the size of the workpiece. Fig. 3.11 illustrates the movement of ruby rod on the machined rod surface to quantify the volume of chipping. As per availability, the least probe diameter of 0.5 mm and with a least count of 0.1 µm is installed.

Here, the machined/chip rod is used to validate the exit chipping on the hole. The reasons for using the machined rod as a means of exit hole chipping as already explained in Section 1.4.2.2. The CRD is derived as the difference between the exit radius of chip rod (R_c) and the entrance radius of chip rod (r_c) as shown in Equation 2.

$$CRD = R_c - r_c \quad (2)$$

The chip thickness (t_c) is stated as the vertical distance between the chip initiation point where the chipping propagates and the machined rod base point surface as in Fig. 3.11.

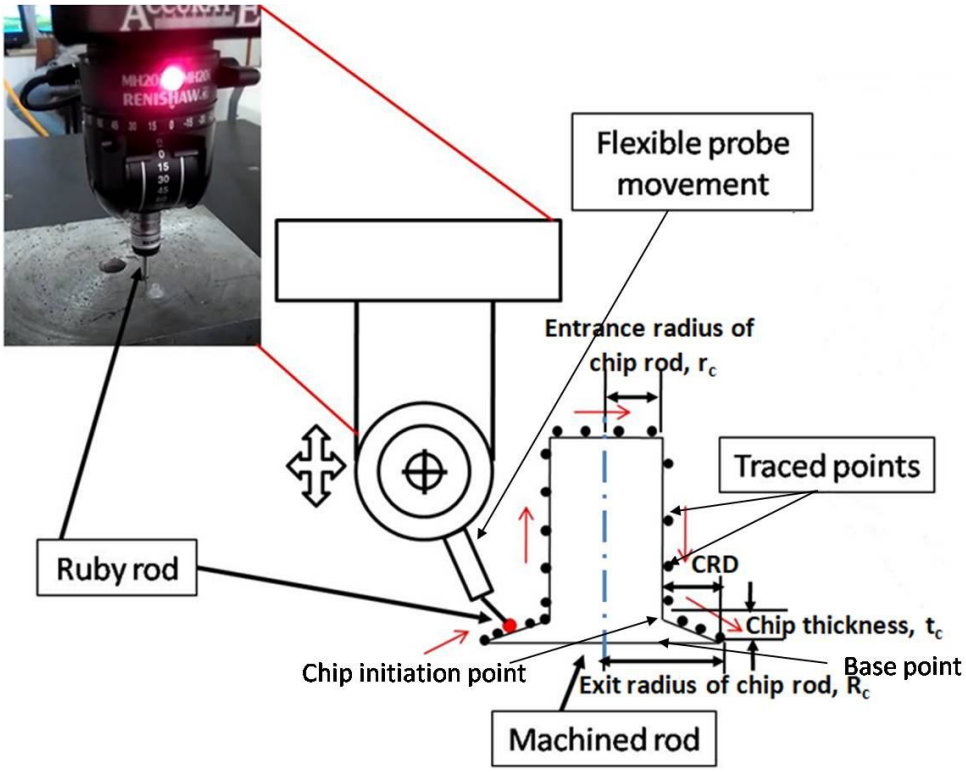

Fig. 3.11: Illustration of the movement of ruby rod on machined rod surface to quantify the CRD and t_c

Fig. 3.12 describes the entire CMM's set up which includes elements probe system and stylus, software connected PC and fixture. Fig. 3.13 and Fig. 3.14 depict the CMM graphical images that contain complete curvature of the machined rod produced after drilling in which several points are traced and the values at these points are deliberate in 2-D coordinates, which aided to evaluate the entrance radius of chip rod (rc), exit radius of chip rod (R_c) and chip thickness (t_c) for each trial. Hence, CMM traced the position data based on geometrical data. These traces generate better detailed information of the workpiece's measuring surface.

As shown in Fig. 3.13, a view of the ideal chip rod and original chip rod are stated. Initially, in tracing the values over the machined rod, troublesome related to irregular curve shape (represent as dash line) are occurring near hole entrance edges, the reason is machined rod is not fixed properly over the table. Also, owing to probe setting error, the round shapes are observed at the entrance corners of the machined rod. The movement of probe in the narrow curvature is complex to reach.

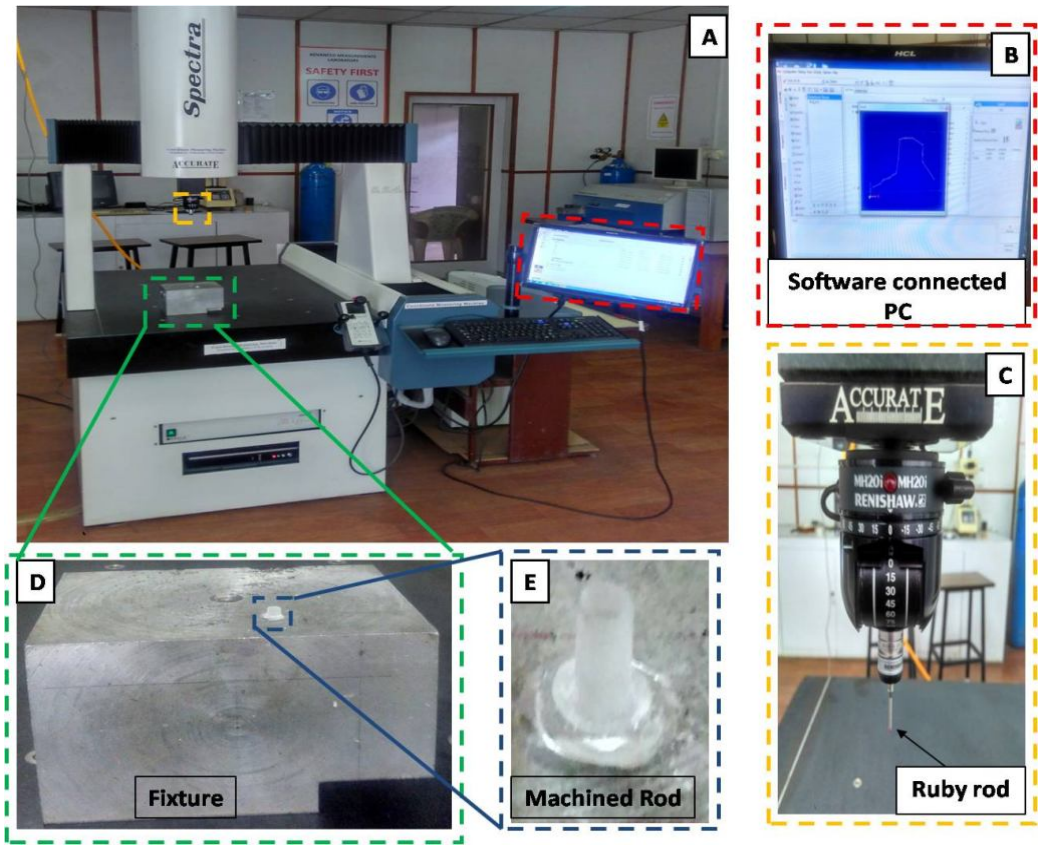

Fig. 3.12: Description of CMM's set up which includes: a) Complete CMM equipments; b) Probe system and Stylus; c) Software connected PC; d) Fixture e) Machined rod

Deviation error is an additional hindrance that occurs during point's tracing. It is observed that the increase in the quantity of measuring points on machined rod specimen leads to decrease in the deviation error.

In the case of Fig. 3.13, 16 discrete tracing points are considered. On another side, 22 tracing points are estimated in Fig. 3.14 for better accuracy. Hence, later on, appropriate machined rod shape is considered. As the machined rod size is too small, the diameter of the probe in CMM itself is a barrier to trace the maximum points. Hence at the maximum 22 points were traced as shown in Fig. 3.14.

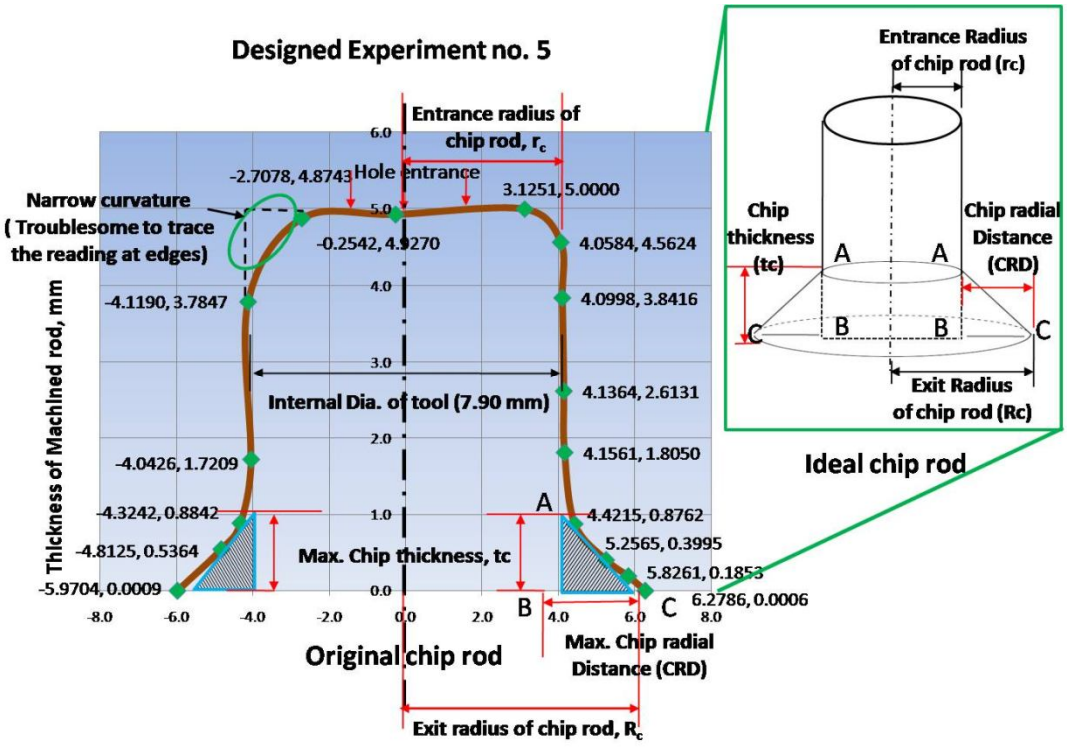

Fig. 3.13: Traced values captured on machined rod periphery deploying CMM; Inset: An ideal machined rod

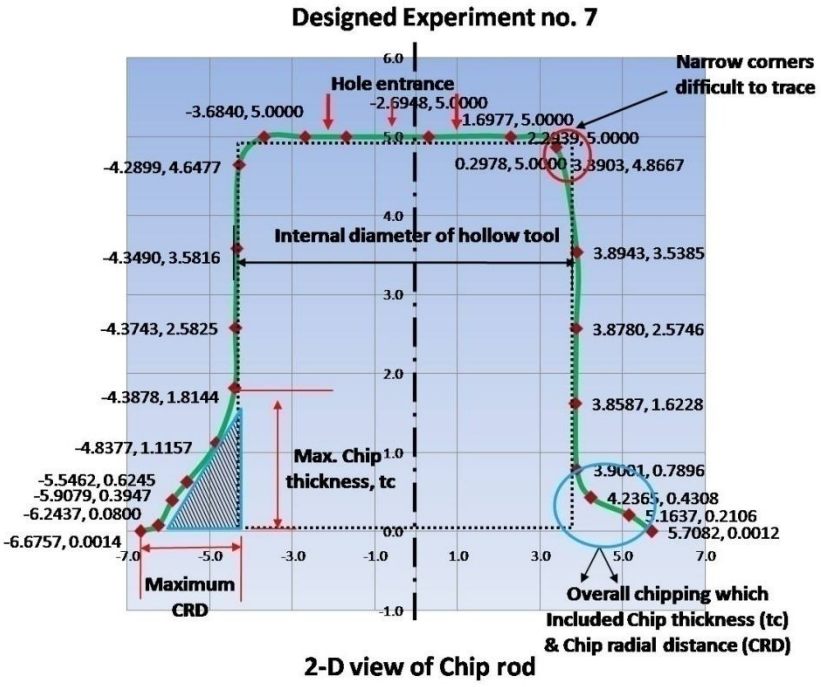

Fig. 3.14: Description of 2-D (X-Z cordinates) values at machined rod for estimating volume of chipping

Fig. 3.14 describes the extended (represent as hash type) line at the bottom of CMM's graph which demonstrates the required 'chipless' rod shape. In Fig. 3.13, points A to B is depicted as the maximum chip thickness (t_c), and points B to C are depicted as the maximum chip radial distance (CRD).

3.5.2 Tool wear

To evaluate the tool wear, weighing balance is used to weigh the different tools at various stages. It is applied to evaluate the weight loss (in %) between fresh tool, used tool after rotary ultrasonic machining (RUM), and conventional drilling (CD) process. After drilling blind holes by conventional drilling (CD) and rotary ultrasonic machining, the digital microscope (Celestron 44302 deluxe) is used for observing the tool wear of various diamond tools. Fig. 3.15 illustrates the equipments used in evaluating tool wear: (a) Weighing balance, (b) Digital microscope, and (c) Personal computer (PC). To evaluate the tool wear, the digital microscope is equipped with a personal computer and microscopic images are estimated at 3 different stages. These stages are: fresh tool, after RUM and after CD. For all 5 tools, wear is evaluated at two portions (lateral faces and end faces). A scanning electron microscope (SEM) is also used to observe the microscopic structure of the multi-shaped tool as shown in Fig. 3.7.

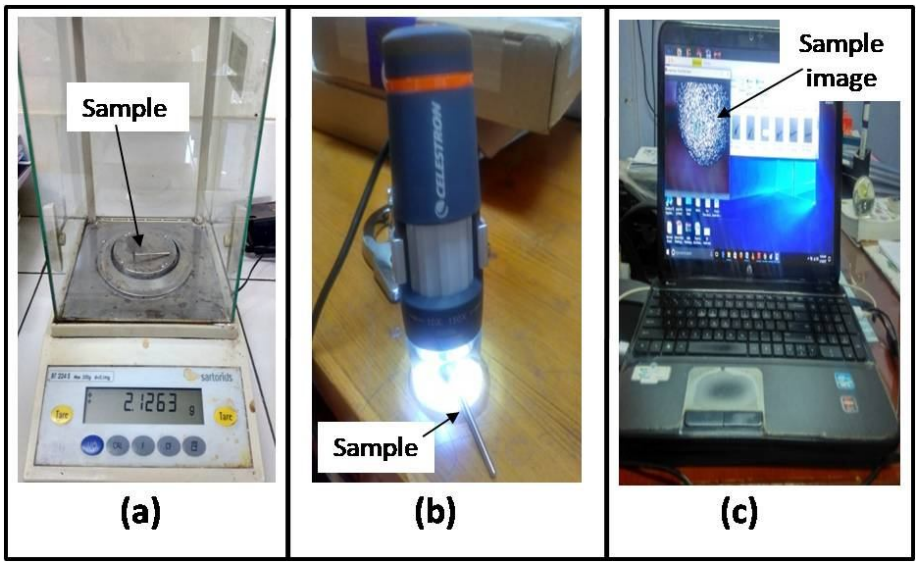

Fig. 3.15: Illustration of the equipments used in evaluating tool wear: (a) Weighing balance, (b) Digital microscope and (c) Personal computer (PC)

3.5.3 Average Surface Roughness

To evaluate the average (avg.) surface roughness of the internal region of the drilled hole, Mitutoyo surface roughness tester (Model: SJ 400) with a cut-off length of 0.25 mm is used. Fig. 3.16 illustrates the complete surface roughness tester including its parts. Avg. surface roughness quantification has been carried out on four different points on the inner surface of the drilled float glass hole specimen.

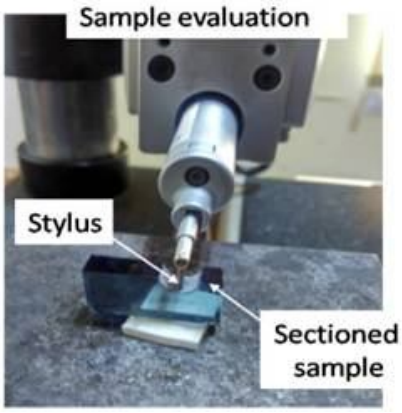

Fig. 3.16: Illustration of the complete surface roughness tester including its parts

Average surface roughness (R_a) is measured by moving the stylus on the inner region of the float glass samples parallel to its central axis. For the smaller size of the float glass samples, the samples are sectioned into two pieces for the appropriate measurement.

3.6 Evaluation of Volume of Chipping

After a closer of the machined rod, it is visualized that using the measurements such as CRD and t_c, the volume of chipping can also quantify. It is revealed that the total volume of the machined rod is equal to the volume of a cylinder plus the volume of a truncated cone. Fig. 3.17 depicts the evaluation scheme of a machined rod with all its measurements. Therefore, volume of chipping at hole exit is revealed as volume of truncated portion minus volume of cylinder portion (which is situated inside truncated portion only). It is a novel attempt to show the extent of the chipping at exit of the hole.

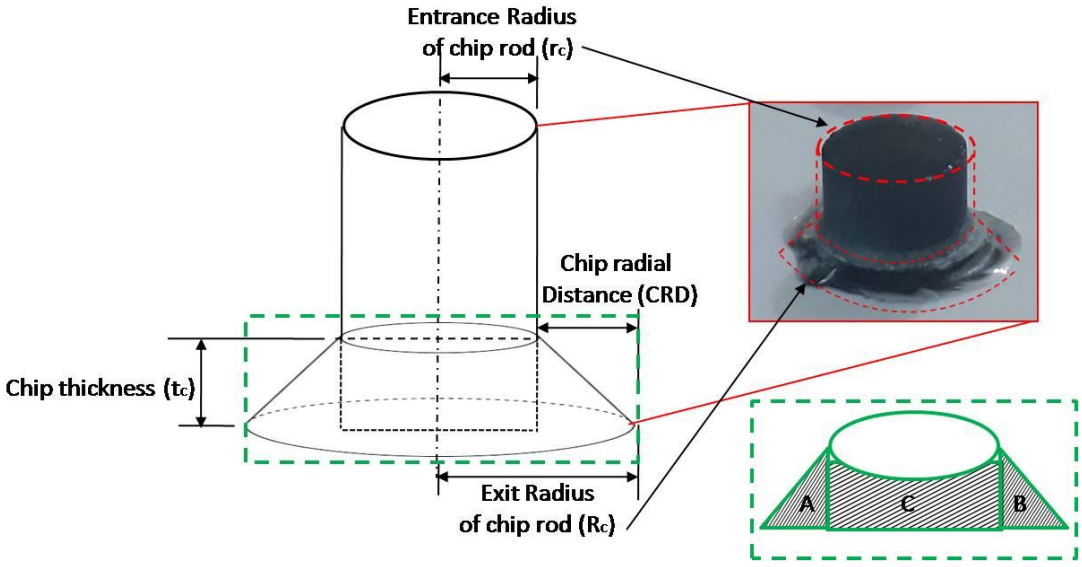

Fig. 3.17: Schematic diagram of machined rod in 3-D including its measurements

Volume of chipping = Volume of truncated portion – Volume of cylinder portion (3)

Volume of truncated portion,

$$V_t = (A + B + C) \quad (4)$$

$$V_t = \tfrac{1}{3}\pi(r_c^2 + r_c.R_c + R_c^2)t_c \quad (5)$$

Volume of cylinder portion,

$$V_{cyl} = C \quad (6)$$

$$V_{cyl} = \pi r_c^2 t_c \quad (7)$$

Volume of chipping,

$$V_c = V_t - V_{cyl} = (A + B + C) - (C) \quad (8)$$

$$V_{c=}\ \tfrac{1}{3}\pi(r_c^2 + r_c.R_c + R_c^2)t_c - \pi r_c^2 t_c \quad (9)$$

$$V_{c=}\ \pi t_c\ [\tfrac{1}{3}(r_c^2 + r_c.R_c + R_c^2) - r_c^2] \quad (10)$$

Where,

V_c – Volume of chipping, mm^3

V_t – Vol. of truncated portion, mm^3

V_{cyl} - Volume of cylinder portion, mm^3

r_c - Entrance radius of chip rod or Internal tool radius, mm

R_c - Exit radius of chip rod, mm

t_c - Chip thickness, mm

(R_c - r_c) - Chip radial distance (CRD), mm

The response result is consists of two sub responses, these are: a) Chip radial distance (CRD), (maximum); b) Chip thickness (t_c), (maximum). The values of chip radial distance (CRD), and chip thickness (t_c) are estimated using CMM in which at specific points on the machined rod, 2-D values are traced constantly. On another hand, entrance radius of chip rod (r_c) is equivalent to the internal tool radius. Hence, the volume of chipping at hole exit proximity could also be evaluated using Equation no. 10. These obtained values could further considered for parameter optimization.

3.7 Summary

The following summary is describing the experimental work performed for drilling the float glass samples. The rotary ultrasonic machining experimental setup is developed to drill holes in the float glass workpiece. There are 5 multi-shaped tools are used to create blind holes and 1 hollow abrasive coated tool is used for creating through hole. There are three categories of experimentation are performed. Firstly, multi-shaped tools based experimentation are performed for making blind hole and choosing the best tool among them for the least entrance hole chipping. Correspondingly, the best tool while considering least wear has been carried out using multi-shaped tools investigation. Secondly, the L18 experimental method is used to make through hole so that chipping at hole entrance and exit are further analyzed to optimize the parameters. Along with it, average surface roughness is also evaluated to enhance the overall hole quality. Thirdly, conventional and rotary ultrasonic drilling experimentation are performed on pre-tempered float glass at optimize parametric condition. Where, its prime concern is to compare the hole entrance chipping size before and after tempering process. The characterization techniques used for analysing the drilled hole quality such as coordinate measuring machine (CMM), scanning electron microscope (SEM), optical microscope and profile projector, weighing balance and surface roughness tester are used for measuring and computing the hole quality and tool wear. Where, coordinate measuring machine (CMM) is a novel technique to use for chipping evaluation at hole exit.

CHAPTER 4: RESULTS AND DISCUSSION

This chapter contains the results and discussion related to the drilling of float glass specimen and subsequently its outcome responses into six categories. In the first category, results related to the effect of using multi-shaped tools while making blind hole on entrance chipping are analyzed. In the second category, the effect on multi-shaped tool wear is discussed in which the tools' end and lateral faces are analyzed. In the third, fourth, and fifth category, Taguchi optimization technique is performed in which effects of various parameters (i.e. spindle speed, feed rate, and vibration amplitude) on hole entrance chipping, hole exit chipping, and hole internal surface roughness (avg.) region are elaborated, respectively. In the last category, the comparison between the hole entrance chipping near hole edges before and after the tempering process has been carried out.

4.1 Effect of Multi-Shaped Tools on Entrance Chipping during Blind Hole

During the drilling process using various multi-shape tools, it is noticed that the tool surface (face) area that is initially in contact with the surface area of float glass is considered as the most effective cutting zone for the generation of stress. Where, the lesser stress concentration leads to the minimum amount of chipping as well as cracking on the work sample. When the impact forces are applied by the tool over the workpiece periphery, at that moment the micro-cracking as well as chipping are propagated around the top edges of the work sample and consequently dislocate the chips particle over the workpiece. Chipping and cracking are occurring by the high tensile stresses in the sub-surface region (Jiao et al. (2005)). Because it is reported that the float glass material having the compressive strength of 212 MPa, that is much better than the tensile strength (50 MPa) (Wang et al. (2018)). Therefore, major concern while drilling is to reduce the stress value up to the tensile strength of the workpiece sample, where the chippings nearby edges were assumed to be initiated (Xu et al. (2014)). It is expected that the maximum amount of tensile stress was generated at 30° axis on both sides of the impact axis (Ghahramani and Wang (2001)). In the case of multi-shape tools, the angle of impact on the workpiece surface varies, consequently, it could affect the chipping quantity. It could be possible that chipping could be diminished by using sharp tools (Jiao et al. (2005)), because, the rolling action and angle of penetration of the tool's abrasive are contributed to the chipping over hole periphery.

Float glass specimen undertakes to combine the effect of tensile stress and shear stress during drilling process that effects the chipping measurement. Hence, as the stress propagation reduced, the chances of chip formation also decreased (Ding et al. (2014)). It was stated that shear force is always maximum at the outer region and minimum or negligible near neutral axis. Also, in a research study, it was mentioned that the maximum amount of shear stress was observed at 45° from the axis where the impact force happened. The reason behind the occurrence of chipping in each tool case is described as follows.

4.1.1 Pinpointed conical tool: Tool 1

In this case, tool tip firstly touches the float glass sample with some impact and the tensile forces which are not equally distributed. Because it is acted on a single point, where the initial angle of contact is larger (near about 60^0) which leads to an increase in tensile and shear stresses and reached its critical value (where the cracks, as well as chipping, starts to propagate drastically). Fig. 4.1 depicts the criteria of drilling by the pinpointed conical tool. Fig. 4.2 (a) shows the profile image of drilled hole after CD and Fig. 4.2 (b) represents the image of drilled hole after RUD.

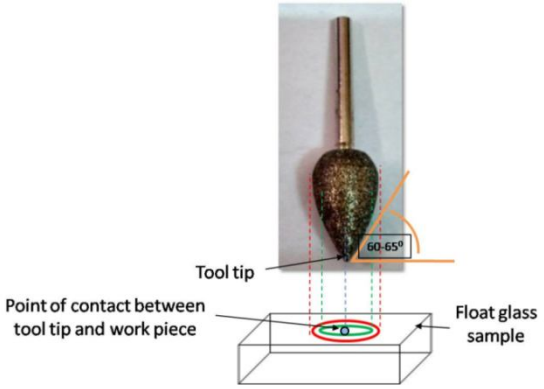

Fig. 4.1: Criteria of drilling by the pinpointed conical tool

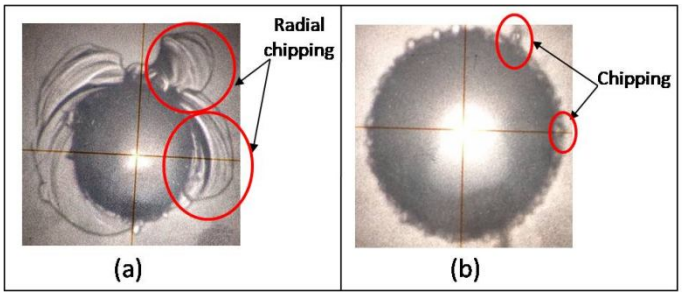

Fig. 4.2: Profilometer images of machined blind holes by the pinpointed conical tool (a) By conventional drilling (CD) (b) By rotary ultrasonic drilling (RUD)

Therefore, the angle of impact on the workpiece surface affects the chipping quantity (Ghahramani and Wang (2001)). Hence, this tool creates a maximum of chipping, and the same is also validated in a successive portion of this chapter. Hence, it seems that pin pointed conical tool is not appropriate to drill hole with minimum chipping.

4.1.2 Flat cylindrical tool (Height > Dia.): Tool 2

In this type of tool, tool pressure exerted over the workpiece periphery is equivalent throughout the contact surface. At the time of machining, the tool is perpendicular to the work sample which is 90^0 angle of contact. Fig. 4.3 depicts the criteria of drilling by a flat cylindrical tool (Height > Diameter). In the profile picture of Fig. 4.4 (a) and Fig. 4.4 (b), it was also noticed that conventional drilling generating more chips in form RCD (the reason is explained in section 4.1.1.). In the case of CD, some rotational streaks are also visualized that reduce its hole quality.

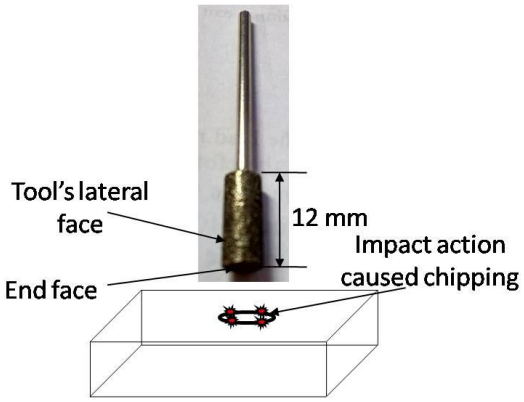

Fig. 4.3: Criteria of drilling by a Flat cylindrical tool (Height > Diameter)

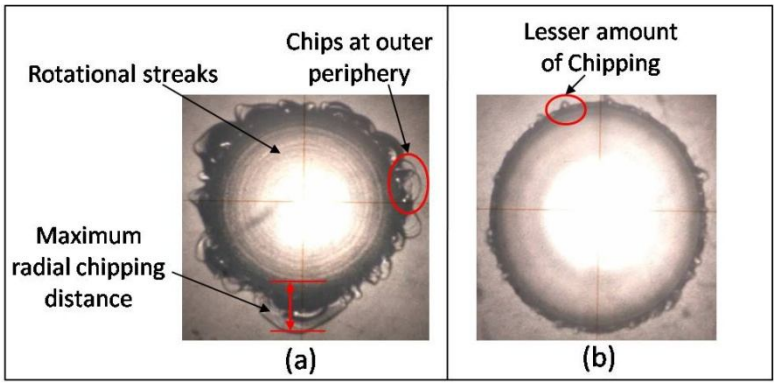

Fig. 4.4: Images of machined blind holes by CD and RUD by a Flat cylindrical tool (Height > Diameter) (a) Blind hole by CD (b) Blind hole by RUD

The chipping is easily formed to the extreme edge of the tool owing to the uniform pressure of the end face. Also, the chipping is suppressed by the end face in the middle and there is a free contact of the abrasives at the extreme edge of the end face. Therefore, it is abrasive at the lateral face of the tool which dominates the shearing mechanism at the outer periphery of the hole. That could be the cause of extreme chipping (Malkin and Guo (1996)).

4.1.3 Flat cylindrical tool (Height < Diameter): Tool 3

For this kind of tool as in case of Tool 2, a similar trend of shearing action followed by tensile action take place. In Tool 3, as the height of the tool is less than the diameter, the lesser tool's height means the lesser effective area in contact with the workpiece periphery for drilling that plays a vital role to reduce a little bit of chipping than Tool 2. Where lesser effective cutting area means less cutting stresses and it is expected a low rate of chipping. Fig. 4.5 illustrates the criteria of drilling by a flat cylindrical tool (Height < Diameter). Fig. 4.6 (a) and Fig. 4.6 (b) shows the chipping images of machined blind holes by CD and RUD by a Flat cylindrical tool (Height < Diameter).

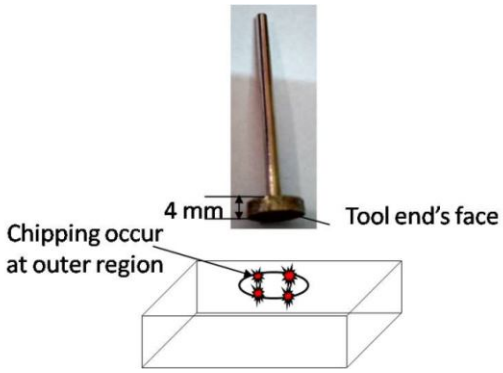

Fig. 4.5: Criteria of drilling by a Flat cylindrical tool (Height < Diameter)

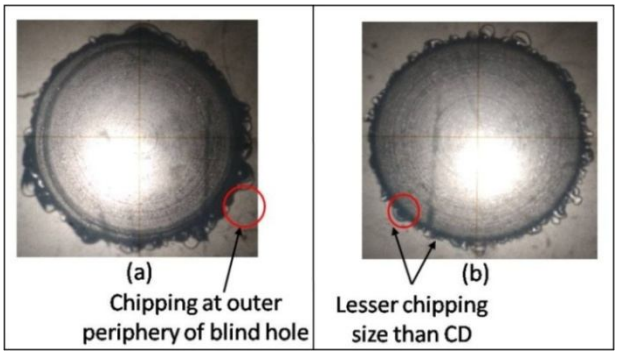

Fig. 4.6: Chipping images of machined blind holes by CD and RUD by a Flat cylindrical tool (Height < Diameter) (a) Blind hole by CD (b) Blind hole by RUD

Therefore, it shows a better result than Tool 1 and Tool 2. Yet, chipping is still occurring.

4.1.4 Hollow abrasive tool: Tool 4

Hollow tools are widely used in industries and researchers' work (Liu et al. (2014); Jiao et al. (2005); Li et al. (2006)). It generates a lesser amount of shear stress as well as tensile stress, because of their contact area. Fig. 4.7 represents the criteria of drilling by the hollow abrasive tool. . The outer and inner regions shown in Fig. 4.8 (a) and Fig. 4.8 (b) is due to the hollow tool. The thickness of the tool is predicted by the images as shown in Fig. 4.8 (b). The problem of chip formation remains there.

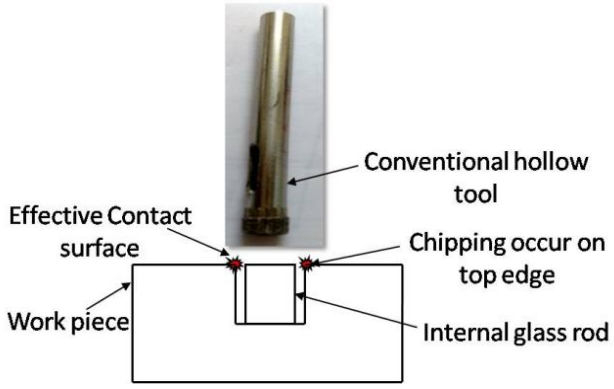

Fig. 4.7: Criteria of drilling by the hollow abrasive tool

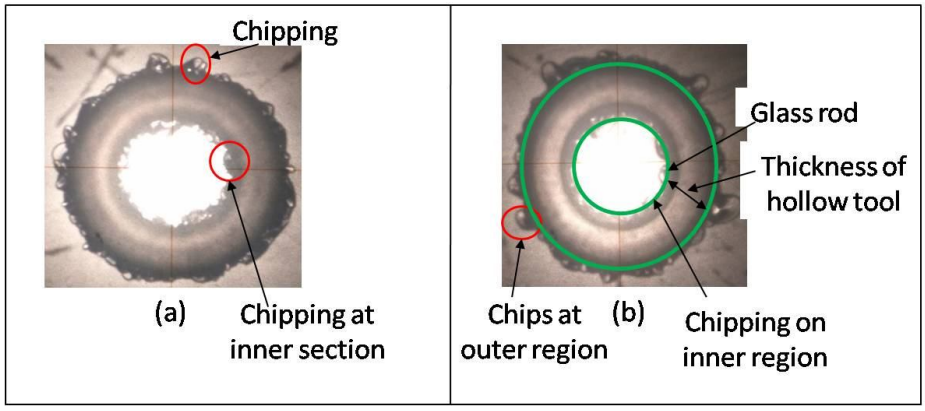

Fig. 4.8: Chipping images of machined blind holes by the hollow abrasive tool (a) Blind hole by CD (b) Blind hole by RUD

In this case, less area is subjected to lesser cutting stresses and it is expected a low rate of chipping there. It is usually round in shape from the tool end face

4.1.5 Concave circular tool: Tool 5

In this technique, the grinding mechanism has played a crucial role in the formation of the hole. Fig. 4.9 represents the criteria of drilling on float glass by the concave circular tool. Initially, drilling occurred near the central region as visible in a first smaller ellipse (red dash) on the workpiece sample. In this region, maximum tensile force and shear force occur. Afterward, as the tool exerts pressure towards the workpiece, depth of cut keeps on increasing as noticeable in the second largest ellipse (green round dot). Similarly, drilling takes place continuously up to the size of tool diameter. Therefore, maximum of combined (tensile and shearing) action is not reached to the outer region of the hole. Another reason is that the angle of contact between the tool and workpiece region is near about 20^0 approx. which states that the maximum tensile stress value point (i.e. 30^0) is not reached (Malkin and Guo (1996)). Hence, the chipping is least in that case. Fig. 4.10 shows the images of blind hole machined by the concave circular tool at two conditions i.e. after CD and after RUD process.

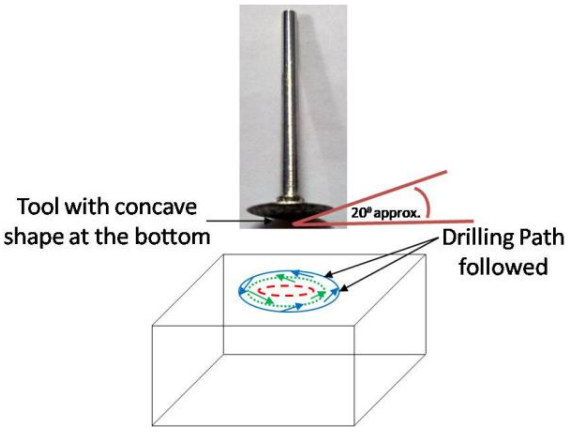

Fig. 4.9: Criteria of drilling by the concave circular tool

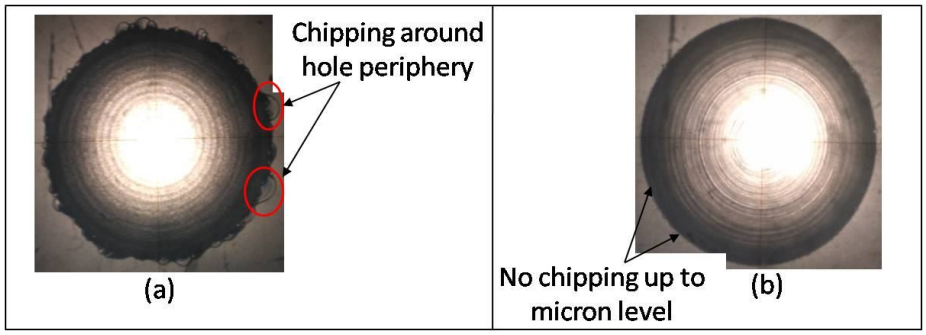

Fig. 4.10: Profilometer images of blind hole machined by the concave circular tool (a) Blind hole by CD (b) Blind hole by RUD

In the concave shaped tool, shearing action is very significant. Whereas, float glass material has more shearing strength which means chances of occurrence of the critical point (chipping) is least. Therefore, concave shape tool is considered most efficient than other tools.

It is noticed after visualizing each profilometer image of all five tools; found that lesser radial chip distance (RCD) is noticed by RUD as compare to CD. The reason is explained that during RUD, the tool vibrates at some specific ultrasonic frequency; it is observed that the diamond sintered on the end face of the drilling tool is not in continuous contact with the workpiece (*www.makeitfrom.com)*. During each vibration cycle, the diamond particles on the end face of the tool penetrate the workpiece sample for a specific period. It means effective cutting time is lesser in RUD than CD process (Wang et al. (2017a)). Hence, as per this mechanics, low chipping is expected in case of RUD. During CD, abrasives over the tool are in constant contact with an effective cutting surface of float glass sample, because there is no vibration generated during drilling as in case of RUD. Hence the machining occurs by the action of direct shearing and extrusion and it leads to more chipping over float glass periphery rather than RUD.

Hence, according to the tool shapes, each tool has its own path of drilling and effective contact area which influences the chip formation and hole quality. Specifically, only in the case of pin pointed tool, the effective contact area is concentrated only on a single point over the workpiece and that impactful strike of the tool tip over the specimen leads to drastic incline in stresses over the tool face. On another side, concave circular tool has a negligible effect of tensile stress. Only the shearing action is a major cause of chipping that is negligible during RUD as compare to CD. Also, stated that during CD, abrasives loaded over the tool periphery are in continuous contact on the specimen's drilled to be surface. As there is no simple harmonic motion of the abrasives, the tool is only rotated and feeding in the direction of its axis with respect to the workpiece. Hence, the cutting force is continuous throughout the process and machining occurs by the action of direct shearing and extrusion leads to more chipping over float glass periphery. It is one of the major reasons for hole chipping.

In rotary ultrasonic machining, the diamond abrasives electroplated over the hollow tool was rotated at a high constant speed, and in the meantime, the tool also vibrates in simple harmonic motion with an ultrasonic frequency (Lv et al. (2016). Coating thickness is taken as 1 mm for the abrasive coated hollow tool. In RUM process, the abrasive impregnated over the tool end face is

traveled in definite sinusoidal paths in the axis of the workpiece with some specific tool revolution. Therefore, it exerts low tool pressure on the cutting periphery of the workpiece and also provides lesser tool wear rate. That shows the mechanism behind the material removal during drilling process.

The trajectory motion of the abrasive impregnated over the tool end face could be assumed as:

$$x = r\sin(\omega t) \quad (12)$$

$$y = r\cos(\omega t) \quad (13)$$

$$z = f_r t + A\sin(2\pi f t) \quad (14)$$

where x-y-z is the path followed by the abrasive in the directions, ω is the angular velocity in radian per sec, t is the effective time in sec, r is the tool radius in mm, f_r is the feed rate in mm/min, A is the vibration amplitude in μm and f is the ultrasonic frequency in cps. As per trajectory motion equations, the periodic oscillation of the abrasive trajectories is illustrated in Fig. 4.11.

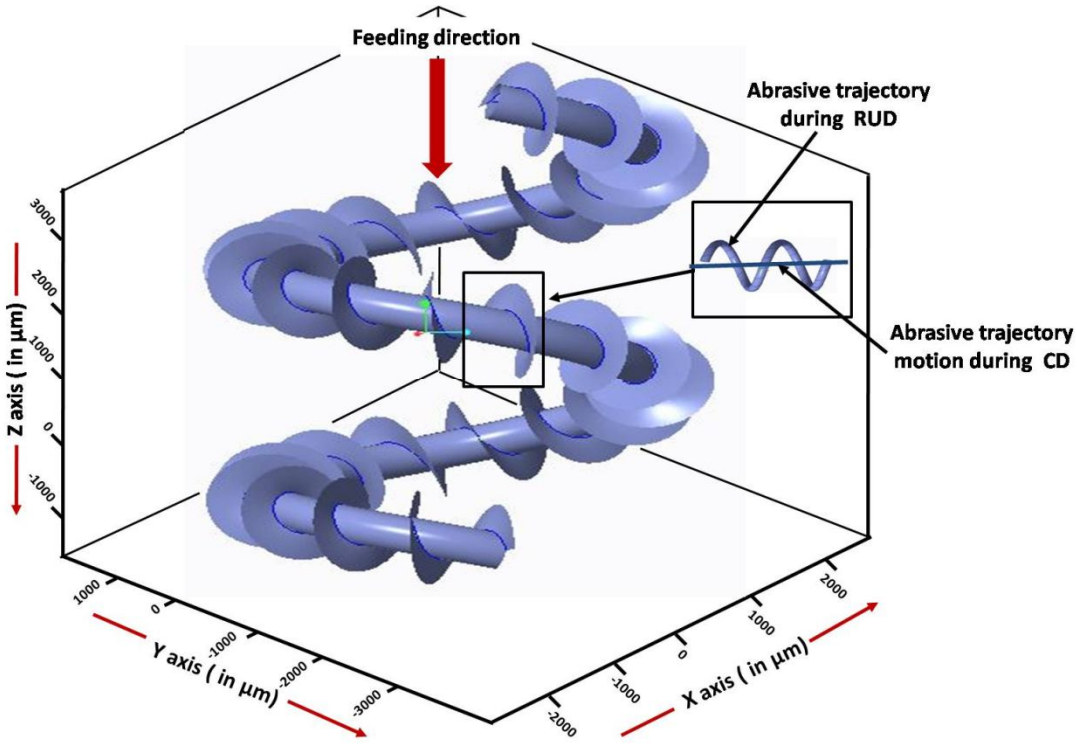

Fig. 4.11: Schematic representation of the abrasive feeding motion with ultrasonic vibration (Case of RUD process) and without ultrasonic vibration (Case of CD process

Hence, it is revealed that there is no continuous contact throughout machining (Feucht et al. (2014)). Fig. 4.12 represents the abrasive feeding motion with and without ultrasonic vibration.

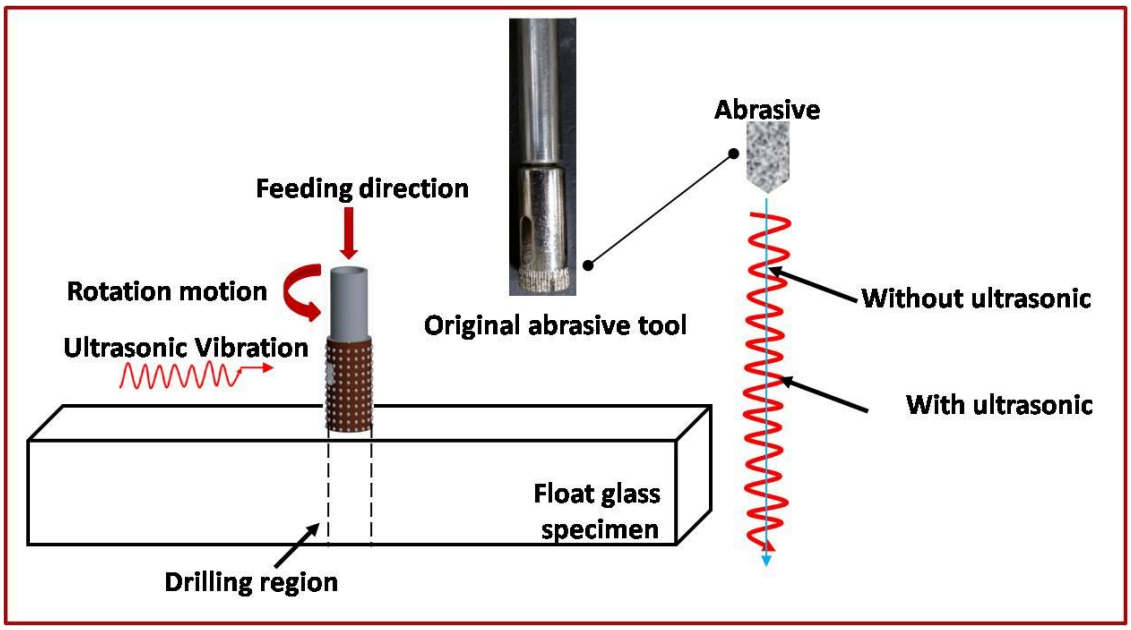

Fig. 4.12: Representation of the abrasive feeding motion with and without ultrasonic vibration

Furthermore, low pressure owing to ultrasonic actuation over the tool help to resist the maximum first principal stress to reach up to the ultimate tensile strength of the workpiece. Hence, as per this mechanics, low chipping is expected during rotary ultrasonic drilling process.

4.1.6 Quantification of Entrance Chipping of Multi-Shaped Tools

Radial chip distance (RCD) is computed precisely on each hole, the outcome of maximum, minimum and average RCD observed (according to section 3.6.1) while using different tools with CD and RUD processes are shown in Table 4.1. Fig. 4.13 shows a comparative trend of average RCD with respect to their corresponding tools by CD and RUD. During CD, it is cleared by visualizing the bar chart that among all 5 tools, the pinpointed conical tool possessed the highest average RCD i.e. 0.8125 mm.

Table 4.1: Radial chip distance (RCD) for CD and RUD process by 5 tools

S. no.	Types of Tool	Maximum /Minimum RCD for CD, mm	Maximum /Minimum RCD for RUD, mm	Avg. RCD for CD, mm	Avg. RCD (mm) for RUD, mm
1.	Pin pointed conical tool	1.387/0.238	0.803/0.182	0.8125	0.4925
2.	Flat cylindrical tool (Height > Dia.)	1.23/0.231	0.371/0.108	0.7305	0.2395
3.	Flat cylindrical tool (Height < Dia.)	1.195/0.182	0.344/0.098	0.6885	0.221
4.	Hollow abrasive tool	1.115/0.150	0.407/0.102	0.6325	0.2545
5.	Concave circular tool	0.745 /0.138	0.208/0.021	0.4415	0.1145

The concave circular tool has creating lowest average RCD i.e. 0.4415 mm. A similar trend is found during RUD process, highest average RCD by the pinpointed conical tool is 0.4925 mm and the lowest average RCD is 0.1145 mm by the concave circular tool.

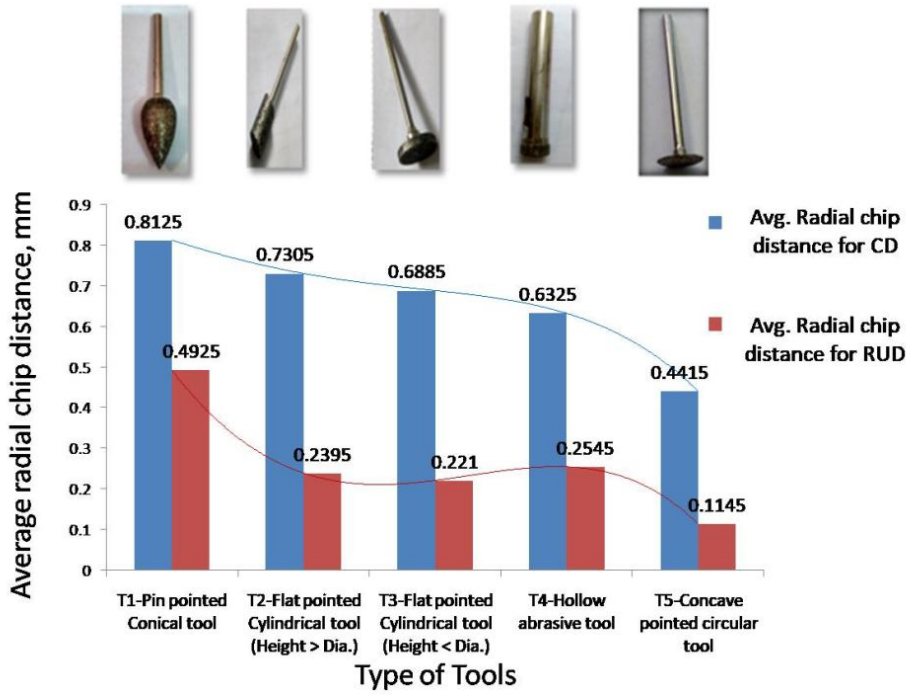

Fig. 4.13: Comparative trend of RCD with respect to their corresponding tools by CD and RUD

Hence, after analyzing profile images and trends of RCD, the following points are postulated. These are: a) Blind holes produced during RUD possess lesser average RCD than CD b) Sequence of descending order of average RCD with respect to different tools are:

T1>T2>T3>T4>T5 = Very high>High>Medium>Low>Very low

Hence, concave circular tool is found as the best tool among others particularly to get low average RCD. Fig. 4.14 depicts the microscopic image of the best blind hole created by concave circular tool during RUD.

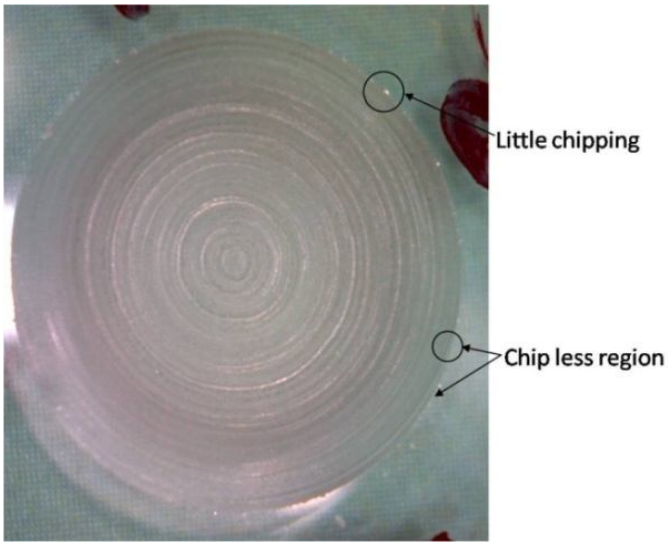

Fig. 4.14: Microscopic image of the blind hole created by concave circular tool

It is visualize that concave circular tool has possessed a negligible chipping amount near hole corners. It can boost up the application of float glass material in the micro-electronics and energy based industries.

4.2 Effect on Multi-Shaped Tool Wear during Blind Hole Drilling

All the five tools and its individual faces are observed in Fig. 4.15 and Fig. 4.16. Fig. 4.15 depicts the wear over the tool's lateral face while creating blind holes in three stages: (a) Fresh tool; (b) After RUD; (c) After CD. Fig. 4.16 illustrates the wear over tool's end face in three stages i.e. fresh tool, after RUD and after CD. Here, all the tool wear studies have been reported at constant machining time. Although, more machining time leads to more tool wear. But, for the present study machining time (theoretically) is expected to be constant for every cutting

condition. Subsequently, machining time (T_m) is estimated as 12.0 seconds using $T_m = L/f_r$ for all the cases. Where, L = length/depth of hole (3 mm), feed rate (f_r) is 0.25 mm/sec.

For the diamond abrasive coated tools, wear occur because of three combined mechanisms such as attrition wear, grain fracture, and bond fracture (Tsuwa (1964)). In case of attrition wear, a combination of a cutting force and sliding force directly affects the formation of chips and growth of wear flat. Maximum of tool's distortion was noticed by attrition wear. Remaining tool's deformation is happened by the fracture within the grains and it removes abrasive fragments. Some distortion also found by a bond fracture because of dislodging of abrasive grains over tool surface.

4.2.1 Tool's Lateral Face

The lateral face of the tool is not in direct contact with the machined to be surface. So, stress concentration near this region is much lesser. There is a small amount of noticeable discrepancy in the microstructure of the diamond grains on the tool lateral faces of 5 tools as prescribed in Fig. 4.15. Some dislodging of grains could be visible at the corner of the tool (close to the end face) as in case of Tool 5 (Fig.4.14). Correspondingly, length of the lateral face can be reduced up to certain extent. Microscopic images are captured here, to validate the tool wear in CD and RUD with respect to the unused tool. After examining the lateral face of all the tools, it was found that grains are dislodged over the tool's periphery, which is heavily visible in CD's used tool than RUD's used tool. In case of tool 3, size of wear flat is more after CD as compare to RUD. Flat is defined as the straight surface initiated over the face of the abrasive (like in a single point cutting tool) by the action of feeding of tool towards the workpiece. Wear flat stated that when the frictional forces increase drastically between the tool and workpiece interface and significantly cause the surface damage. During RUD process, the contact between the tool and workpiece is in discontinuity that permits the heat to dissipate rapidly. Later on, lesser generation of friction and stresses take place as compare to CD process.

TOOL 1: Pin pointed conical tool's Lateral face

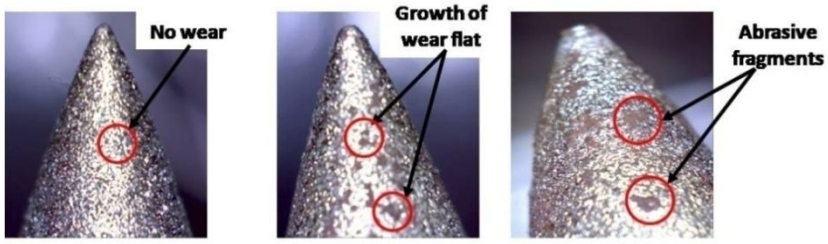

TOOL 2: Flat cylindrical tool's Lateral face (Height > Dia.)

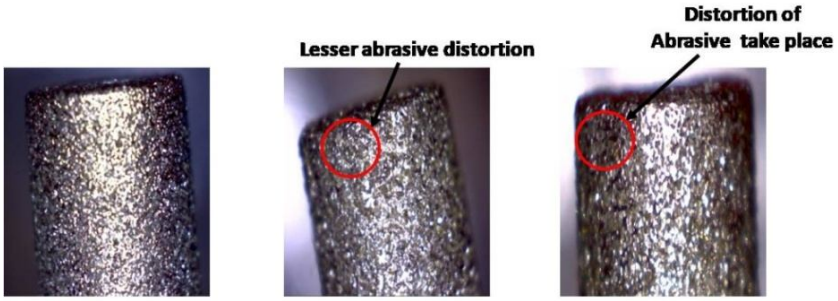

TOOL 3: Flat cylindrical tool's Lateral face (Height < Dia.)

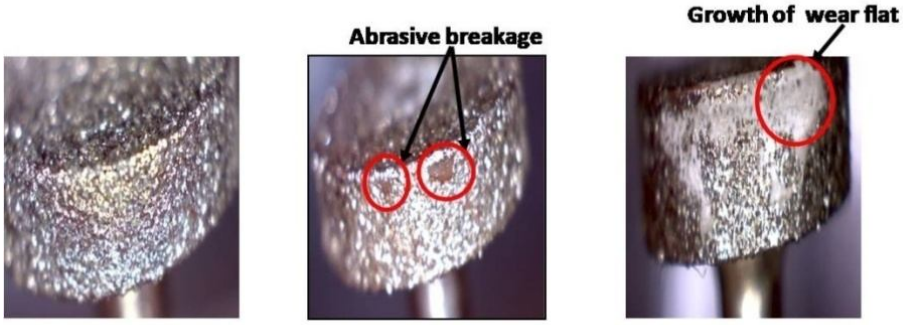

TOOL 4: Hollow abrasive tool's Lateral face

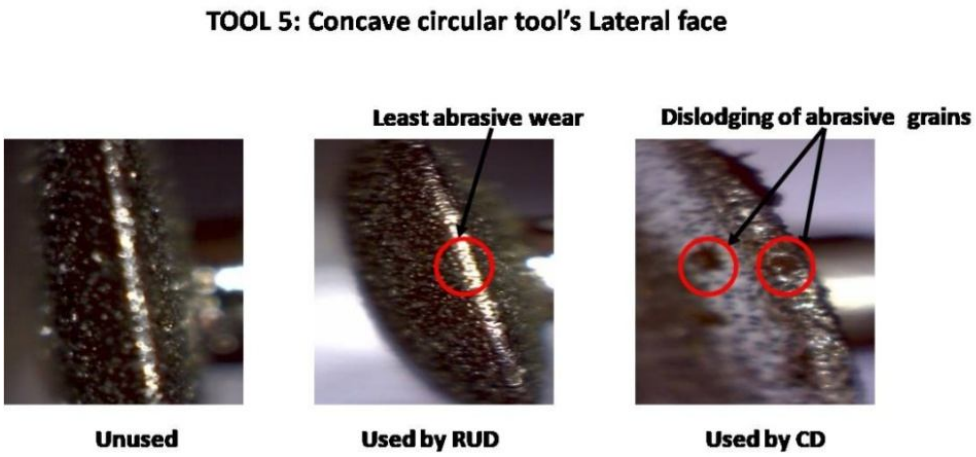

Fig. 4.15: Microscopic images of the lateral face of all the tools at three stages

Added, in case of the hollow abrasive tool (tool 4) and concave circular tool (tool 5), little dissimilarity in the microstructure of diamond grains is noticed in microscopic images. Also, it is observed that in most of the cases lateral face of the tool is not in direct contact with the machined to be surface. So, stress concentration near this region is much lesser such as in concave circular tool (tool 5). The reason for lesser stress generation at lateral face of the tool is because of the occurrence of lesser cutting force that subsequently provides lesser tool wear (Jain and Pandey (2016); Singh and Singhal (2015)). On a flip side, the lateral face of the pin-pointed conical tool (tool 1) is continuously in contact with the machined surface. So, it could also generate heavy chipping and cracking over the hole periphery.

4.2.2 Tool End Face

During drilling by the diamond abrasive coated tool, at the tool's end face, few diamond grains are dislodged and washed away after machining because of bond fracture action. Fig. 4.16 illustrates the end face of the tools in different stages. Some diamond grains were pulled out of the metal bond prematurely, before completing their effective working lives. It was mentioned that the impact force and high temperature leads to deterioration of the interfaces between diamond grains and base metal bond. It will further lead to the occurrence of chipping over the workpiece. Normally, wear at the tool end face occurs due to grain fracture (Li et al. (2006)). More tool wear observed in CD than RUD (Zeng et al. (2005)). Hence, attrition wear dominates in case of RUD followed by bond fracture wear.

TOOL 1: Pin pointed conical tool's end face

TOOL 2: Flat cylindrical tool's end face (Height > Dia.)

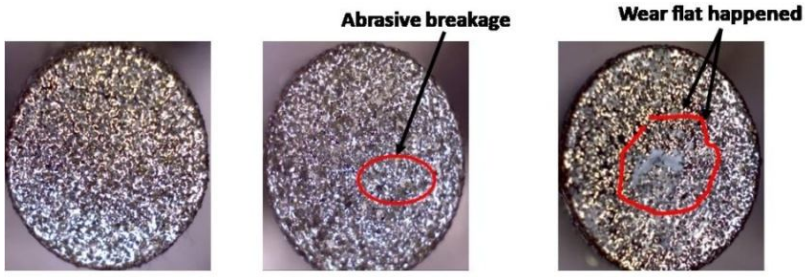

TOOL 3: Flat cylindrical tool's end face (Height < Dia.)

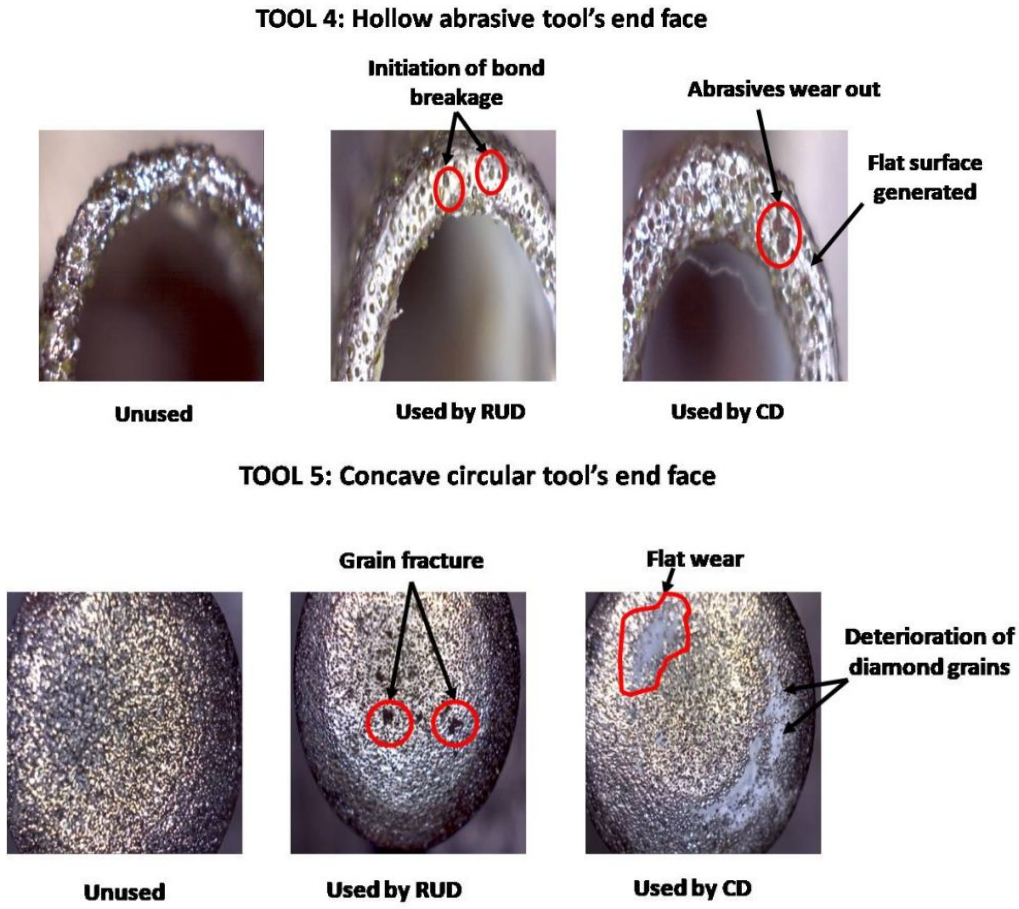

Fig. 4.16: Microscopic images of all tools' end face surfaces at three stages. These are unused, used by RUD, and used by CD

Flat cylindrical tools (tool 2 and tool 3) are showing deterioration of the diamond grains which is caused by the impact force. This deterioration can also cause chipping and cracking over work specimen.

Fig. 4.17 (a) represents the grain particles on tool face for a fresh tool. Abrasive distortion is visualized on used tool periphery after drilling holes on float glass specimen by CD process as shown in Fig. 4.17 (b). Fig. 4.18 (a) shows the image of the fresh face of hollow abrasive tool and Fig. 4.18 (b) demonstrates the end face of the hollow tool which is showing the occurrence of wear flat and grain fracture after creating 9 holes by RUD. By aiding these magnified images, better understanding is achieved about tool wear for various aspects. It is noticed that during drilling process the conical shape of the abrasive got tear apart. The reason behind the tearing distortion of the abrasives is caused by impact action that leads to continuous increase in cutting

temperature. Latterly, reduces its internal strength then the actual abrasive shape has started changing and finally it becomes wear flat as shown in Fig. 4.18 (b). In the magnified image of Fig. 4.18 (c), the dislodging of abrasives is noticed on the tool periphery. The reason is that the abrasive dislodging is generally occurred because of weak bond strength between the tool's metal base and abrasive particle. Sometimes, during drilling process, the abrasive has been dislodged over the tool face even starting the cutting operation because of its fragile bond strength.

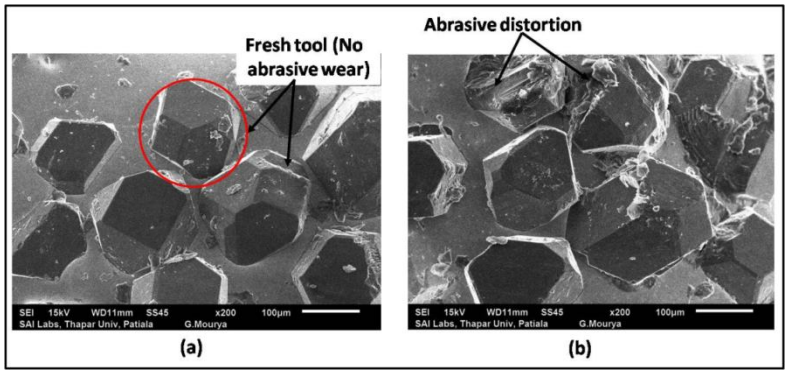

Fig. 4.17: Illustration of grain particles on tool face. (a) Fresh tool with no abrasive grain wear, and (b) Used tool after performing CD process showing abrasive distortion

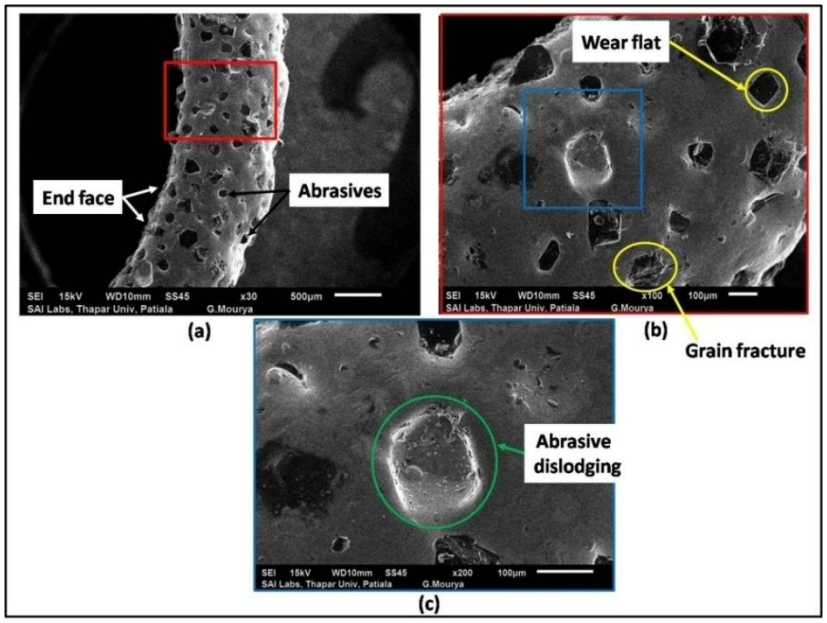

Fig. 4.18: Microscopic images showing tool wear with different magnification after drilling holes by RUD process. (a) End face of Hollow abrasive tool. (b) Magnified image of hollow tool depicting grain fracture. (c) Tool image showing abrasive dislodging

4.2.3 Tool Wear Weight Analysis

In this study, to estimate the tool wear after RUM and CD processes, weight (in gm) of the 5 tools are computed. In Table 4.2, weight loss (in %) between the unused tool and used tool by CD as well as an unused tool with respect to the used tool by RUM are evaluated.

Fig. 4.19 represents the comparison of weight loss (in %age) between new tool and CD tool as well as new tool and RUM tool, respectively.

Table 4.2: Percentage change in weight loss between unused tool, used tool by CD and used tool by RUM process

Tool no.	Tool type	New tool weight (gm)	Used tool weight after CD (gm)	Used tool weight after RUM(gm)	Weight loss (in %) between New tool and CD	Weight loss (in %) between New tool and RUM	Weight loss (in %) between CD and RUM
Tool 1	Pin-pointed Conical tool	5.772	5.150	5.222	10.78 %	9.53 %	1.38 %
Tool 2	Flat cylindrical tool (Height > Dia.)	2.772	2.546	2.582	8.15 %	6.85 %	1.39 %
Tool 3	Flat cylindrical tool (Height < Dia.)	2.238	2.085	2.132	6.84 %	4.74 %	2.20 %
Tool 4	Hollow abrasive tool	3.826	3.580	3.674	6.43 %	3.97 %	2.56 %
Tool 5	Concave circular tool	2.234	2.124	2.190	4.92 %	1.96 %	3.01 %

Additionally, the highest percentage of weight is reduced in case of tool 1 by both CD and RUM i.e. 10.78 % and 9.53 %, respectively. Correspondingly, tool 5 possessed a minimum percentage of weight loss i.e. 4.92 % after CD and 1.96 % after RUM process, respectively.

Overall, in case of each tool, the RUM mode is showing lesser tool wear. It may be because, in RUM process, the contact between the tool and workpiece is in discontinuity that permits the heat to dissipate rapidly, and consequently, lesser generation of friction and stresses take place as compare to CD process.

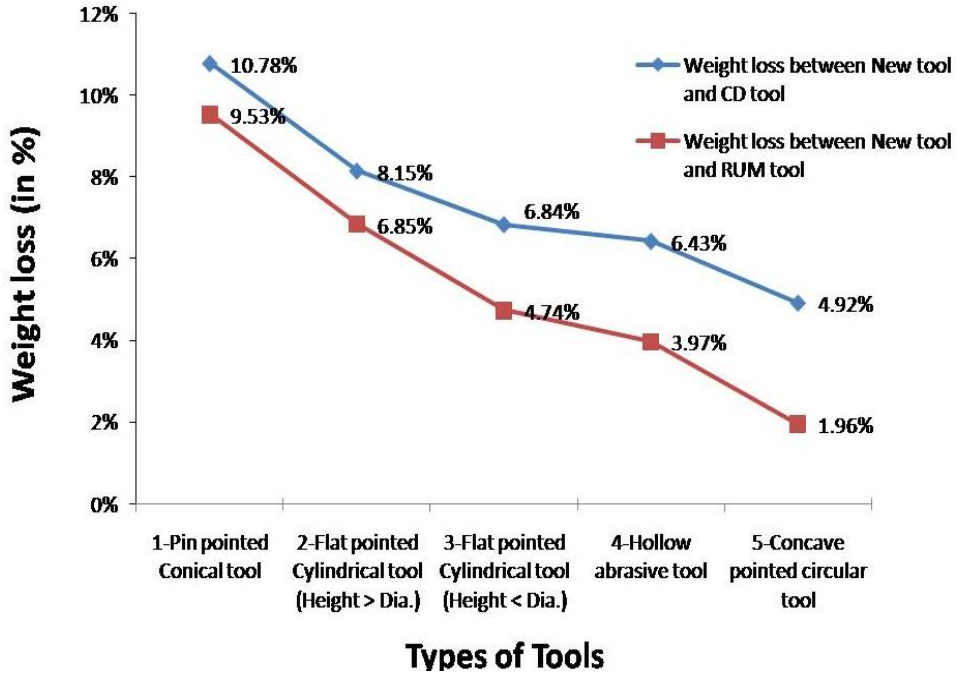

Fig. 4.19: Comparison of weight loss (in %age) between new tool and CD tool as well as new tool and RUM tool

In RUM process, the tool vibrates at some ultrasonic frequency; where the diamond abrasives are impregnated on the tool face which is not in continuous contact with the work specimen. Through each vibration cycle, the abrasive particles on tool's face are penetrated into the work specimen for specific time duration. In CD process, impregnated abrasives over the tool face are in continuous contact with an effective cutting surface of glass specimen, since there is no vibration produced while drilling as in case of RUM. Hence, it revealed that the effective cutting time is lesser during RUM process as compare to CD process. Consequently, RUM possessed lower pressure on the tool and generates lesser tool wear amount.

Hence, it is recommended that the tool's lateral face should be optimum. Because the tool which has smaller lateral face require less amount of diamond grains and it leads to lesser fabrication cost. Subsequently, after analyzing the overall tools wear outcomes, it is investigated that the tool conditions after RUM process is far superior to CD.

4.3 Effect of Various Parameters on Hole Entrance Chipping

The parameters such as spindle rotation speed (rpm), feed rate (mm/min), and vibration amplitude (μm) are the major factors on which hole entrance chipping is based. The radial chip distance is quantified and visualized using profile projector and optical microscope. The effect of these parameters on hole entrance's RCD and the cause of its decrease or increase has been explained in the section.

4.3.1 Effect of Spindle Rotational Speed, Feed Rate and Vibration Amplitude

According to Taguchi L18 optimization technique, the designed experiment matrix is mentioned in Table 4.3. During optimization, the signal noise (S/N) ratio are estimated by considering three conditions i.e. Larger-is-better, smaller-is-better condition and Nominal-the-best. Author has proposed the smaller-is-better condition. The reason of choosing the smaller-is-better condition is that the chipping is usually known as defects. These are undesirable characteristics whose ideal value is zero. Hence, the suitable condition has been used to minimize the chipping size (hole's entrance and exit chipping). Hence, other conditions are not for the required outcome factors. Table 4.3 represents the input factors (spindle speed, feed rate, and vibration amplitude) along with response values of their respective mean and S/N ratio of average RCD values for every designed trial. As per industrial requirement least chipping leads to better hole tolerance limit and correspondingly nourish the surface characteristics of float glass. As in Table 4.3, RCD readings are estimated three times at each drilling condition and then the average of its RCD is computed and carried out for further study i.e. $RCD_{(Average)} = (RCD_1 + RCD_2 + RCD_3)/3$.

Table 4.3: Input and response values table for avg. RCD

Exp. no.	Rotational Speed (rpm)	Amplitude (µm)	Feed rate (mm^3/min)	Radial chip distance (RCD_1)	RCD_2	RCD_3	MEAN of Avg. radial chip distance	S/N ratio of Avg. radial chip distance
1.	3000	0	6	0.91	0.95	0.93	0.93	0.63034
2.	3000	10	12	0.99	0.98	0.97	0.98	0.17548
3.	3000	20	18	1.08	1.05	0.99	1.04	-0.34067
4.	4000	0	6	0.55	0.57	0.56	0.56	5.03624
5.	4000	10	12	0.67	0.62	0.63	0.64	3.87640
6.	4000	20	18	0.66	0.68	0.64	0.66	3.60912
7.	5000	10	6	0.50	0.46	0.45	0.47	6.55804
8.	5000	20	12	0.51	0.53	0.55	0.53	5.51448
9.	5000	0	18	0.60	0.57	0.60	0.59	4.58296
10.	3000	20	6	0.61	0.67	0.64	0.64	3.87640
11.	3000	0	12	1.14	1.18	1.13	1.15	-1.21396
12.	3000	10	18	1.24	1.26	1.25	1.25	-1.93820
13.	4000	10	6	0.59	0.55	0.60	0.58	4.73144
14.	4000	20	12	0.61	0.58	0.61	0.60	4.43697
15.	4000	0	18	1.350	1.350	1.347	1.349	-2.60024
16.	5000	20	6	0.424	0.427	0.424	0.425	7.43222
17.	5000	0	12	0.85	0.87	0.89	0.87	1.20961
18.	5000	10	18	0.86	0.86	0.83	0.85	0.63034

As per Fig. 4.20 of S/N graphs, it was observed that the spindle speed and amplitude have a tremendous effect on average RCD. It is estimated that at the designed parameters of spindle speed (4000 rpm), amplitude (0 µm), and feed rate (18 mm/min), the maximum RCD is observed i.e. 1.349 mm as in Table 4.3. Increase in spindle speed from S1 (3000 rpm) to S2 (5000 rpm) and vibration amplitude from A1 (0 µm) to A2 (20 µm) created a lesser rate of RCD as shown in Fig. 4.20 and Fig. 4.21.

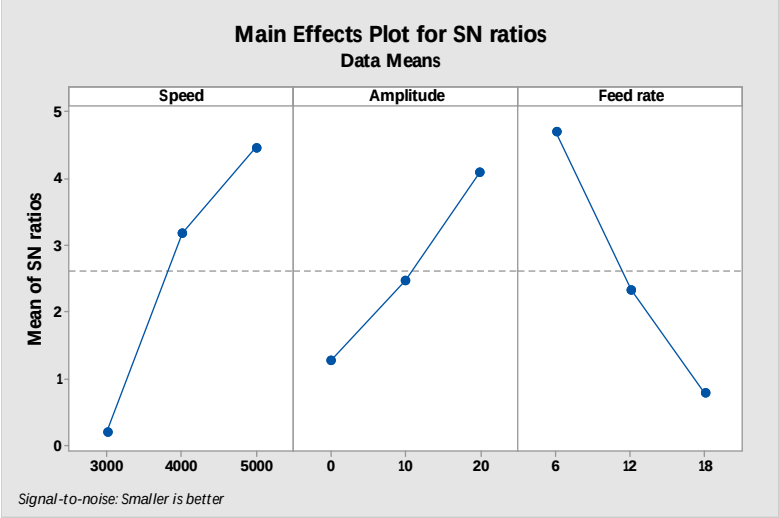

Fig.4.20: Response graph between the S/N ratio values with respect to spindle speed, vibration amplitude and feed rate at hole entrance chipping for RCD

On another hand, it is noticed that as the value of feed rate declined from 18 mm/min to 6 mm/min, it would lead to decrease in RCD as represented in Fig. 4.20 and Fig. 4.21. It is stated that during high spindle speed, the cutting load is distributed over more number of tool's abrasive particles, and the depth of cut per particle reduces. It fascinates the lowering of extraction action and increasing the cutting (abrasion) action of the diamond particles on the glass surface. That leads to lesser stress generation in the machining region which is the cause of chip formation (Anwar et al. (2016)).

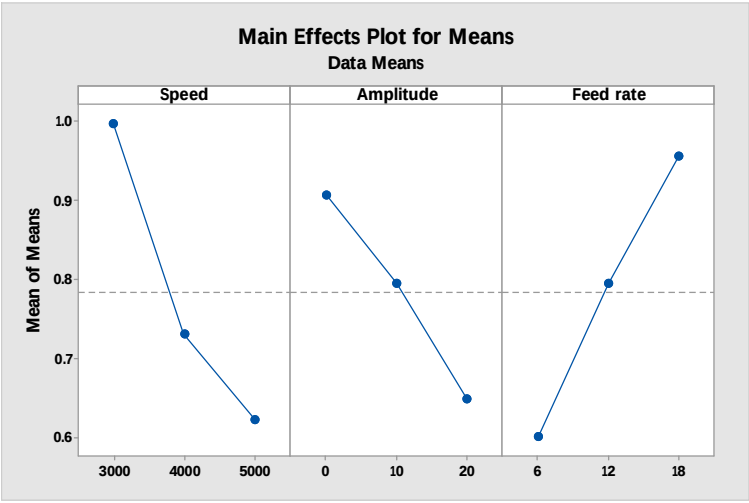

Fig. 4.21: Response graph between the mean values with respect to spindle speed, vibration amplitude and feed rate at the hole entrance chipping for RCD

In Fig. 4.21, it is revealed that increase in feed rate leads to increase in chip size or vice versa. As the selected workpiece 'float glass' has non-crystalline structure, hence the lesser feed rate reduced the constant impact action which helps to resist in building stresses that carry out lesser chipping. Vibration amplitude means the distance of contact between the workpiece and tool face is discontinues. Since as the amplitude increased constantly, it is further created longer discontinuity, which deliberates lesser impact on hole periphery and consequently lesser chipping radial distance and thickness on hole entrance (Singh and Singhal (2016)). Another reason is that during no ultrasonic vibration condition, it is complicated to circulate the water coolant flow through drilling region that results as the generation of more heat and thermal stresses and finally exaggerates the chipping quantity.

The Regression equation of radial chip distance has been reported as:

Radial Chip Distance (RCD) = 1.286 - 0.000186 (Spindle Rotational Speed) - 0.01255 (Vibration Amplitude) + 0.03064 (Feed rate)

For RCD, the value of coefficient of determination (R^2) is noticed as 76.82 %. It reveals that 76.82 % of the data fit the regression model. Minitab displays the lack of fit test when the response data contain replicates (multiple observations with identical input values). Replicates represent "pure error" because only random variation can cause differences between the observed response values. In this study no response data contain replicates. To check whether the model accurately fits the data, P-value has been carried out to the significant level. Generally, P-value significance level is works well up to 0.05. Table 4.4 illustrates that as per ANOVA for the S/N ratio, all the input process parameters have a drastic effect on the average RCD i.e. ($P < 0.05$).

Table 4.4: Analysis of variance (ANOVA) for SN ratios for the average RCD

Source	Degree of Freedom (DOF)	Sum of squares (SS)	Variance	F-ratio	P-value	Contribution (%)
Spindle speed	2	57.21	28.603	12.34	0.002	31.31
Feed rate	2	23.93	11.967	5.16	0.026	33.13
Vibration amplitude	2	46.87	23.435	10.11	0.003	14.90
Residual Error	11	25.49	2.318			20.65

The least radial chip distance (avg.) i.e. 0.425 mm is noticed at spindle speed and amplitude of 5000 rpm and 20 µm, respectively with a feed rate of 6 mm/min as in Table 4.5. At the optimized parameters as mention in Table 4.5, the best hole entrance picture is considered with minimize the chipping amount in Fig. 4.22.

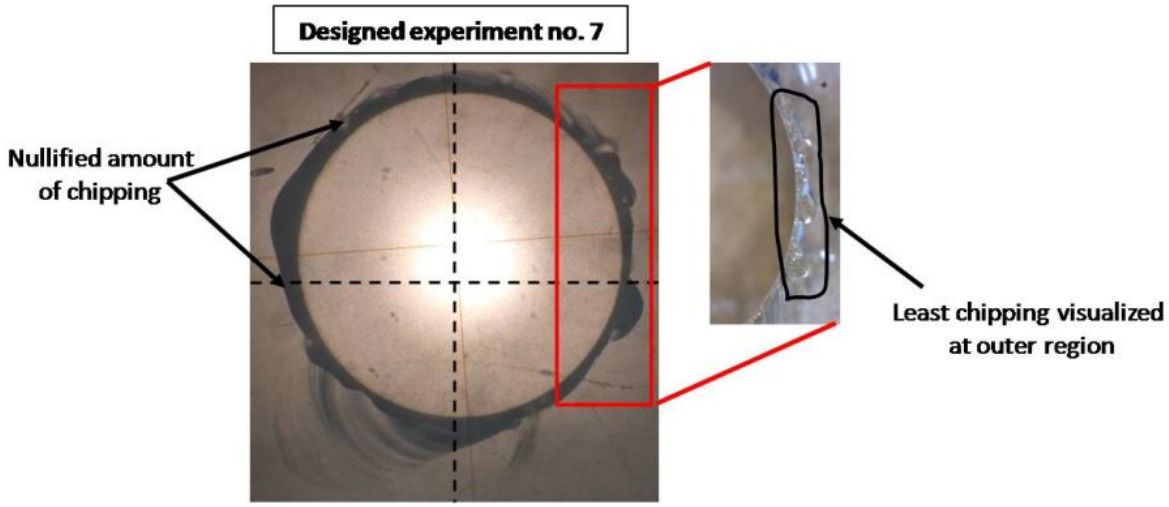

Fig. 4.22: Hole chipping at entrance at optimized parameters

Table 4.5: Optimum parameters to get least RCD (average) at hole entrance

Process parameters	Level	Value
Spindle speed	S3	5000 rpm
Feed rate	F1	6 mm/min
Vibration amplitude	A3	20 µm
Outcome with least RCD	0.425 mm	

4.4 Effect of Various Parameters on Hole Exit Chipping

After creating drilled hole as per parametric conditions by following the Taguchi L18 optimization technique, the hole exit quality is estimated by deploying a machined rod. Machined rod is the best alternate to quantify chipping near hole exit region in form of chip radial distance (CRD) and chip thickness (t_c). Characterization techniques like coordinate measuring machine (CMM), SEM and optical microscope are used to quantify and visualize the chipping amount.

4.4.1 Effect of Spindle Rotational Speed, Feed Rate and Vibration Amplitude

To analyze the effect of spindle rotational speed, feed rate, and vibration amplitude on hole exit chipping, CMM technique is used. It helps to trace the points on the machined rod and determine the chip radial distance (CRD) and chip thickness (t_c). CMM traced the position data based on geometrical data. These traces generate better detailed information of the workpiece's measuring surface. It gives an indication of the quantification of chipping and deviation from the true shape of the hole at hole exit. The CMM pictures of machined rod illustrate the complete curvature of rod created after drilling operation in which various points are considered and the values of these points are quantified in 2-D coordinates. The procedure for making a numerical assessment of the deviation of this trace is to note down the maximum horizontal distance and vertical distance from the true shape of the rod. A trace produced by a CMM which is an amplified record of the displacement of the stylus of the measuring instrument on different machined rods are depicted in Fig. 4.23, 4.24 and 4.25.

As described in Fig. 4.23, initially problems related to the creation of irregular curve shape (represent as a red color solid line) are occurring, the reasons are probe setting error, machined rod setting up issue, and deviation error. It is noticed that the increase in measuring point's numbers on the workpiece sample leads to decrease in deviation error which is further concluded as diminish result dispersion. As in Fig. 4.23, 16 discrete measuring points are considered. Whereas in Fig. 4.24, and Fig. 4.25, measurement points increase up to 18 and 19 points, respectively. Therefore, later on, appropriate machined rod shape is noted. Hence to make the accurate formed path of machined rod sample is a significant task. The rectangular shape inset in the machined rod (represent as dotted lines) is symbolized as the desired shape of the machined rod as shown in Fig. 4.23.

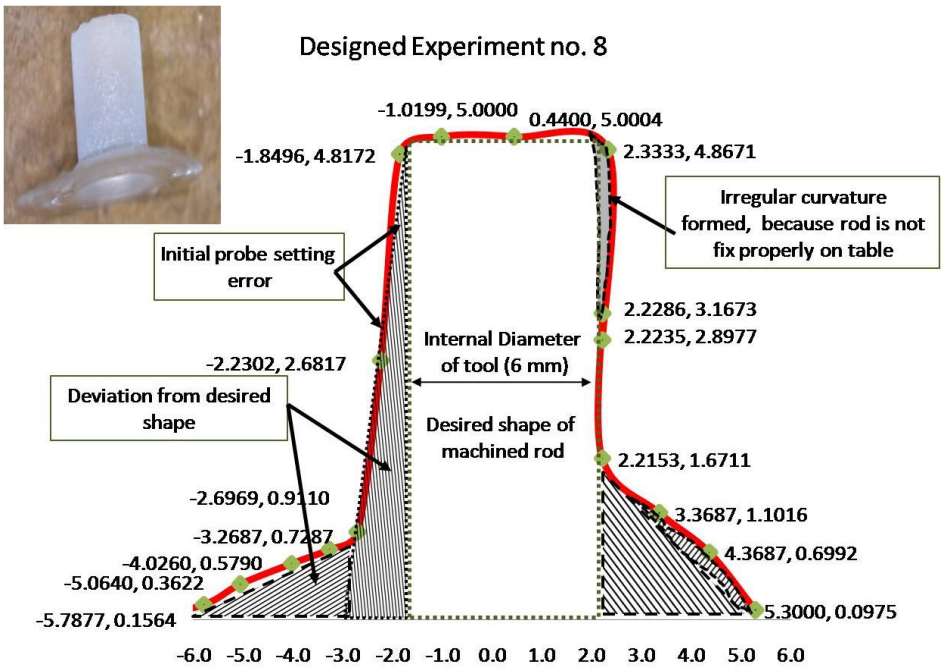

Fig. 4.23: Trace of a machined rod produce by CMM, Inset: Actual machined rod

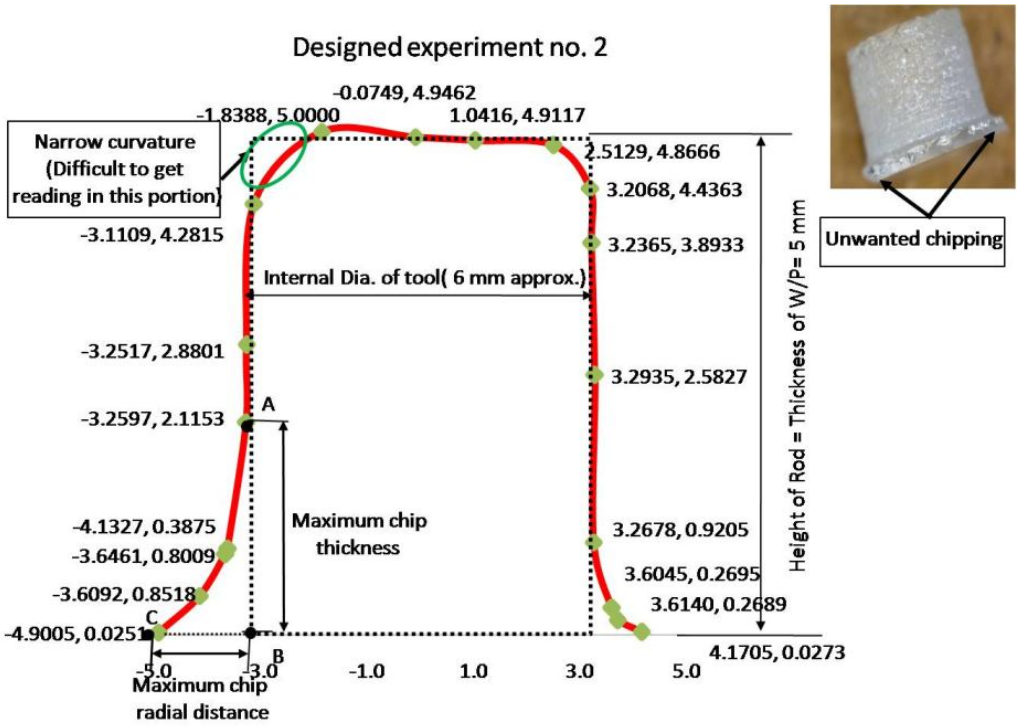

Fig. 4.24: CMM image: Machined rod generated by hollow diamond coated abrasive tool

After overcoming, the setting problems such as machined rod attachment, error deviation, and initial probe error, the machine rod curvature is quantified efficiently. Fig. 4.24 shows that the height of rod is equal to the thickness of the workpiece (W/P) i.e. 5 mm, where; bottom corner on each side represented as unwanted chipping. As shown in Fig. 4.24, the points B to C has depicted the maximum CRD, and points A to C is reflecting the maximum t_c. Hence, the maximum CRD and maximum t_c are estimated.

Similarly, Fig. 4.25 shows the unwanted t_c and CRD in graphical form. In this case, maximum of 19 scanning points are considered which provide refine tracing values. Also, the extended (represent as round dot type) line at the bottom of CMM's graphs shows the required 'chipless' rod shape.

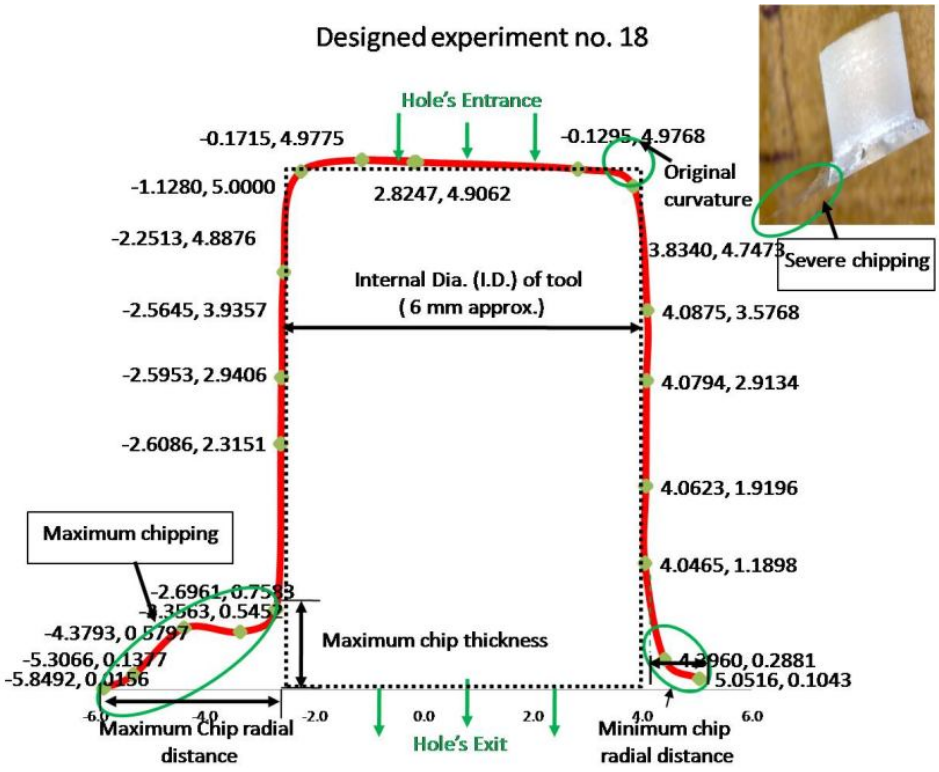

Fig. 4.25: Machined rod illustrate the complete detail related to formation of chips at hole exit

The chipping amount evaluated on machined rods that are trace by CMM is taken into microscopic consideration too. The images of the machined rod (Fig. 4.26) visualize the exit hole chipping. It represents the chipping in both aspects; in the form of chip radial distance and chip thickness. Fig. 4.26 demonstrates the various views of machined rods which are aided during

CMM evaluation. In the same way, unwanted chipping at the hole's exit is noticed, which varies during each designed experimentation.

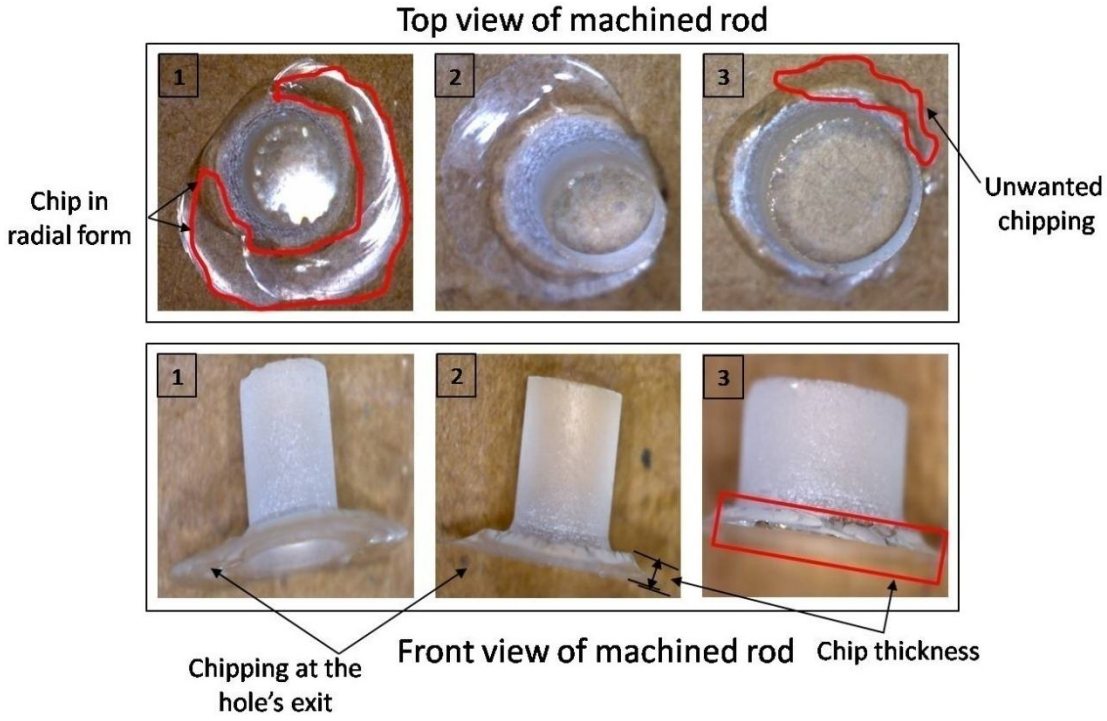

Fig. 4.26: Microscopic pictures of machined rod which is showing the top and front view

After getting hole exit's chipping outcomes, parametric optimization takes place by a designed matrix that estimated the signal noise (S/N) ratio and mean values by considering the smaller-is-better trend. The input and result outcomes are notified as in Table 4.6, which is associated with S/N ratio values and the mean values of maximum CRD and t_c for every experiment trial. The average values of maximum CRD and t_c are estimated three times at each drilling condition to get a precise outcome which is incorporated in Table 4.6. Fig. 4.27 and Fig. 4.28 represents the response graphs between the S/N ratio and mean values with respect to spindle speed at hole exit chipping for CRD, respectively. Fig. 4.29 and Fig. 4.30 represents the response graphs between the S/N ratio and mean values with respect to spindle speed at hole exit chipping for t_c, respectively.

Table 4.6: Input and result table for maximum CRD and t_c on the machined rod

Experiment no.	Rotational Speed (rpm)	Amplitude (micron)	Feed rate (mm/min)	Mean of Max. chip radial distance (mm)	S/N ratio of Max. chip radial distance (mm)	Mean of Max. chip thick. (Exit)	S/N ratio of Max. chip thick. (Exit)
1.	3000	0	6	1.200	-1.58362	1.010	-0.08643
2.	3000	10	12	1.330	-2.47703	1.290	-2.21179
3.	3000	20	18	1.240	-1.86843	1.320	-2.41148
4.	4000	0	6	0.990	0.08730	0.870	1.93820
5.	4000	10	12	0.996	0.03481	0.890	1.11035
6.	4000	20	18	1.100	-0.82785	0.900	0.53744
7.	5000	10	6	0.840	1.51441	0.590	4.43697
8.	5000	20	12	0.800	1.93820	0.580	4.73144
9.	5000	0	18	0.982	0.15777	0.905	1.72372
10.	3000	20	6	0.900	0.91515	0.910	0.81917
11.	3000	0	12	1.110	-0.90646	1.100	0.26457
12.	3000	10	18	1.300	-2.27887	1.020	-0.17200
13.	4000	10	6	0.980	0.17548	0.750	2.49877
14.	4000	20	12	1.070	-0.58768	0.770	0.44553
15.	4000	0	18	1.390	-2.86030	1.130	-1.06157
16.	5000	20	6	0.700	3.09804	0.550	5.19275
17.	5000	0	12	0.980	0.17548	0.820	1.72372
18.	5000	10	18	0.920	0.72424	0.800	1.93820

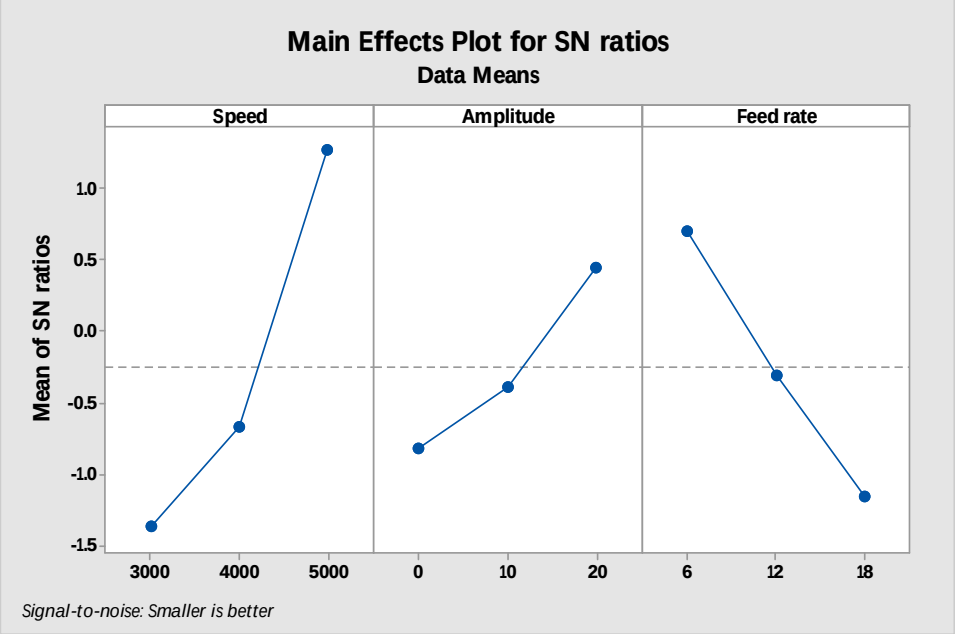

Fig. 4.27: Response graph between the S/N ratio values with respect to spindle speed, vibration amplitude and feed rate at hole exit chipping for CRD

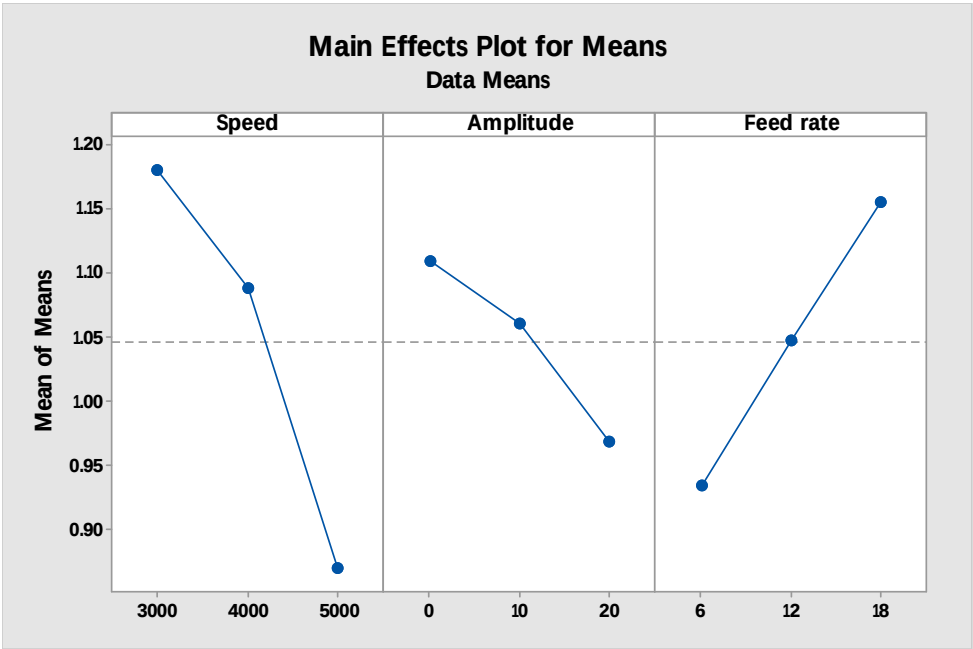

Fig. 4.28: Response graph between the mean values with respect to spindle speed, vibration amplitude and feed rate at hole exit chipping for CRD

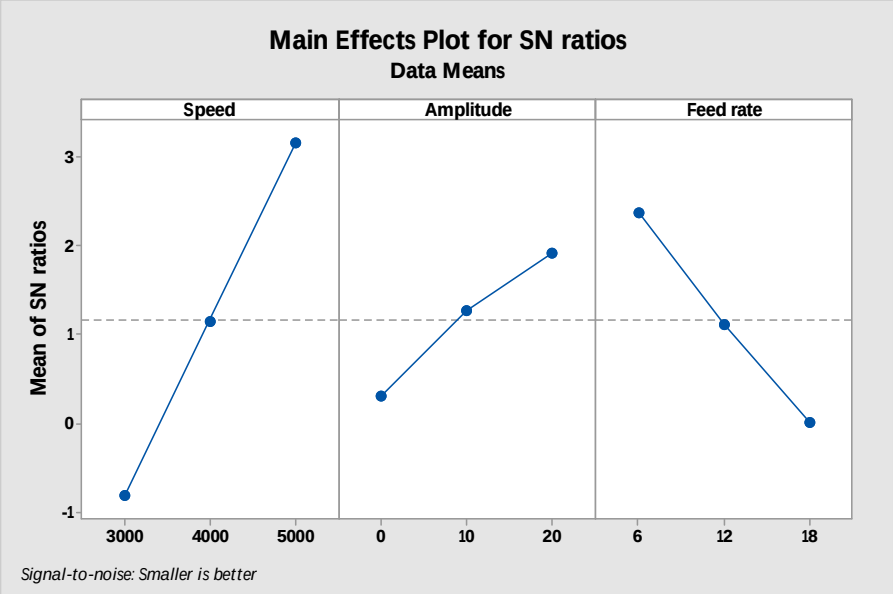

Fig. 4.29: Response graph between the S/N ratio values with respect to spindle speed, vibration amplitude and feed rate at hole exit chipping for t_c

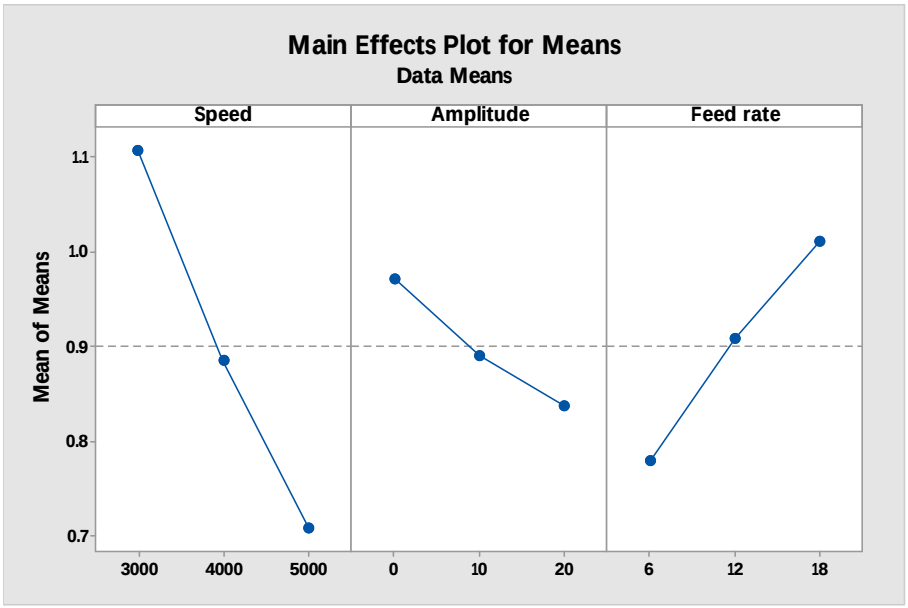

Fig. 4.30: Response graph between the S/N ratio values with respect to spindle speed, vibration amplitude and feed rate at hole exit chipping for t_c

After analyzing the graphs (Fig. 4.27, Fig. 4.28, Fig. 4.29 and Fig. 4.30), it was found that as the spindle speed increased from 3000 rpm to 5000 rpm, the overall chipping in form of CRD and t_c at hole exit is decreased. After investigating the finest parametric arrangement, it was revealed

that the spindle rotation speed is the most influencing parameter among others (Wang et al. (2016b)).

On a flip side, the increase in feed rate from F1 (6 mm/min) to F3 (18 mm/min) caused an unwanted hike in chipping in form thickness and maximum radial distance as represented in Fig. 4.27 and 4.30. Because the lesser feed rate helps out in declining the constant impact action that further aid to reduce the stresses, which subsequently decreased the overall chipping (Jiao et al. (2005)). After visualizing Fig. 4.27 & Fig. 4.29, it is noticed that the increase in vibration amplitude from A1 (0 µm) to A2 (10 µm) and finally then A3 (20 µm) causes a reasonable decline in CRD and t_c too. Consequently, vibration amplitude shows somehow similar trend as in case of spindle speed that chipping amount is reduced by increasing them. In the case of vibration amplitude, the discontinuity produced during drilling is the key reason for lesser chipping thickness and radial distance on the machined rod.

The Regression equation of chip radial distance has been reported as:

Chip Radial Distance (CRD) = 1.515 - 0.000155 (Spindle Rotational Speed) - 0.00702 (Vibration Amplitude) + 0.01836 (Feed rate)

The Regression equation of chip thickness (t_c) has been considered as:

Chip thickness (t_c) = 1.537 - 0.000200 (Spindle Rotational Speed) - 0.00671 (Vibration Amplitude) + 0.01938 (Feed rate)

For CRD, the value of coefficient of determination (R^2) is noticed as 80.62 %. It is stated that 80.62 % of the data has fitted with the regression model. In case of tc, the value of coefficient of determination (R^2) is reported as 84.54 %. It shows the 84.54 % of the data is fitted with the regression model.

As per ANOVA tables of the S/N ratio, all the input source factors have a significant influence on the maximum chip radial distance and thickness. Table 4.7 and Table 4.8 demonstrate the value of P less than 5 % ($P < 0.05$).

Table 4.7: Analysis of variance (ANOVA) for SN ratios for the maximum CRD

Source	Degree of Freedom (DOF)	Sum of Squares (SS)	Variance	F-ratio	P-value	Contribution (%)
Spindle speed	2	22.33	11.1649	21.88	0.000	51.56
Feed rate	2	10.402	5.2008	10.19	0.003	24.01
Vibration amplitude	2	4.963	2.4817	4.86	0.031	11.46
Residual Error	11	5.612	0.5102			12.95

Table 4.8: Analysis of variance (ANOVA) for SN ratios for the maximum t_c

Source	Degree of Freedom (DOF)	Sum of Squares (SS)	Variance	F-ratio	P-value	Contribution (%)
Spindle speed	2	47.712	23.8561	29.25	0.00	58.68
Feed rate	2	16.688	8.3438	10.23	0.003	20.52
Vibration amplitude	2	7.935	3.9676	4.86	0.031	9.75
Residual Error	11	8.973	0.8157			11.0389

According to the response curves, it is revealed that the third level of rotational speed (S3), the first level of feed rate (F1), and third level of vibration amplitude (T3) demonstrate the finest parametric arrangement to get the lowest value of CRD. Table 4.9 shows the optimum parameters to get the least value of CRD and t_c at hole entrance.

Table 4.9: Optimum parameters to get least CRD at the hole entrance

Process parameters	Level	Value
Spindle speed	S3	5000 rpm
Feed rate	F1	6 mm/min
Vibration amplitude	A3	20 µm
Outcome with least CRD	0.70 mm	
Outcome with least t_c	0.55 mm	

The SEM images of the machined rod and backside view of drilled hole with different magnifications are illustrated in Fig. 4.31. At optimized parametric conditions, while performing experiments, least amount of chipping at hole exit is noticed.

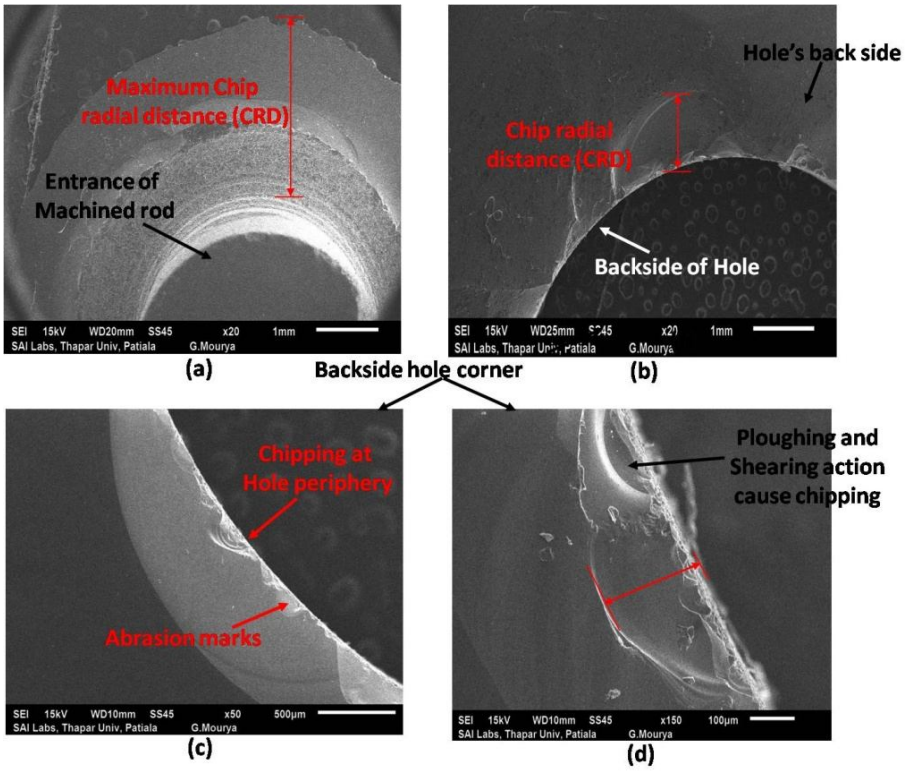

Fig. 4.31: (a) Microscopic images of the machined rod and backside view of drilled hole with different magnifications (a) Machined rod (b) Hole back side with 20 x magnification (c) Hole back side with 150 x magnification (d) Back side of hole with 20 x magnification

CRD and t_c values at the optimize parameters are 0.700 mm and 0.550 mm, respectively which is evaluated at the parameter of spindle speed (5000 rpm), vibration amplitude (20 μm), and feed rate (6 mm/min). Fig. 4.31 shows the microscopic images of the machined rod and drilled hole on which the least amount of chipping amount is estimated. Fig. 4.31 (b) depicts the back side pictures of the hole and also notified the severe chipping nearby hole boundary. It visualizes the formation of CRD on the chip rod. As shown in Fig. 4.31 (c), the abrasion marks are noticeably observed on the backside corners of the hole periphery. Due to shearing and ploughing action, heavy chipping is observed in Fig. 4.31 (d). These microstructure images are an attempt to check the applicability of the measured chip sizes. The abrasives scratch marks lead to pits and cavities

formation that will further propagate into CRD. The abrasive scratching depth is transformed into t_c. The lateral ploughing marks evoke the chip in length as CRD and depth as t_c beyond the hole periphery (Lv et al. (2016)). After analyzing the outcomes, it is implicit that the proper combination of the factors (spindle speed, vibration amplitude, and feed rate) leads to decrease in the chipping amount at utmost.

4.5 Effect of Various Parameters on Avg. Surface Roughness of Hole Internal Region

By following the Taguchi L18 optimization technique, the designed matrix of experiments is described in Table 4.9. The input factors i.e. spindle speed; vibration amplitude and feed rate along with response values of their respective mean and S/N ratio of average surface roughness (R_a) values are predicted by considering smaller-is-better order. According to the requirement to improve the surface characteristics of the float glass specimen, the smallest amount of surface roughness at the internal region of the drilled hole leads to better hole quality.

Surface roughness (R_a) readings are calculated four times at several positions axially parallel to the direction of drill feed and then its average surface roughness value is estimated using: $R_{a(Average)} = (R_{a\,1} + R_{a\,2} + R_{a\,3} + R_{a4})\ /4$ as mention in Table 4.10.

Fig. 4.31 and Fig. 4.32 shows the response graph represents the S/N ratio for the spindle speed, vibration amplitude, and feed rate at hole internal region for avg. surface roughness, respectively. After visualizing the graphs (Fig. 4.32 and Fig. 4.33), it is noticed that increase in spindle speed from 3000 rpm to 5000 rpm possessed decrease in avg. surface roughness (R_a). Whereas, feed rate shows an opposite trend, and increase in feed rate from 6 mm/min to 18 mm/min would increase the avg. surface roughness (R_a) value.

Table 4.10: Illustration of input and response values table for surface roughness (average)

Exp. no.	Rotational Speed (rpm)	Amplitude (μm)	Feed rate (mm^3/min)	Mean of avg. surface roughness, R_a (μm)	S/N ratio of avg. surface roughness, R_a (μm)
1.	3000	0	6	2.20	-6.84845
2.	3000	10	12	1.91	-5.62067
3.	3000	20	18	2.47	-7.85394
4.	4000	0	6	1.53	-3.69383
5.	4000	10	12	1.45	-3.22736
6.	4000	20	18	1.48	-3.40523
7.	5000	10	6	1.12	-0.98436
8.	5000	20	12	1.15	-1.21396
9.	5000	0	18	1.30	-2.27887
10.	3000	20	6	1.84	-5.29636
11.	3000	0	12	2.24	-7.00496
12.	3000	10	18	2.32	-7.30976
13.	4000	10	6	1.35	-2.60668
14.	4000	20	12	1.38	-2.79758
15.	4000	0	18	1.58	-3.97314
16.	5000	20	6	1.09	-0.74853
17.	5000	0	12	1.19	-1.51094
18.	5000	10	18	1.24	-1.86843

Hence, it is clear that the combination of high spindle speed and low feed rate value would create enhanced surface quality. The reason for better avg. surface roughness is that increase in spindle speed with less feed rate would lead the diamond abrasive of the hollow tool to cut and shear the holes' internal machined region for a longer period, which reduced the surface roughness (Mandegari and Behbahani (2013)). As shown in Fig. 4.32 and Fig. 4.33, it is stated that the vibration amplitude influences the surface roughness of the machined region. It is found that, at amplitude of 10 μm and 20 μm, the avg. surface roughness initiates decreasing.

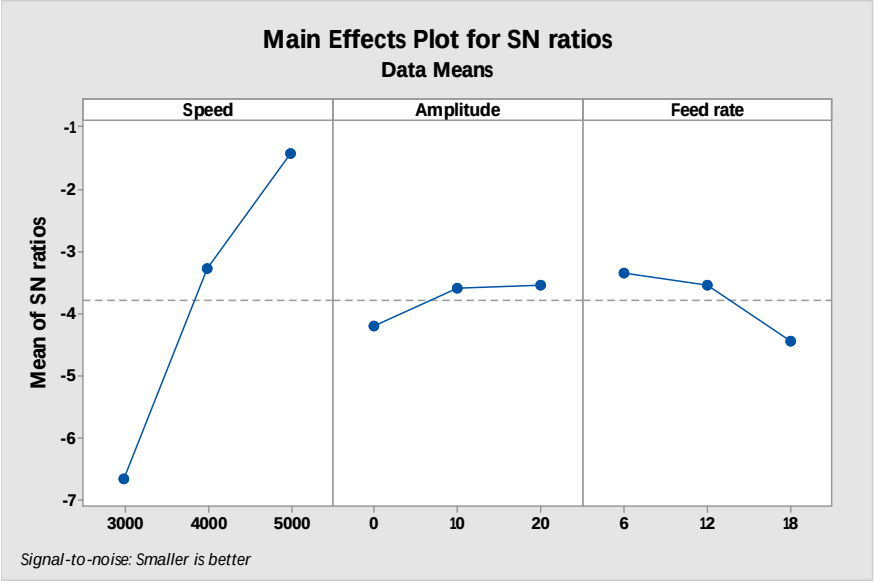

Fig. 4.32: Response graph represents the S/N ratio for the spindle speed, vibration amplitude and feed rate at hole internal region for avg. surface roughness

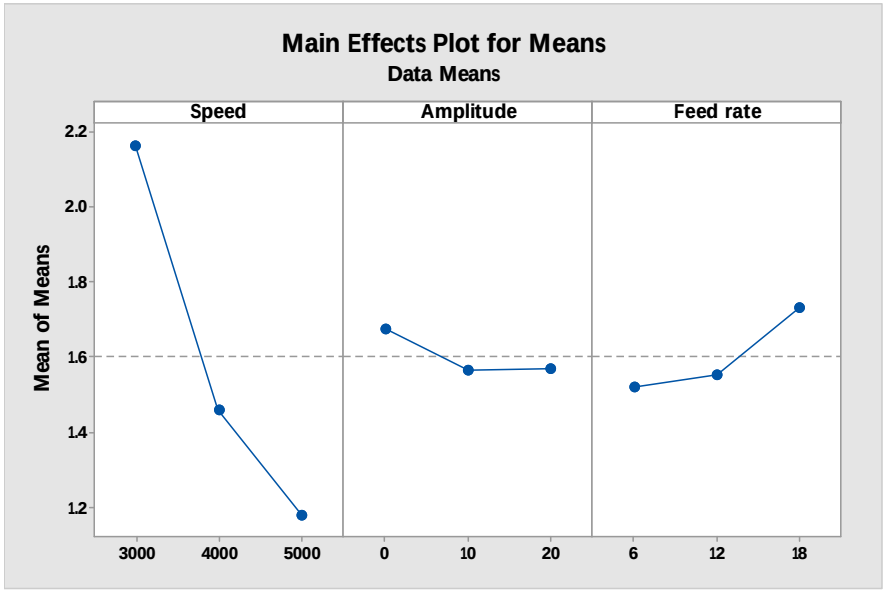

Fig. 4.33: Response graph represents the Mean data for the spindle speed, vibration amplitude and feed rate at hole internal region for avg. surface roughness

Hence, it is reported that an increase in amplitude provides better hole quality. The Regression equation of average surface roughness (R_a) has been reported as:

Average Surface roughness (R_a) = 3.408 - 0.000491 (Spindle Rotational Speed) - 0.00525 (Vibration Amplitude) + 0.01750 (Feed rate)

For Surface roughness (R_a) output response, the value of coefficient of determination (R^2) is found as 89.05 %. It represents that the 89.05 % of the data is fit with the regression model. For checking the model that it fits fits the data accurately or not, the P-value has been carried out to the significant level. Generally, a significance level is works well up to $P < 0.05$. As per the ANOVA table of the S/N ratio, it is confirmed that all three input factors have a significant effect on the avg. surface roughness. Table 4.11 illustrates the value of P less than 5 % ($P < 0.05$).

Table 4.11: Table illustrates the Analysis of Variance (ANOVA) for SN ratio for the avg. surface roughness (R_a)

Source	Degree of Freedom (DOF)	Sum of squares (SS)	Variance	F-ratio	P-value	Contribution (%)
Spindle speed	2	84.109	42.0544	203.43	0.000	58.42
Feed rate	2	1.649	0.8246	3.99	0.050	8.82
Vibration amplitude	2	4.004	2.0018	9.68	0.004	22.55
Residual Error	11	2.274	0.2067			

In Table 4.12, it is mentioned that the least avg. surface roughness (R_a) i.e. 1.09 µm is noticed at spindle speed (5000 rpm), vibration amplitude (20 µm) and feed rate (6 mm/min). By selecting this input parametric combination, the float glass specimen would attain better finishing that could decrease the occurrence of fatigue failure at the time of functioning. Hence, it would increase the life span and service span of float glass applications.

Table 4.12: Illustration of the optimum parameters to get the least avg. surface roughness

Process Parameters	Level	Value
Spindle speed	S3	5 000 rpm
Feed rate	F1	6 mm/min
Vibration amplitude	A3	20 µm
Outcome with least avg. surface roughness (R_a)	1.09 µm	

Fig. 4.34 (a) and (b) depict the surface roughness profiles of the drilled holes on float glass specimen. It is found that experiment no. 3 is generated maximum values of avg. surface roughness i.e. arithmetical mean avg. surface roughness (R_a) is reached to 2.47 μm, ten-point mean roughness (R_z) is 7.3 μm and root mean square average roughness (R_q) value is 1.42 μm. In the case of experiment no. 16, the avg. surface roughness values of hole on the specimen are found as R_a is 1.09 μm, R_z is 7.3 μm and R_q is 1.42 μm. As it is cleared that the profile with the least roughness values is taking place by experiment no. 16, which is stated as the optimum parametric combination.

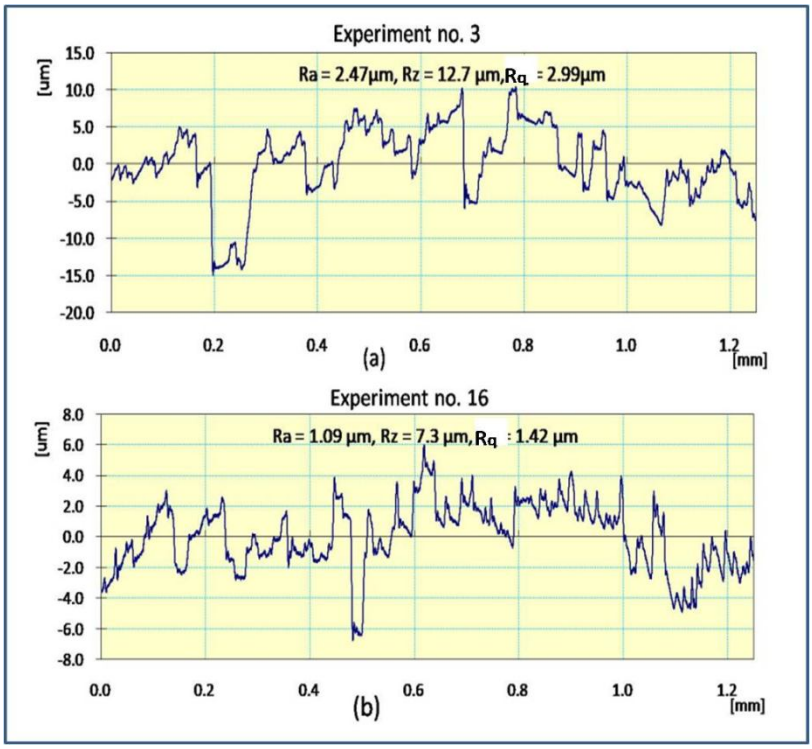

Fig. 4.34: Surface roughness profiles of the internal drilled region of float glass specimen: (a) Illustration of experiment no 3 with maximum average surface roughness (R_a), (b) Profile of experiment no 16 with least average surface roughness (R_a) at optimum parameters

Hence, to achieve the overall hole quality, the combination of hole's side corners and inner machined region are needed to be machined efficiently without drilling defects. Therefore, all the process parameters are optimized to get the best of applications of float glass in the area of solar, metrology, optical.

4.6 Comparison of Edge Chipping Before and After Tempering Process during CD and RUD

To get the appropriate measurement outcome, radial chip distance (RCD) is measured at eight different points and then the average values of radial chip distance (at the entrance) are obtained during CD and RUD processes. The detail procedure of measurement is as shown in Fig. 3.10. Later on, same float glass samples are evaluated again after tempering process, so that changes occurred on pre-tempered float glass and post tempered glass specimens is estimated precisely. Fig. 4.35 shows the profile images of the drilled hole entrances by CD and RUD process at two conditions i.e. before tempering and after tempering.

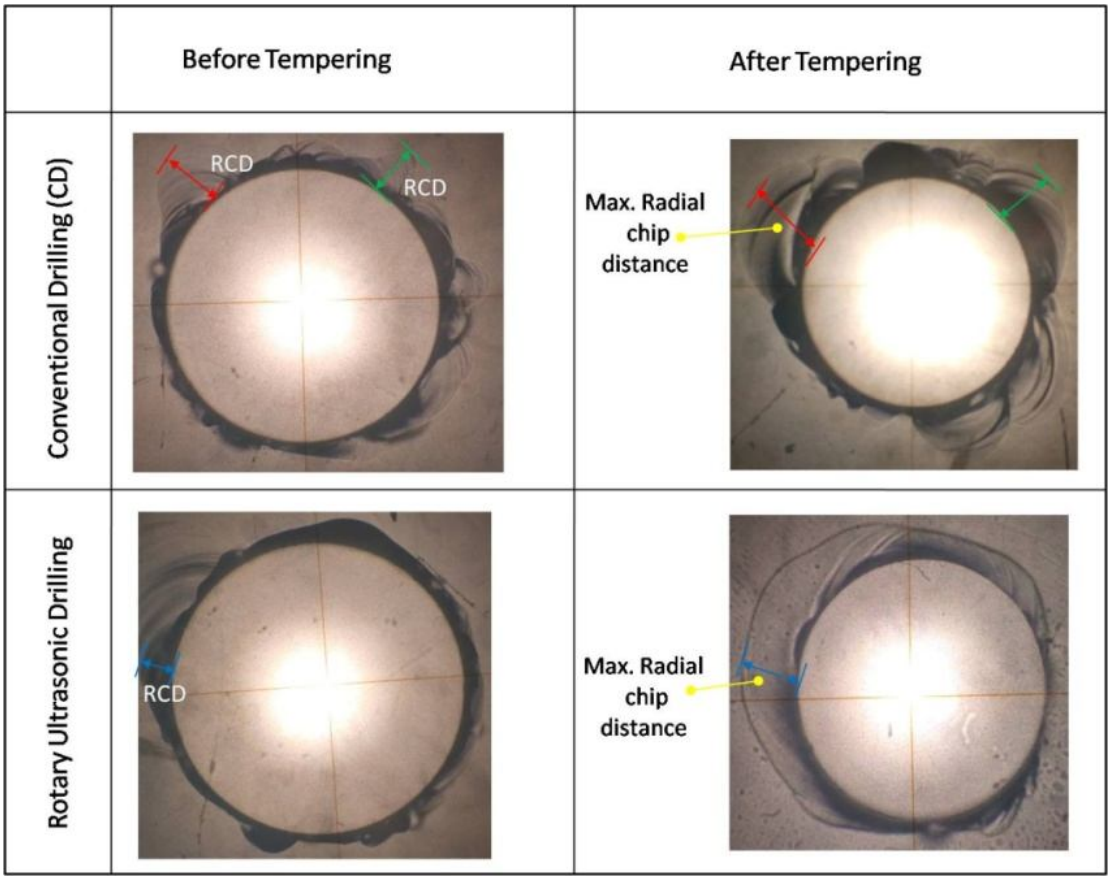

Fig. 4.35: Profile images of drilled hole entrances by CD and RUD process at conditions i.e. before and after tempering process

RCD obtained on pre-tempered drilled samples by their respective drilling processes (CD and RUD), are again evaluated after tempering process, so that change in RCD after tempering process is estimated. From previous results, it is found that holes created after RUM process has

lesser amount of chipping than CD process. Table 4.13 represents the increase in RCD for CD during 'before tempering' and 'after tempering'. Table 4.14 represents the increase in RCD for RUD during 'before tempering' and 'after tempering' process. As mentioned in section 3.4.3, 5 holes are drilled in each case (CD and RUD) for further analysis.

Table 4.13: Increase in RCD for CD: Before and after tempering process

Hole no.	Before tempering: *Radial chip distance* (RCD) by CD, mm	After tempering: RCD by CD, mm	% increase in RCD (Edge chipping size)
Hole 1	1.46	1.99	36.301
Hole 2	1.35	1.92	42.222
Hole 3	1.17	1.67	42.735
Hole 4	1.24	1.86	50
Hole 5	1.29	1.93	49.612
$RCD_{Avg.}$ by CD	1.302	1.874	43.93

Table 4.14: Increase in RCD for RUD: Before and after tempering process

Hole no.	Before tempering: *Radial chip distance* (RCD) by CD, mm	After tempering: RCD by RUD, mm	% increase in RCD (Edge chipping size)
Hole 6	0.87	1.23	41.37
Hole 7	0.92	1.26	36.95
Hole 8	0.785	1.14	45.22
Hole 9	0.75	1.11	48.00
Hole 10	0.82	1.18	43.90
$RCD_{Avg.}$ by RUD	0.829	1.182	42.58

It is stated that radial chip distance (RCD) has smaller size during RUD process as compare to CD at each hole, respectively. Table 4.15 illustrates the change in average RCD for CD and

RUD and also describes the change in average RCD during "before tempering' and 'after tempering process'.

Table 4.15: Percentage of increase in RCD before and after tempering process for CD and RUD

Condition	After CD	After RUD	% decrease in RCD by RUD w.r.t. CD
Before tempering: ***Avg. radial chip distance*** (RCD), mm	1.302	0.829	36.32 %
After tempering: ***Avg. radial chip distance*** (RCD), mm	1.874 (Not acceptable)	1.182 (Acceptable)	36.92 %
Increased in RCD (in %)	43.93 %	42.58 %	

After drilling 5 holes each by CD and RUD process, the average RCD is noticed. It is examined that before and after the tempering process, the average RCD during RUD process is smaller in size than CD process. It is found that the value of RCD is 1.302 mm by CD and 0.829 mm by RUD before the tempering process at a constant optimized parametric combination. On another hand, after tempering process, the RCD is 1.874 mm by CD and 1.182 mm by RUD. As per the industrial requirement for 5 mm thickness of float glass specimen, generally, the value of RCD should be less than 1.5 mm after tempering process. So, the float glass specimen is further used in different applications. Hence, it is only the initial RCD, obtained by the process on which rejection of the component depends. Owing to the value of RCD is lesser than 1.5 mm by RUD process as shown in Table 4.15. A rotary ultrasonic machining technique is recommendable to generate to get fine hole quality. Therefore, a RUD technique is recommendable as it gives an initial RCD of 0.829 mm before tempering which is almost 36.32 % lesser than CD process. An attempt has been done on the present work just to show the effect of tempering on RCD with both the processes.

It has been observed from Table 4.15 that increases in RCD for both the cases (i.e. RUD and CD) are almost the same (42.58 % and 43.93 %, respectively) after tempering. It means tempering process leads to an increase in radial chip distance (chipping size). During tempering process, float glass is heated to a definite temperature range and afterward, rapid air cooling has

been carried out to make thermally tempered glass. Consequently, the post-tempered float glass specimen becomes extensively hard and it could generate severe internal stresses especially nearby corners of the drilled hole. Hence, during tempering process, the float glass sample is facing increase in temperature from room temperature to processing temperature up to 690^0c. Further, air blast pressure on the corners of drilled hole samples could cause more distortion because it is the most sensitive section of the glass. Subsequently, the combined effect of elevated temperature and high pressure creates some breakage as chipping due to changes in the metallurgical behavior of the float glass material. Fig. 4.36 shows the micro-level picture of the same drilled hole before and after the tempering process.

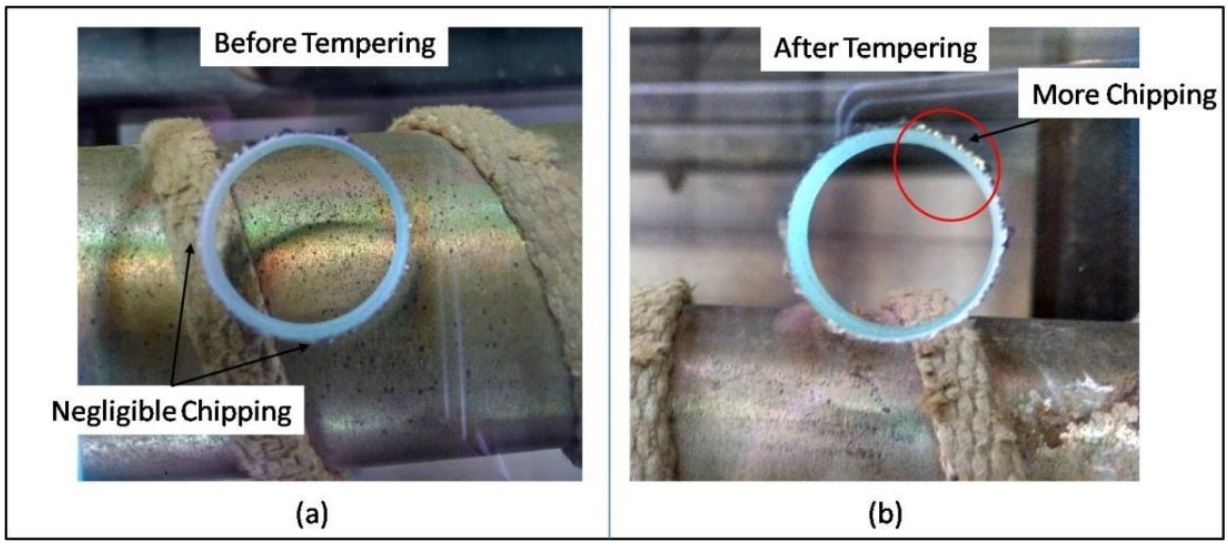

Fig. 4.36: Picture of drilled hole before and after tempering process during RUM process

Fig. 4.37 depicts the SEM images of the drilled hole samples which includes: (a) Drilled hole with 16x magnification, (b) Hole corner of pre-tempered float glass with 50x magnification, and (c) Hole corner of post-tempered float glass with 50x magnification. As represented in Fig. 4.36 and Fig. 4.37, it was noticed that pre-tempered float glass has negligible chipping near hole entrance corner. On another side, post-tempered glass has possessed severe edge chipping which is validating the presumption mentioned about the increase in edge chipping after tempering process. Hence, during the drilling operation, it should be kept in mind that the chipping should be as least as possible.

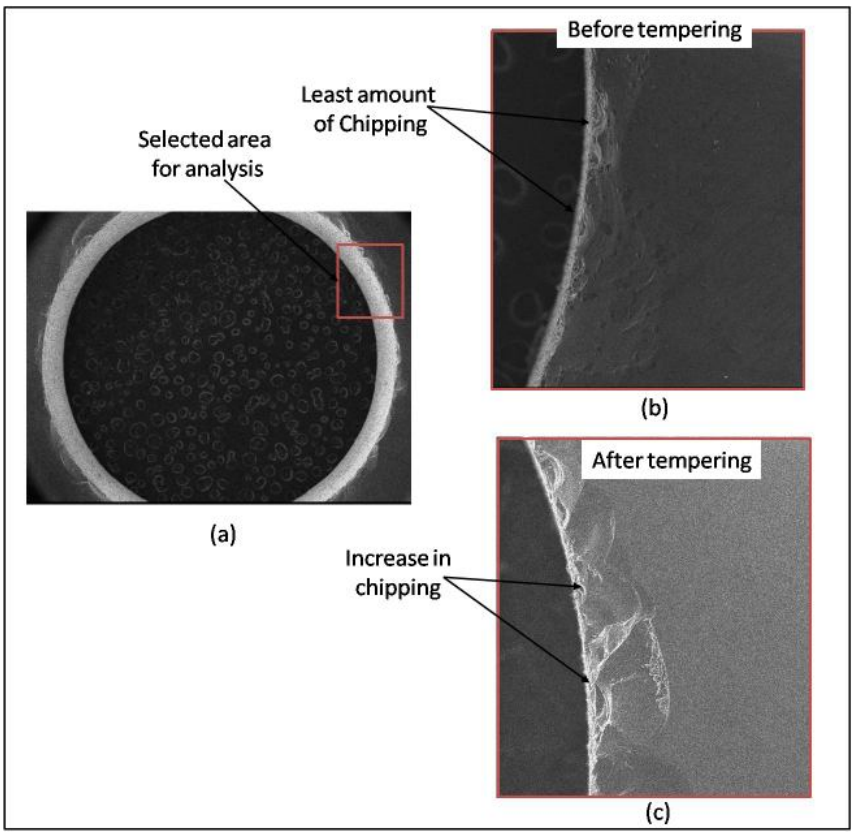

Fig. 4.37: SEM images of the drilled hole of the float glass specimen which include: (a) Drilled hole with 16x magnification; (b) Hole corner of pre-tempered float glass with 50x magnification; (c) Hole corner of post-tempered float glass with 50x magnification

Also, if the chipping near machined corners is found after all the primary processes it could lead to heavy monetary loss in from of operation cost, tempering cost, labor cost, time wastage, human fatigue.

4.7 Summary

The following summary explains the results and discussions related to the formation of hole chipping, hole internal machined region, and multi-shaped tool wear while drilling float glass material using rotary ultrasonic machining (RUM) and conventional drilling. Effect of tempering on drilled hole corner (entrance chipping) are also investigated.

Initially, the blind hole produced during RUD process, has possessed lesser radial chip distance (RCD) than conventional drilling (CD). Also, the tool wear rate is smaller in quantity by RUD process as compared to CD. Overall, Concave circular tool is found as the best tool among others to get negligible chipping at hole entrance (RCD) with negligible tool wear. Secondly, the

parametric effects on hole entrance, hole exit chipping, and hole internal machined region are also elaborated while following the Taguchi L18 optimization technique. It is revealed that the higher values of spindle speed and vibration amplitude and lower value of feed rate detected as the best parametric arrangement to get the lowest value of radial chip distance (RCD), chip radial distance (CRD), chip thickness (t_c) and avg. surface roughness (R_a) to achieve overall enhanced hole quality. Lastly, during the float glass tempering process, the combined effect of elevated temperature and high pressure creates some breakage (such as chipping) due to change in the metallurgical behavior of the float glass material. Accordingly, before the tempering process; the chipping amount should be as least as possible. Before the tempering process, it is found that the value of RCD is 1.302 mm by conventional drilling and 0.829 mm by rotary ultrasonic drilling. On another hand, after the tempering process, the RCD is 1.874 mm by CD and 1.182 mm by RUD. Hence, as the RCD size is smaller after RUD process as compared to CD. Therefore, the rotary ultrasonic machining technique is recommended to generate to get better hole quality.

CHAPTER 5: FINITE ELEMENT ANALYSIS OF FLOAT GLASS DRILLING

This chapter presented a FE analysis to investigate the effect of stress generation on hole exit during rotary ultrasonic glass drilling (RUD) and conventional drilling (CD) of float glass. A numerical model has been prepared in ANSYS APDL R 15.0. A relation between the von Mises stress failure criterion and chipping produced at hole exit after float glass drilling has been noticed. Simulation results analyze the reduction in stress generation after rotary ultrasonic drilling as compare to CD of float glass specimen.

5.1 Assumption and Boundary Condition

A Finite element analysis has been performed in ANSYS APDL R 15.0. Mesh was generated considering the SOLID quad 4 node 182 elements. A 2D static model has been prepared in ANSYS APDL R 15.0. The float glass specimen model is prepared to evaluate the behavior during the drilling process. The workpiece was modeled as a rectangle with measurements of 30*5 mm^2 with a rectangular recess (in form of the machined rod) as shown in Fig. 5.1. Float glass material is assumed as pure isotropic in nature. The property of the float glass specimen which is considered during modeling is mentioned in Table 3.1.

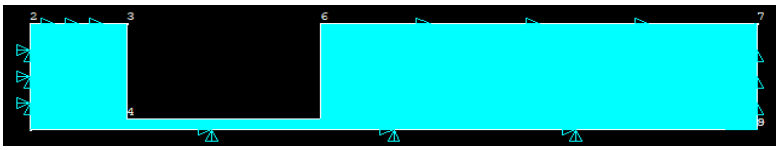

Fig. 5.1: Float glass specimen model

The following assumptions are made while the execution of simulation. These are:

- In the case of CD and RUD process, boundary conditions are imposed that the workpiece is constrained from all (X-Y-Z) directions (Fig. 5.2) by using glass holding fixture (experimentally too).
- The depth of drilling is assumed to reach up to 4.5 mm by hollow abrasive coated tool. The specification of the hollow tool is mentioned in Table 3.2.
- A hollow abrasive tool is loaded in form of critical cutting force (F_c).
- Float glass material is isotropic in nature.

- The von Mises stress failure criteria are expected to be an appropriate condition to consider failure for isotropic materials.

5.2 Cutting Forces during Experimentation

To presume the tool is to be loaded in form of cutting force (F_c) on float glass specimen, experimentation is performed. The value of cutting force was measure using dynamometer (Kistler Dynoware type 9272) during drilling by CD and RUD process, which is used as an input condition in simulation. Cutting (dynamic) forces during both the conventional drilling & rotary ultrasonic drilling processes has been made. As the direction of cutting force is steady in the z-direction of a dynamometer, hence the force curve of Fz from Dyno Ware is considered as driving force. Fig. 5.2 illustrates the cutting force with respect to time recorded during RUD and CD process, which shows the maximum driving force.

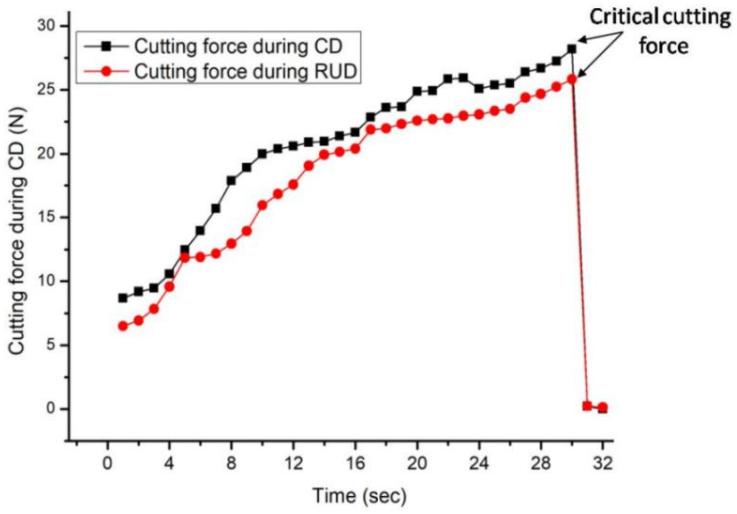

Fig. 5.2: Obtaining of critical cutting force with respect to time by CD and RUD processes

After attaining a maximum position, the driving force decreases quickly to zero. This signifies the initiation of chipping at hole exit. This maximum driving force was accordingly defined as the critical cutting force. During RUD process, the critical cutting force reached to 25.85 N approx. whereas, 28.20 N of critical cutting force is noticed in CD process. Finally, the cutting force as an input parameter is further used in simulation work for both drilling process.

5.3 Von Mises Stress Failure Criterion

In the case of isotropic materials such as float glass, it is predicted that the chipping has been propagating, when the maximum stress value satisfies the failure criterion. Hence, in this study; von Mises stress failure criterion is applied (Nikumb et al. (2005)). According to this criterion, chipping is assumed to propagate if $\sigma \geq \sigma_{ut}$, where σ is stated as maximum principle stress taken from the FEA simulation, and σ_{ut} is defined as the ultimate tensile strength of the workpiece material (Li et al. (2006)). The value of the ultimate tensile strength of the float glass specimen is considered as 50 MPa (Khan and Haque (2007)). The von Mises equivalent stress (σ_{von}) is stated as:

$$\boldsymbol{\sigma_{von}} = \sqrt{\frac{(\boldsymbol{\sigma_1}-\boldsymbol{\sigma_2})^2+(\boldsymbol{\sigma_2}-\boldsymbol{\sigma_3})^2+(\boldsymbol{\sigma_1}-\boldsymbol{\sigma_3})^2}{\mathbf{2}}} \qquad (11)$$

Where, σ_1, σ_2, and σ_3 are principle stresses in x-y-z direction taken from the FEA simulation, respectively. σ_{ut} is defined as the tensile strength of the workpiece material.

Hence, during the drilling process, as the value of principle stress would reach equal to and above the ultimate tensile strength of float glass specimen, then chipping is considered as initiated.

5.4 Geometrical Modeling and Mesh Design

A finite element analysis has been performed in ANSYS APDL R 15.0. Quadrilateral mesh has generated considering the SOLID quad 4 node 182 elements with a mesh size of 0.5 mm. To achieve the close comparison among the FE analysis and experimental measurements, the mesh size of 0.5 mm has been taken. The mesh size was selected corresponding to the probe size availability i.e. 0.5 mm as shown in Fig. 5.3. Total of 536 nodes and 99 elements are used in the simulation. It is an explicit simulation study. Fig. 5.3 illustrates the Snapshot of the initial state of the simulation model of the workpiece with hollow abrasive coated tool. It is showing that the actual position of the force i.e. 4 mm from the left side of the workpiece.

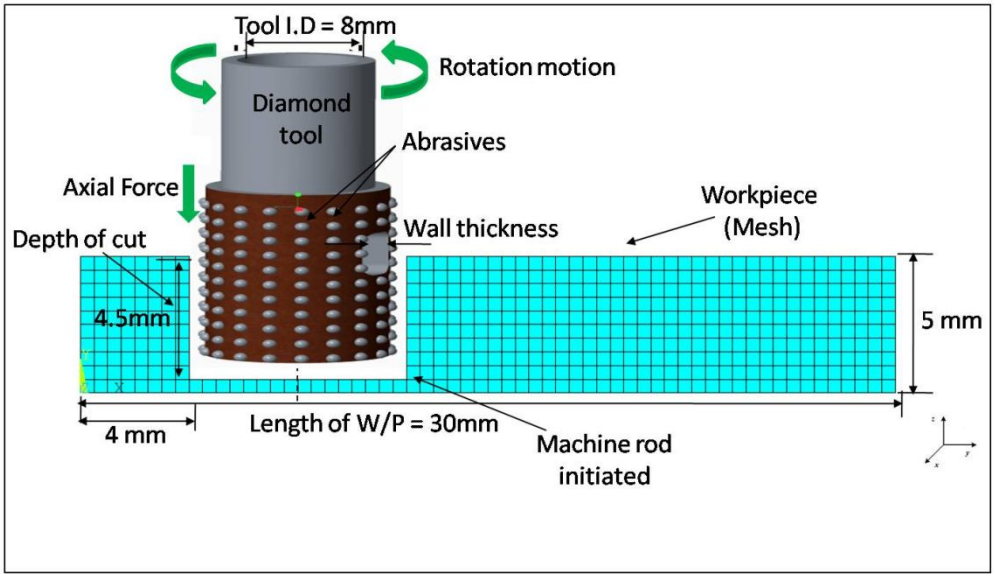

Fig. 5.3: Initial state of the simulation model of the workpiece with hollow abrasive coated tool

The elements are progressively considered on whole workpiece. Estimate boundary conditions for the numerical analysis which emulate the phenomena in a real system with proper accuracy. Fig. 5.4 shows the complete boundary condition and distributed axial force applied over the float glass periphery. Here, it is represented by the front view and top view that the hollow tool exerted axially distributed force that could lead the defects in form chipping.

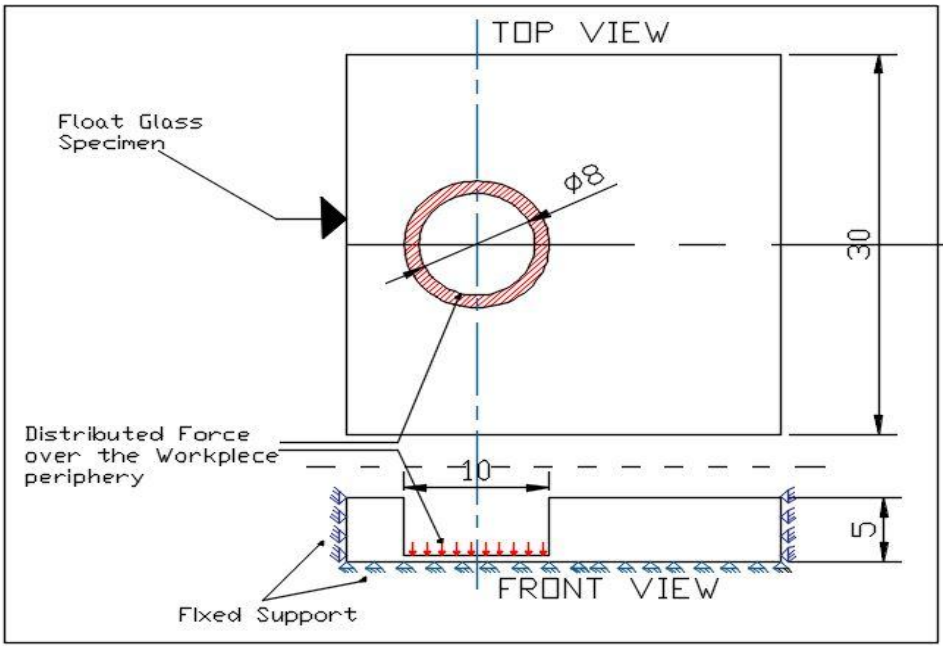

Fig. 5.4: Illustration of boundary condition and distributed force applied over the float glass periphery

5.5 Simulation Results

5.5.1 Distribution of von Mises stress at hole exit during CD and RUD

Fig. 5.5 shows the 2-D distribution of the von Mises stress in the region of chipping propagate at constant optimized parameters by CD. During CD, it is visualized that as the von Mises stress value goes beyond the 50 MPa (i.e. ultimate tensile strength of the specimen), the deformation has been carried out as chipping. The maximum von Mises stress value reaches up to 82.11 MPa. Fig. 5.6 shows the 2-D distribution of von Mises stress in the region of chipping propagate at hole exit for RUD process. Similarly, the maximum von Mises stress value is reported as 76.24 MPa.

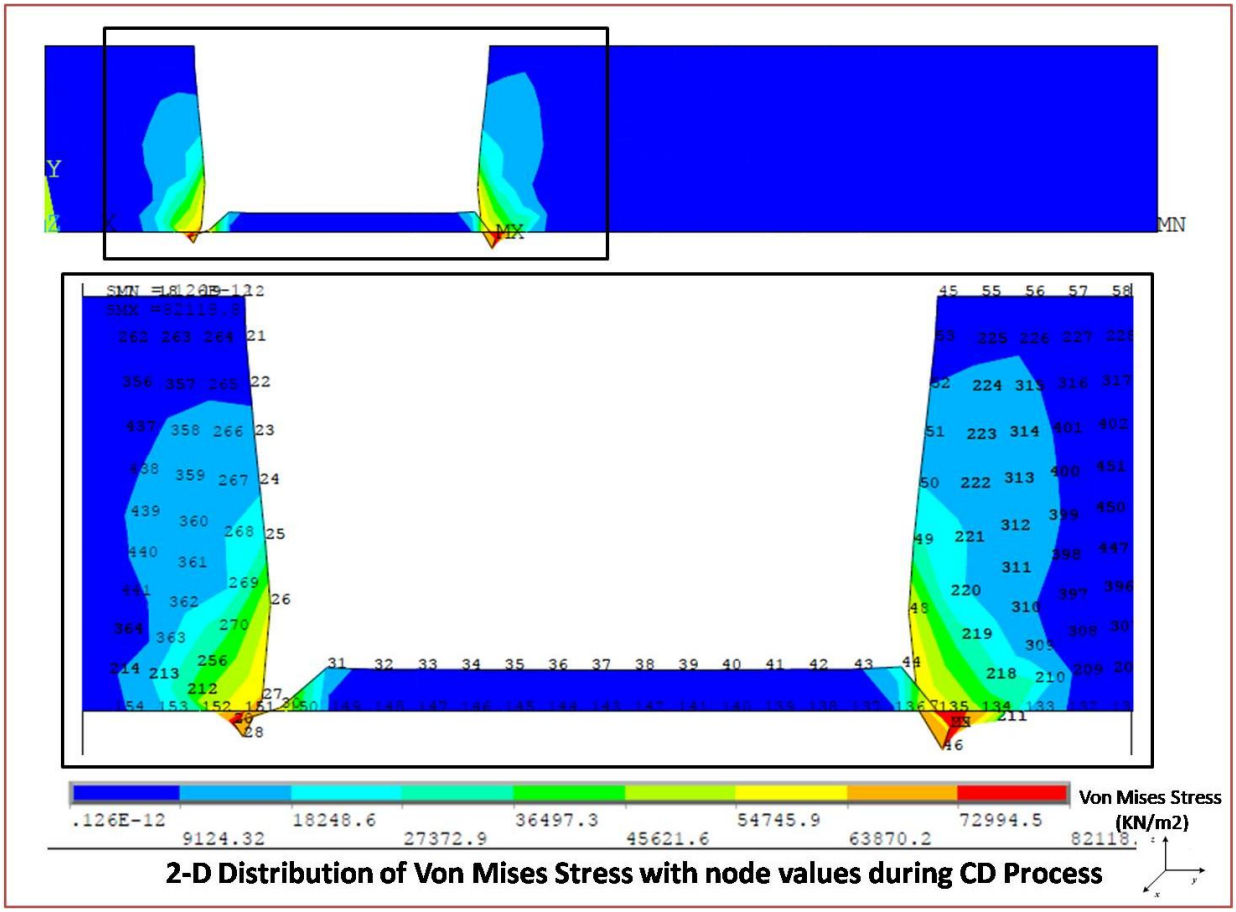

Fig. 5.5: 2-D distribution of von Mises stress in the region of chipping propagate at hole exit for CD process at constant optimized parameters

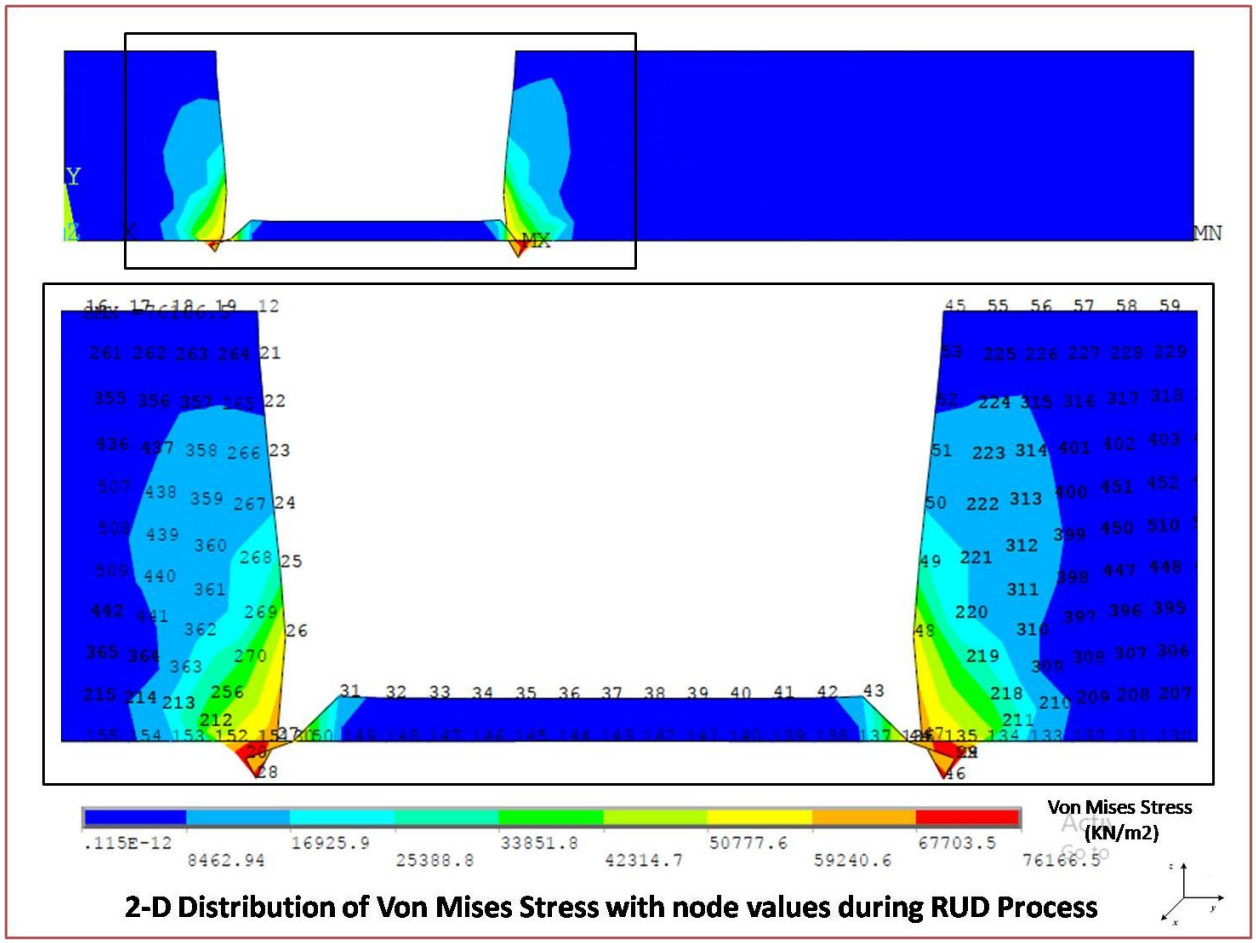

Fig. 5.6: 2-D distribution of von Mises stress in the region of chipping propagates for RUD

It is found that near hole exit region, von Mises stress values reached above 50 MPa i.e. the ultimate tensile strength of the float glass specimen. Similar trends are noticed in CMM graph (Fig. 5.8 & Fig. 5.9) that the chipping propagation is visualized at hole exit region.

As it is cleared that the stress region and the chipping region occur on the same bottom portion of the hole. Hence, there could be a relation between the overall chipping (CRD and t_c) with respect to von Mises stress during RUD and CD processes.

5.5.2 Stress Distribution at Chipping Initiated Region

To undertake the von Mises stress values at its corresponding nodes near to hole exit region, Fig. 5.7 (a) shows the left and right portion of the workpiece specimen. Selected nodes are shown in boxes (Blue color) and out of them, 5 nodes from each portion are found to be exceeding in von Mises stress values from the ultimate tensile strength of the specimen. In Fig. 5.7 (b), scatter plot

illustrates the von Mises stress value which corresponds to the chipping initiated region on the left portion of the hole. This indicates that the chipping is initiated in the same region, where the stresses are above the specimen's tensile strength. An utmost, similar trend of von Mises stress values would be noticed on the right region of chip initiation nodes because the critical force is applied uniformly on float glass specimen (Wang et al. (2016). But for explanation purposes only the left portion is considered as greater chipping/stress is formed in this region.

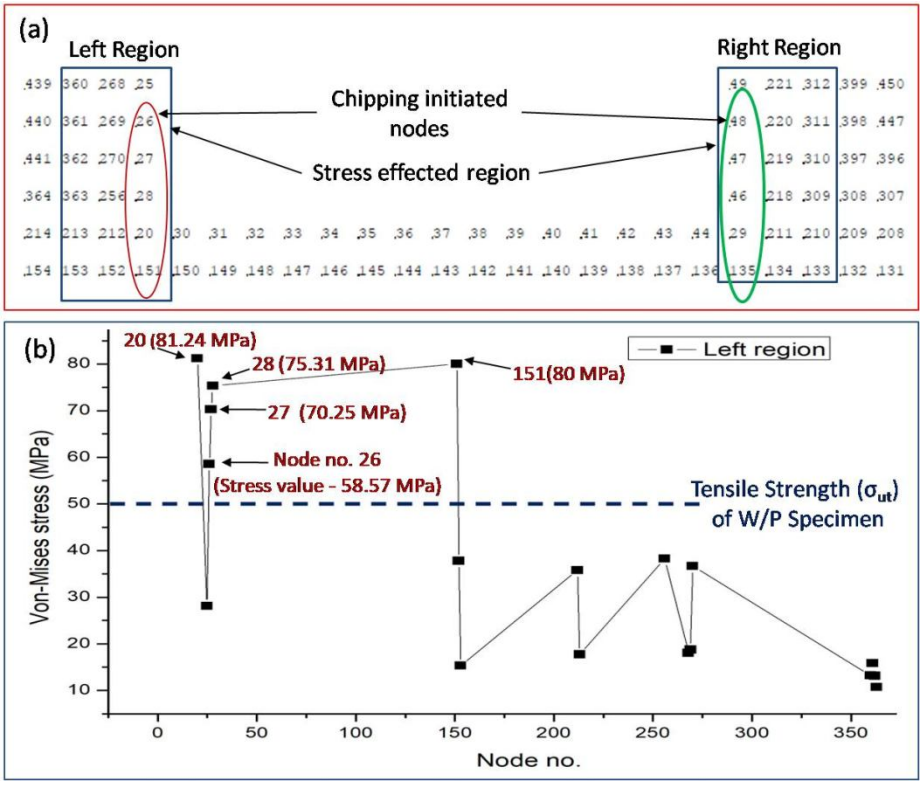

Fig. 5.7: (a) Representation of selected nodes where Von Mises stress could go beyond the Workpiece's tensile strength, (b) Scatter plot illustrates the value of Von Mises stress w.r.t. its corresponding node number on left chipping initiated region

5.5.3 Relation between von Mises *Stress and Hole Exit Chipping*

For precise validation of simulation results (von Mises stress) with experimentation outcome (chipping measurements), machined rod (Fig. 5.8 & Fig. 5.9) is taken under consideration to validate the chipping near hole exit with respect to von Mises stress generation at the same location. The cause of opting machined rod is to accurately quantify the chip radial distance (CRD) and chip thickness (t_c) on machined rod and consequently, predicted by the FE analysis in

form of stress generation. A coordinate measuring machine (CMM) is taken to estimate the CRD and t_c through the machined rod. CMM diagram of machined rod which is drilled by CD process is depicting the chipping (CRD and t_c) measurements with its microscopic images of the machined rod in front and top view (Fig. 5.8).

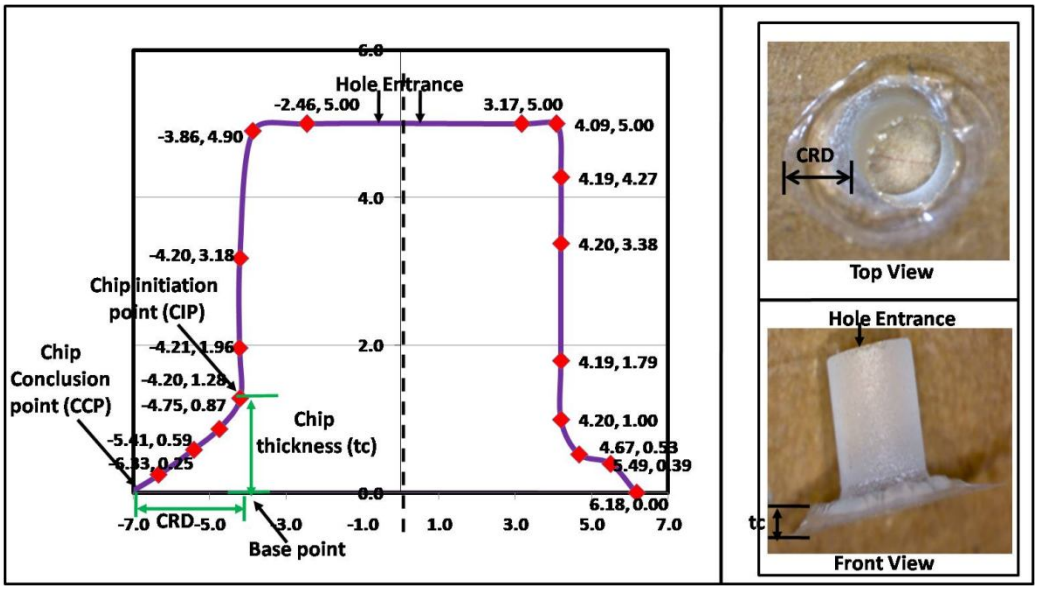

Fig. 5.8: CMM diagram of machined rod which is drilled by CD process: Depicting of chipping (CRD and t_c) measurements with its microscopic images of the machined rod in front and top view

CMM diagram (Fig. 5.8) shows the complete curvature of the machined rod which was formed after drilling. 18 spots are traced and measured the values in form of 2-D coordinates. These tracing points are helping out in measuring the CRD and t_c. By tracing values from the CMM graph during CD process, chip radial distance (CRD) and chip thickness (t_c) is computed as 0.98 mm and 0.87 mm, respectively. Fig. 5.9 depicts the CMM image of machined rod which is drilled by RUD process which is showing the chipping (CRD and t_c) measurements. After RUD process, chip radial distance (CRD) is 0.75 mm and chip thickness (t_c) is 0.53 mm, which means RUD has possessed smaller CRD and t_c in size than CD.

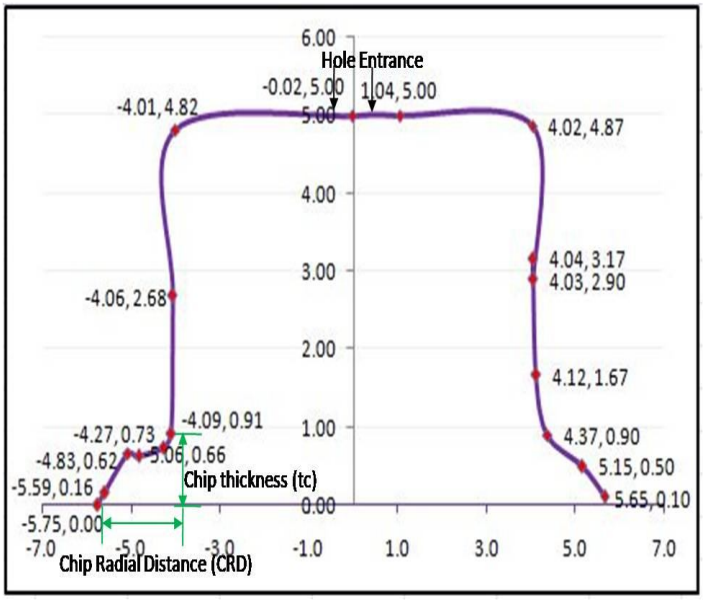

Fig. 5.9: CMM image of machined rod which is drilled by RUD process: Depicting of chipping (CRD and t_c) measurements

Fig. 5.10 portrays the left section of the machined rod which shows the trend of von Mises stress distribution with respect to chipping at hole exit (a) During CD and (b) During RUD. After noticing the machined rod section, it is revealed that the chip thickness (t) size directly depends on the point where the chipping initiates; it is the point where the value of von Mises stress just reached above ultimate tensile strength (i.e. 50 MPa). Whereas, chip radial distance (CRD) size depends upon the chipping conclusion point (CCP). As chipping moves from chip initiation point (CIP) to chipping conclusion point (CCP) the CRD increases and at this point the von Mises stress value is maximum i.e. 82 MPa approx. Therefore, the chipping measurement is depending on the stress values at a particular point. The chipping segment demonstrates the various stress regions, where von Mises stress value is going beyond 50 MPa (Fig. 5.10).

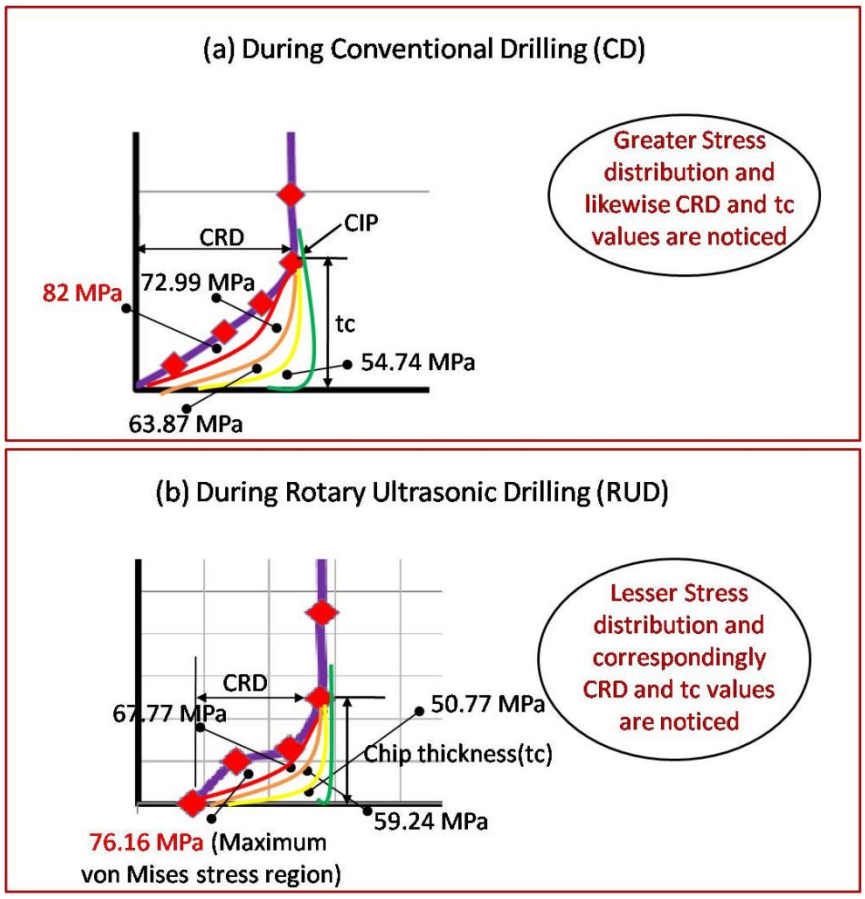

Fig. 5.10: Comparison between numerical and experimental results: Illustration of the left portion of the machined rod shows the trend of von Mises stress distribution with respect to chipping sizes (a) During CD (b) During RUD

During CD, chip radial distance (CRD) and chip thickness (t_c) is approaching under the range of 54.74 MPa to 82 MPa. In RUD, the range of von Mises stress region is coming under 50.77 MPa to 76.16 MPa. Subsequently, it is found that 7.12 % decrease in von Mises stress has been carried out using RUD as compare to CD. Similarly, decrease in CRD and decrease in t_c are also noticed as 4.43 % and 39.08 %, respectively using RUD process. Hence, it has been found that (Fig. 5.10) the chipping and von Mises stress values are following a similar trend (Li et al. (2005)). The reason of lesser value of maximum von Mises stress during RUD as compare to CD is that during RUD, the tool is not in continuous contact with the specimen's drilled to be surface. As there is a simple harmonic motion has been taken place by the tool owing to the vibration frequency. On another hand, during CD; the tool is continuously in contact with the specimen's periphery during drilling which provides more stress generation as compare to RUD

process which is the crucial reason behind cutting force and chip initiation. Therefore, during RUD proess low tool pressure has been exerts on the cutting periphery of the workpiece and also provides lesser tool wear rate.

Hence, it is stated that von Mises stress distribution has a significant influence on the chip radial distance (CRD) and chip thickness (t_c). As the von Mises stress increased, it would lead to increase in the overall chipping in both directions (horizontal as well as vertical) near hole exit region. Overall, a fine agreement is achieved which helps to reduce the chipping at hole exit that may amplify the utility of the float glass material.

5.6 Summary

The summary is drawn after developing the FE analysis which investigates the effect of stress generation on hole exit during rotary ultrasonic glass drilling (RUD) and conventional drilling (CD) of float glass specimen. It is noticed during FE analysis, the maximum von Mises stress value is 82 MPa for conventional drilling (CD) and 76.16 MPa by rotary ultrasonic drilling process, during drilling operation at the hole exit corner. Similarly, RUD has possessed smaller CRD and t_c in size than CD. It is found that 7.12 % decrease in von Mises stress has been carried out using RUD as compare to CD. Similarly, decrease in chip radial distance (CRD) and decrease in chip thickness (t_c) are also noticed as 4.43 % and 39.08 %, respectively using RUD process. Hence, it has been found that the chipping and von Mises stress values are following a similar trend.

CHAPTER 6: CONCLUSIONS AND SCOPE OF FUTURE WORK

6.1 Conclusions

In this study, the multi-shaped tools are used to create blind holes by rotary ultrasonic machining and conventional drilling. The concern is to selecting the best tool among all to get negligible chipping at hole entrance along with the least tool wear. The influence of various process parameters (such as: spindle speed, feed rate, vibration amplitude) during drilling of float glass specimen by rotary ultrasonic machining (RUM) technique has been presented while considering hole entrance, exit, and internal machined region quality. After optimization, the best parametric combination is purposed to achieve the least amount of chipping near hole corners and the least value of avg. surface roughness (Ra) at hole internal region. Also, the comparison between the edge chipping near hole corners before and after the tempering process has been investigated.

A FE analysis based upon von Mises stress failure criterion has been established to investigate the effect of stress generation on hole exit during rotary ultrasonic glass drilling and conventional drilling of float glass. It is investigated there is a relation between the von Mises stress failure criterion and chipping produced after conventional drilling (CD) and Rotary ultrasonic drilling (RUD). A strategy to reduce the overall chipping (chip thickness and chip radial distance) through monitoring the stress generation is proposed.

The following results as evidence showed that the present strategies would be competent and capable to resolve the challenges like chipping produced during drilling and machining of hard and brittle material i.e. float glass. Also, the machining characteristics such as avg. surface roughness and tool wear are reported during rotary ultrasonic drilling. Based on the results obtained from the present research work, the following conclusions have been drawn.

1. During blind hole drilling by multi-shaped tools, it is found that the tool which possessed the lesser amount of combined stress (tensile or shear stress) because of their shape and angle of contact, creates lesser chipping. It is noticed that according to the tool shapes, each tool has its own path of drilling and effective contact area which influences the chip formation and hole quality.

2. During conventional drilling, the lowest and highest chipping size at the entrance is 0.4415 mm & 0.8125 mm by using a concave circular tool and pinpointed conical tool respectively. The trends are same with Rotary Ultrasonic Drilling viz concave circular tool has lowest chipping size (radial chip distance) i.e. 0.1145 mm, where the pinpointed conical tool possessed the highest chipping (radial chip distance) i.e. 0.4925 mm.
3. The blind holes results show that RUD process has attained minimum chipping as compare to CD for all types of tools.
4. Concave circular tool possessed least overall (both lateral and end face) wear and Pin-pointed conical tool have created the highest amount of total wear in both the cases (RUD and CD). Added, the maximum amount of grain fracture and wear flat are noticed on the end face of the tool during CD rather than RUM.
5. The concave circular tool has possessed the least weight loss i.e. 4.92 % after CD and 1.96 % after RUM process.
6. For blind holes, concave circular tool is found as the best tool with the least values of chipping and tool wear.
7. In case of through hole drilling, as the spindle speed and vibration amplitude increases, the overall chipping and average surface roughness decreases. On the other hand, at lower feed rate, least chipping has generated in both the cases (entrance and exit chipping) with lesser surface roughness.
8. The optimal values of RUD parameters for least amount of chipping (at entrance and exit of the hole) and avg. surface roughness are concluded as:

Process parameters	Level	Value
Spindle speed	S3	5000 rpm
Feed rate	F1	6 mm/min
Vibration amplitude	A3	20 µm

- After optimizing the RUD parameters, the least amount of chipping (at entrance and exit of the hole) and avg. surface roughness are concluded as:

Chipping at hole entrance (mm)	Chipping at hole exit(mm)	Max. chip thickness at hole exit(mm)	Hole surface roughness (μm)
0.425	0.70	0.55	1.09

- After the tempering process, the chipping amount at the entrance is reduced by 36.92 % with RUD as compare to CD process.
- The hole quality for pre-tempered float glass while using rotary ultrasonic machining is enhanced as compared to conventional drilling.
- During FE analysis, it is noticed that the maximum von Mises stress value is 82 MPa for conventional drilling (CD) and 76.16 MPa by rotary ultrasonic drilling process at the hole exit corner.

6.2 Scope of Future Work

The present work provides some outcomes to get the least amount of chipping which would be used in the future to get high quality drilling or machining purposes. It can also help to boost up the applications of the float glass. The following are the scopes of future work which could be deployed in the future endeavor:

- Using rotary ultrasonic machining on several other hard and brittle materials such as zerodur and titanium which could be machined using above types of multi-shape tools.
- In future work, tools with some other specifications could be used which have different abrasive types, abrasive structure, bond, the shape of abrasives such as conical, rectangular, spherical etc.
- Various profile formation, slots cutting and thread formation could also take place using rotary ultrasonic machining on glass material.

REFERENCES

Anil Kumar Jain and Pulak M. Pandey (2016); “Study of Peck drilling of borosilicate glass with the μRUM process for MEMS”; Journal of manufacturing processes, 22, pp. 134–150.

Anil Kumar Jain and Pulak M. Pandey (2017); “Modeling of un-deformed chip thickness in RUM process and study of size effects in μ-RUM”; Ultrasonics, 77, pp. 1–16.

Anish Roy, Farrukh Makhdum, DNP Norddin and Vadim V. Silberschmidt (2012); “Ultrasonically assisted drilling of carbon fibre reinforced plastics”; Solid State Phenomena, 188, pp. 170–175.

A. A. Khan and M. M. Haque (2007); “Performance of different abrasive materials during abrasive water jet machining of glass”; Journal of Materials Processing Technology, 191, pp. 404–407.

A. M. Abrao, P. E. Faria, Juan Campos Rubio, P. Reis, J. Paulo Davim (2007); “Drilling of fiber reinforced plastics: A Review” Journal of Materials Processing Technology, 186, pp. 1–7.

A. Navanth and T. Karthikeya Sharma (2013); “A Study of Taguchi Method Based Optimization of Drilling Parameter in Dry Drilling of Al 2014 Alloy At Low Speeds”; International Journal of Engineering Sciences & Emerging Technologies, 6 (1), pp. 65–75.

A. Salama, L. Li, Paul Mativenga and A. Sabli (2016a); “High-power picosecond laser drilling/machining of carbon fibre-reinforced polymer (CFRP) composites”; Applied Physics A, 122 (73), pp. 1–11.

A. Salama, L. Li, Paul Mativenga and David J. Whitehead (2016b); “TEA CO_2 laser machining of CFRP composite”; Applied Physics A., 122, pp. 479–497.

Avanish Kumar Dubey and Vinod Yadava (2008); “Laser beam machining- A review” International Journal of Machine Tools & Manufacture, 48, pp. 609–628.

B. Ghahramani and Z Y. Wang (2001); “Precision ultrasonic machining process: A case study of stress analysis of ceramic (Al2O3)”; International Journal of machine tools & manufacture, 41, pp. 1189–1208.

B J Park, Y J Choi and C N. Chu, (2002); “Prevention of Exit Crack in Micro Drilling of Soda-Lime Glass”; CIRP Annals, 51 (1), pp. 347–350.

B. Yang, X. Shen X and S. Lei (2009) “Mechanisms of edge chipping in laser-assisted milling of silicon nitride ceramics”; International Journal of Machine Tools & Manufacture, 49, pp. 344–350.

Chakguy Prakasvudhisarn and Shivakumar Raman (2004); “Framework for Cone Feature Measurement Using Coordinate Measuring Machines”; Journal of Manufacturing Science and Engineering, 126, pp. 169–177.

Chandrashekhar S. Jawalkar, Pradeep Kumar and Apurbha Kumar Sharma, (2014); “Investigations on performance of ECDM process using NaOH and NaNO3 electrolytes while micro machining soda lime glass”; International Journal Manufacturing Technology and Management, 28, pp. 80–93.

Chandra Nath, G C Lim and H Y Zheng (2012); “Influence of the material removal mechanisms on hole integrity in ultrasonic machining of structural ceramics”; Ultrasonics, 52, pp. 605–613.

Chenglong Zhang, Pingfa Feng, Jianfu Zhang, Zhijun Wu and Dingwen Yu (2012); “Investigation into the rotary ultrasonic face milling of K9 glass with mechanism study of material removal”; International Journal of Manufacturing Technology and Management, 25 (4), pp. 248–266.

Chenglong Zhang, Weilong Cong, Pingfa Feng and Zhijian Pei (2014); “Rotary ultrasonic machining of optical K9 glass using compressed air as coolant: A feasibility study”; 228(4), pp. 504–514.

Chwan Huei Tsai and Hong Wen Chen (2003); “Laser milling of cavity in ceramic substrate by fracture machining element technique”; Journal of Materials Processing Technology, 136, pp. 158–165.

C. Paulmann (1996); “Study of oxygen vacancy ordering in mullite at high temperature”; Phase Trans, 59, pp. 77–90.

Dae Kyun Baek, Tae Jo Ko and Seung Han Yang (2013); “Enhancement of surface quality in ultrasonic machining of glass using a sacrificing coating”; Journal of materials processing technology, 213, pp. 553–559.

Dongxi Lv, Hongxiang Wang, Yongjian Tang, Yanhua Huang, Zhiping Li (2013); “Influences of vibration on surface formation in rotary ultrasonic machining of glass BK7”; Precision Engineering, 37(4), pp. 839–848.

Dongxi Lv, Yuanming Zhang and Yunfeng Peng (2016); “High-frequency vibration effects on hole entrance chipping in rotary ultrasonic drilling of BK7 glass” Ultrasonics, 72, pp. 47–56.

D. Prabhakar (1993); “An experimental investigation of material removal rates in rotary ultrasonic machining”; Transactions of the North American Manufacturing Research, Institution of SME, pp. 211–218.

Eshetu D. Eneyew and Mamidala Ramulu (2016); “Experimental study of surface quality and damage when drilling unidirectional CFRP composites”; Journal of Materials Research and Technology, 3 (4), pp. 354–362.

Florian Feucht, Jens Ketelaer, Alexander Wolff, Masahiko Mori and Makoto Fujishima (2014); “Latest machining technologies of hard to cut materials by Ultrasonic machine tool”; Procedia CIRP, 14, pp. 148–152.

F D Ning, W L Cong, Z J Pei and C. Treadwell (2015); “Rotary ultrasonic machining of CFRP: A comparison with grinding”; Ultrasonics, 66, pp. 125–132.

Fuda Ning, Hui Wang, Weilong Cong and P.K.S.C. Fernando (2017); “A mechanistic ultrasonic vibration amplitude model during rotary ultrasonic machining of CFRP composites”; Ultrasonics, 76, pp. 44–51.

Gurmeet S. Singh (2013); “Federation Of Safety Glass” Printed Prominent Press, Book. www.fosg.in ed.

G. Ya, H. W. Qin, S. C. Yang and Y. W. Xu (2002); “Analysis of the rotary ultrasonic machining mechanism”; Journal of Materials Processing Technology, 129, pp. 182–185.

H. Tsuwa (1964); “An investigation of grinding wheel cutting edges”; Journal of engineering for industry, 86, pp. 371-382.

I. Singh and N. Bhatnagar (2006); “Drilling of uni-directional glass fiber reinforced plastic (UD-GFRP) composite” International Journal of Advanced Manufacturing Technology, 27, pp. 870–876.

I. Singh, N. Bhatnagar and P. Vishwanath (2008); “Drilling of uni-directional glass fiber reinforced plastics : Experimental and finite element study”; Materials & Design, 29, pp. 546–553.

Jamal Y. Sheikh Ahmed (2016); “Hole Quality and Damage in Drilling Carbon / Epoxy Composites by Electrical Discharge Machining Hole Quality and Damage in Drilling Carbon / Epoxy Composites by Electrical Discharge Machining”; Materials and Manufacturing Processes. 31, pp. 941–950.

Jianjian Wang, Pingfa Feng, Jianfu Zhang, Chenglong Zhang and Zhijian Pei (2016a); “Modeling the dependency of edge chipping size on the material properties and cutting force for rotary ultrasonic drilling of brittle materials”; International Journal of Machine Tools & Manufacture, 101, pp. 18–27.

Jianjian Wang, Pingfa Feng, Jingzhen Zheng, Jianfu Zhang (2016b); “Improving hole exit quality in rotary ultrasonic machining of ceramic matrix composites using a compound step-taper drill”; Ceramics International, 42 (12), pp. 13387–13394.

Jianjian Wang, Huiting Zha, Pingfa Feng and Jianfu Zhang (2016c); “On the mechanism of edge chipping reduction in rotary ultrasonic drilling: A novel experimental method”; Precision Engineering, 44, pp. 231–235.

Jianjian Wang, Pingfa Feng, Jianfu Zhang and Hao Shen (2017a); “Experimental investigation on the effects of thermo-mechanical loading on the vibrational stability during rotary ultrasonic machining”; Machining Science and Technology, 21(2), pp. 239–256.

Jianjian Wang, Pingfa Feng, Jainfu Zhang, Wanchong Cai and Hao Shen (2017b); “Investigations on the critical feed rate guaranteeing the effectiveness of rotary ultrasonic machining”; Ultrasonics, 74, pp. 81–88.

Jianjian Wang, Pingfa Feng and Jianfu Zhang (2018a); “Reducing edge chipping defect in rotary ultrasonic machining of optical glass by compound step-taper tool”; Journal of Manufacturing Processes, 32, pp. 213–221.

Jianjian Wang, Jainfu Zhang, Pingfa Feng and Ping Guo (2018b); “Damage formation and suppression in rotary ultrasonic machining of hard and brittle materials: A critical review”; Ceramics International, 44, pp. 1227–1239.

Jingsi Wang, Keita Shimada, Masayoshi Mizutani and Tsunemoto Kuriyagawa (2018); “Effects of abrasive material and particle shape on machining performance in micro ultrasonic machining”; Precision Engineering, 51, pp. 373–387.

J. Gan, X Wang, M Zhou, B Ngoi and Z Zhong (2003); “Ultra-precision diamond turning of glass with ultrasonic vibration”; International journal advance manufacturing technology, 21, pp. 952–955.

J. Paulo Davim (2010); “Surface Integrity in Machining”; Springer Verlag, 235.

J. Paulo Davim, Pedro Reis, C Conceicao Antonio (2004); “Experimental study of drilling glass fiber reinforced plastics (GFRP) manufactured by hand lay-up” Composites Science and Technology, 64 (2), pp. 289–297.

Jun Wei Liu, Dae Kyuk Baek and Tae Jo Ko (2014); “Chipping minimization in drilling ceramic materials with rotary ultrasonic machining”; International Journal of Advance Manufacturing Technology, 72, pp.1527–1535.

Kai Ding, Yucan Fu, Honghua Su, Yan Chen, Xizhai Yu and Guozhi Ding (2014); “Experimental studies on drilling tool load and machining quality of C/SiC composites in rotary ultrasonic machining”; Journal of materials processing technology, 214, pp. 2900–2907.

Koichi Yamada and Masahide Mohri (1991); “Properties and Applications of Silicon Carbide Ceramics”; Silicon Carbide Ceramics, 1, pp. 13–44.

M A Azmir and A K. Ahsan, (2008); “Investigation on glass/epoxy composite surfaces machined by abrasive water jet machining,” Journal of materials processing technology, 198, pp. 122–128.

M. Kuruc, T. Vopat and J. Peterka (2015); “Surface roughness of Poly Crystalline Cubic Boron Nitride after Rotary ultrasonic machining”; Procedia engineering, 100, pp. 877–884.

Maroju Naresh Kumar, S. KanmaniSubbu, P. Vamsi Krishna and A.Venugopal (2014); “Vibration Assisted Conventional and Advanced Machining : A Review”; Procedia Engineering, 97, pp. 1577–1586.

Md Mahadi Hasan, Jingwei Zhao and Zhengyi Jiang (2017); “A review of modern advancements in micro drilling techniques”; Journal of Manufacturing Processes, 33, pp. 1–33.

Mudimallana Goud and Apurbba Kumar Sharma (2017); “On performance studies during micromachining of quartz glass using electrochemical discharge machining”; Journal of Mechanical Science and Technology, 31 (3), pp. 1365–1372.

Mudimallana Goud, Apurbba Kumar Sharma and Chandrashekhar S Jawalkar (2016); “A review on material removal mechanism in electrochemical discharge machining (ECDM) and possibilities to enhance the material removal rate” Precision Engineering, 45, pp. 1–17.

Muhammad Arif, Mustafizur Rehman and Wong Yoke San (2012); “An experimental study on the machining characteristics in ductile-mode milling of BK-7 glass” International Journal of Advance manufacturing technology, 60, pp. 487–495.

Muhammad Imran, Paul Mativenga, Ali Gholinia and Philip J. Withers (2015); “Assessment of surface integrity of Ni superalloy after electrical-discharge, Laser and mechanical micro-drilling processes”; International Journal of Advance Manufacuting and Technology, 79, pp.1303–1311.

Mohd Sayuti Ab Karim, Ahmed Alu Diaa Mohammed Sarhan and Mohd Hamdi Abd Shukor (2011); “Experimental Study on Minimizing Edge Chipping in Glass Milling Operation Using an Internal CBN Grinding Tool”; Materials and Manufacturing Processes, 26, pp. 969–976.

M. Wiercigroch, R D Neilson and M A. Player (1999); “Material removal rate prediction for ultrasonic drilling of hard materials using an impact oscillator approach”; Physics Letters A, 259: pp. 91–96.

M. Mandegari and S. Behbahani (2013); “Experimental Analysis of a Novel Rotary Ultrasonic Assisted Drilling (RUAD) Machine”; Materials and Manufacturing Processes, 28, pp. 481–487.

Narottam P. Bansal and Jacques Lamon (2014); “Ceramic Matrix Composites: Materials, Modeling and Technology”; Wiley Publishing, Book, pp. 1–714.

N. Bhatnagar, I. Singh and D. Nayak (2004); “Damage Investigation in Drilling of Glass Fiber Reinforced Plastic Composite Laminates”; Materials and Manufacturing Processes, 19 (6), pp. 995–1007.

Paolo Francesco Manicone, Pierfrancesco Rossi Iommetti and Luca Raffaelli (2007); “An overview of zirconia ceramics: Basic properties and clinical applications”; Journal of Dentistry, 35(11), pp. 819–826.

Patrick A Rebro, Yung C Shin and Frank P. Incropera (2004); “Design of operating conditions for crack free laser-assisted machining of mullite”; International Journal of Machine Tools and Manufacture, 44 (7-8), pp. 677–694.

P. L. Guzzo and A. H. Shinohara (2004); “A Comparative study on ultrasonic machining of hard and brittle Materials”; Journal of the brazil society of material science & engineering, 26, pp. 56–61.

Pravin Pawar, Raj Ballav and Amaresh Kumar (2015); “A review on machining process of glass materials”; Journal of Emerging technology in Mechanical science & Engineering, 5 (1), pp. 18–22.

Q H Zhang, J H Zhang, Z X Jia and X. Ai (1998); “Fracture at the exit of the hole during the ultrasonic drilling of engineering ceramics”, Journal of materials processing technology, 84, pp. 20–24.

Ramesh Kumar Singh, V. Roshan Joseph and Shreyes N. Melkote (2011); “A statistical approach to the optimization of a laser-assisted micromachining process”; International Journal of Advanced Manufacturing Technology, 53 (4), pp. 221–230.

Ravi Pratap Singh and Sandeep Singhal (2015); Rotary ultrasonic machining of advanced materials: A review”; International Journal for technological research in engineering, 2 (7), pp. 777–785.

Ravi Pratap Singh and Sandeep Singhal (2016); “Rotary Ultrasonic Machining: A Review” Materials and Manufacturing Processes, 31(14), pp. 1795–1824.

Ravi Pratap Singh and Sandeep Singhal (2017); “Investigation of machining characteristics in rotary ultrasonic machining of alumina ceramic”; Materials and Manufacturing Processes, 32(3), pp. 309–326.

Rees Rawlings, Jeremy Wu and Aldo R. Boccaccini (2006); “Glass-ceramics: Their production from wastes- A Review” Journal of Material Science, 41, pp. 733–761.

Samira Darvishi, Thomas Cubaud and Jon P. Longtin, (2012); “Ultrafast laser machining of tapered microchannels in glass and PDMS”; Optics and Lasers in Engineering, 50 (2), pp. 210–214.

Sara Fanara, Pranesh Sengupta, Hens Werner Becker, Detlef Rogalla and Sumit Chakraborty (2017); “Diffusion across the glass transition in silicate melts Systematic correlations, new experimental data for Sr and Ba in calcium-aluminon silicate glasses and general mechanisms of ionic transport” Journal of Non-crystalline solids, 455, pp. 6–16.

S. C. Rangwala, K.S. Rangwala and P.S. Rangwala (2010); “Engineering materials”; Charotar Publishing House Pvt. Ltd. (37 Edition).

S. Nikumb, Q. Chen, C. Li, H. Reshef, H. Y. Zheng, H. Qiu and D. Low (2005); “Precision glass machining, drilling and profile cutting by short pulse lasers” Thin Solid Films, 477, pp. 216–221.

Saqib Anwar, Mustafa M Nasr, Salman Pervaiz S, Abdulrahman Al-Ahmari, Mohammed Alkahtani and Abdulaziz El Tamimi (2018); "A study on the effect of main process parameters of rotary ultrasonic machining for drilling BK7 glass"; Advances in Mechanical Engineering, 10 (1), pp. 1–10.

Soda-Lime (Float) Glass Material Properties: www.makeitfrom.com.

Stephen Malkin and Chengshen Guo (1996); "Grinding Technology: Theory and Applications of Machining with Abrasives"; Society of manufacturing engineering Industrial press, 2nd edition.

T. Moriwaki, E. Shamoto and K. Inoue (1992); "Ultra-precision ductile cutting of glass by applying ultrasonic vibration"; CIRP Annals - Manufacturing Technology, 41 (1), pp. 141–144.

Vaibhav A. Phadnis, Farrukh Makhdum, Anish Roy and Vadim V. Silberschmidt (2012); "Experimental and numerical Investigations in conventional and ultrasonically assisted drilling of CFRP Laminate"; Procedia CIRP, 1, pp. 455–459.

Vaibhav A. Phadnis, Anish Roy and Vadim V. Silberschmidt (2013); "A finite element model of ultrasonically assisted drilling in carbon/epoxy composites" 14th CIRP Conference on Modeling of Machining Operations (CIRP CMMO), Procedia CIRP, 8, pp. 141–146.

Vincent A. Balogun and Paul T. Mativenga (2017); "Specific Energy Based Characterization of Surface Integrity in Mechanical Machining"; Procedia Manufacturing, 7, pp. 290–296.

Weixing Xu, L. C. Zhang and Yongbo Wu (2014); "Elliptic vibration assisted cutting of fiber reinforced polymer composites: understanding the material removal mechanisms"; Composites science technology, 92, pp. 103–111.

Weixing Xu and L.C. Zhang (2015); "Ultrasonic vibration assisted machining: principle, design and application"; Advance manufacturing, 3, pp. 173–192.

W L Cong, Z J Pei, T W Denies, Anil Srivastava, L Riley and C. Treadwell (2012); "Rotary ultrasonic machining of CFRP composites: A study on power consumption"; Ultrasonics, 52, pp. 1030–1037.

W M. Zeng, Z C. Li, Z J. Pei and C. Treadwell, (2005); "Experimental observation of tool wear in RUM of advanced ceramics"; International Journal of Machine Tools & Manufacture, 45, pp. 1468–1473.

X. Y. Yao, B. Wang, J. H. Wang, H. L. Jin, Y. F. Zhang and S. Dong, (2010); “Chemical machining of Zerodur material with atmospheric pressure plasma jet”; CIRP Annals-Manufacturing Technology, 59 (1), pp. 337–340.

Yaseer Ahmed, W L Cong, Matthew R. Stanco, Z. G. Xu, Z J. Pei, C. Treadwell, Y. L. Zhu and Z. C. Li (2012); “Rotary Ultrasonic Machining of Alumina Dental Ceramics: A Preliminary Experimental Study on Surface and Subsurface Damages”; Journal of Manufacturing Science and Engineering, 134, pp. 1–6.

Yingbin Hu, Hui Wang, Fuda Ning, Weilong Cong and Yuzhou Li (2017); “Surface grinding of optical BK7/K9 glass using Rotary ultrasonic Machining: An experimental study”; 12th International Manufacturing Science and Engineering Conference, Proceedings of the ASME, pp. 1–7.

Y. J. Chang, Y. C. Hung, C. L. Kuo, J. C. Hsu and C. C. Ho (2017); “Hybrid stamping and laser micromachining process for micro-scale hole drilling”; Materials And Manufacturing Processes, 32 (15), pp. 1685–1691.

Youqiang Xing, Jianxin Deng, Guodong Zhang, Ze Wu and Fengfang Wu (2017); “Assessment in drilling of C / C-SiC composites using brazed diamond drills” Journal of Manufacturing Processes, 26, pp. 31–43.

Yue Jiao, W J. Liu, Z J. Pei, X J Xin and C. Treadwell (2005); Study on edge chipping in rotary ultrasonic machining of ceramics: An integration of designed experiments and finite element method analysis”; Journal of manufacturing science and engineering, 127, pp. 752–758.

Z C Li, Y. Jiao, T W. Deines, Z J. Pei and C. Treadwell (2005); “Rotary ultrasonic machining of ceramic matrix composites: feasibility study and designed experiments”; International journal of machine tools & manufacture, 45, pp. 1402–1411.

Z. C. Li, Liang Wu Cai, Z J Pei and C. Treadwell (2006); “Edge-chipping reduction in rotary ultrasonic machining of ceramics: Finite element analysis and experimental verification”; International Journal of Machine Tools & Manufacture, 46, pp. 1469–1477.

Zongyi Wang, Yuanquing Wang, Yufan Liang, Xinxi Du and Yongjiu Shi (2016); “Bearing capacity of tempered glass panel in point supported glass facades against in-plane load”; Archives of Civil and Mechanical Engineering, 16(4), pp. 935–948.

VISIBLE OUTCOMES

Journals:

1. **Ankit Sharma**, Vivek Jain and Dheeraj Gupta (2018) *"Multi-Shaped Tool Wear Study during Rotary Ultrasonic Drilling and Conventional Drilling for Amorphous Solid"*, Journal of Process Mechanical Engineering, 233(3), 551-560. *Status:* ***Published Online****, Publisher: Sage Part E (****Impact Factor: 1.448****,* ***Category: SCI).***
2. **Ankit Sharma**, Vivek Jain and Dheeraj Gupta (2018) *"Characterization of Chipping and Tool wear during drilling of Float glass using rotary ultrasonic machining"*, Measurement, 128, 254-263. *Status:* ***Published Online****, Publisher: Elsevier (****Impact Factor: 2.359****,* ***Category: SCI).***
3. **Ankit Sharma**, Vivek Jain and Dheeraj Gupta (2018) *"Comparative Analysis of Chipping mechanics of Float glass during Rotary Ultrasonic Drilling and Conventional Drilling: For multi-shaped tools"*, Machining Science and Technology, 23, 547-568. *Status:* ***Published Online****, Publisher: Springer (****Impact factor: 1.339****,* ***Category: SCI).***
4. **Ankit Sharma**, Vivek Jain and Dheeraj Gupta (2020) *"A novel investigation study on float glass hole surface integrity & tool wear using Chemical assisted Rotary ultrasonic machining"*, Materials Today Proceedings, 26(2), 632-637. *Status:* ***Published Online****, Publisher: Elsevier (Category: SCOPUS).*
5. **Ankit Sharma**, Vivek Jain and Dheeraj Gupta (2019) *"Effect of Pre and Post tempering on hole quality of Float Glass specimen: For Rotary Ultrasonic and Conventional Drilling"*, Silicon, *Status:* ***Accepted****, Publisher: Springer (****Impact factor: 1.49****,* ***Category: SCI).***
6. **Ankit Sharma**, Vivek Jain and Dheeraj Gupta (2019) *"Mathematical approach on Chipping volume estimation generated during Rotary Ultrasonic Drilling for Float glass"*, Proceedings of the National Academy of Sciences, India, Section A: Physical Sciences, *Status:* ***Major revision****, Publisher: Springer (****Impact Factor: 0.7****, Category: SCI).*
7. **Ankit Sharma**, Vivek Jain and Dheeraj Gupta (2019) *"An Experimental and Finite Element Analysis of Chip size reduction by Rotary Ultrasonic Drilling of Brittle material"*, Machining Science and Technology, *Status:* ***Under review****, Publisher: Springer (****Impact factor: 1.339****,* ***Category: SCI).***

8. **Ankit Sharma**, Vivek Jain and Dheeraj Gupta (2019) "Evaluation and Optimization of Entrance/Exit Float glass Chipping during Rotary ultrasonic drilling: An Experimental approach", Sadhana. *Status: **Under review**, Publisher: Springer (Impact Factor: 0.80, Category: SCI).*
9. Ankit Sharma, Vivek Jain and Dheeraj Gupta (2020) "Experimental investigation of cutting temperature during drilling of float glass specimen", IOP Conference Series: Materials Science and Engineering, 715, 1-12. *Status: **Published Online**, Publisher: IOP Science (Category: SCOPUS).*

International Conferences:

1. **Ankit Sharma**, Vivek Jain and Dheeraj Gupta (2018) *"Tool wear analysis while creating blind holes on float glass using conventional drilling: A multi-shaped tools study"*, International Conference on Engineering Materials, Metallurgy and Manufacturing (ICEMMM), SSN College of Engineering, Chennai, India. 1-7 *Status: **Published**, **Best paper award.***
2. **Ankit Sharma**, Atul Babbar, Vivek Jain and Dheeraj Gupta (2018) *"Optimization of surface roughness during Pre-tempered float glass hole drilling by Rotary Ultrasonic machining"*, International Conference On Mechanical, Materials and Manufacturing (ICMMM), MATEC Web of Conferences 249, **Orlando, USA**. *Status: **Published.***
3. **Ankit Sharma,** Vivek Jain, Dheeraj Gupta (2019) *"In Situ affect of Cutting force and Drilling temperature on Glass hole Surface integrity"*, International Conference on "Emerging trends in Mechanical & Industrial Engineering" (ICETMIE-2019), North Cap University, Gurugram, India**.** *Status: **Accepted.***

Books:

1. **Ankit Sharma**, Vivek Jain and Dheeraj Gupta (2018) *"Tool wear analysis while creating blind holes on float glass using conventional drilling: A multi-shaped tools study"*, Advances in Manufacturing Processes, Lecture Notes Mechanical Engineering, Chapter-17, 175-183. doi: https://doi.org/10.1007/978-981-13-1724-8_17, *Status: **Published in Springer note.***
2. **Ankit Sharma,** Vivek Jain, Dheeraj Gupta (2019) *"In Situ affect of Cutting force and Drilling temperature on Glass hole Surface integrity"*, Advances in Manufacturing Processes, Lecture Notes Mechanical Engineering, *Status: **Accepted in Springer note.***